



23  
2000



This is to certify that the

dissertation entitled

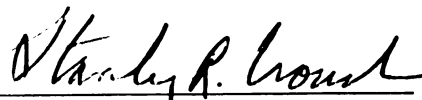
CHEMOMETRIC DATA PROCESSING TECHNIQUES FOR  
KINETIC-SPECTROPHOTOMETRIC DETERMINATIONS

presented by

Thomas Francis Cullen

has been accepted towards fulfillment  
of the requirements for

Ph.D. degree in Chemistry

  
Major professor

Date 9/1/99

**LIBRARY**  
**Michigan State**  
**University**

**PLACE IN RETURN BOX** to remove this checkout from your record.  
**TO AVOID FINES** return on or before date due.  
**MAY BE RECALLED** with earlier due date if requested.

DATE DUE	DATE DUE	DATE DUE
NOV 18 2001		

**CHEMOMETRIC DATA PROCESSING TECHNIQUES FOR  
KINETIC-SPECTROPHOTOMETRIC DETERMINATIONS**

**By**

**Thomas Francis Cullen**

**A DISSERTATION**

**Submitted to  
Michigan State University  
in partial fulfillment of the requirements  
for the degree of**

**DOCTOR OF PHILOSOPHY**

**Department of Chemistry**

**1999**

## **ABSTRACT**

### **CHEMOMETRIC DATA PROCESSING TECHNIQUES FOR KINETIC-SPECTROPHOTOMETRIC DETERMINATIONS**

By

Thomas Francis Cullen

A variety of chemometric data processing techniques were applied to kinetic-spectrophotometric data. In order to acquire these data, a new data acquisition system was designed and built. This redesign of the existing system involved the fabrication of a new optical path for a stopped-flow apparatus as well as the creation of a new computerized interface for a diode array detection system.

A series of simulated experiments were performed. In these simulation studies the effect of an array of experimental variables on the accuracy of a kinetic-spectrophotometric determination of a two component mixture were explored. Methods for quantifying the amount of kinetic and spectral information present in kinetic-spectrophotometric data are discussed. The kinetic and spectral angles were introduced and shown to be good measures of the quantity of information available in each dimension. Kinetic and spectral net analyte signals were also developed and were shown to be good predictors of the relative accuracy with which analytes can be determined. The kinetic angle was shown to have several contributing factors. The ratio of the analyte rate constants is the

largest contributor, but the fraction of the slower reaction for which data is acquired and the number of spectra acquired also impact the kinetic angle.

Ga(III) and Ni(II) were the subjects of a kinetic-spectrophotometric determination. In the studies discussed, the effect of the kinetic angle was explored experimentally; the determination was carried out at two different values of solution pH where the ratios of the reaction rate constants are different. A comparison was drawn between the various chemometric algorithms; continuum regression and multiway partial least squares regression proved most promising.

The effect of kinetic non-linearity on kinetic-spectrophotometric determinations was examined in both simulations and in experimental determinations. In general, it was found that most of the techniques used were fairly tolerant of nonlinear kinetics, though they began to fail in highly nonlinear systems. Again, the various chemometric algorithms were compared, and similar results to those found in the initial studies were obtained. Continuum regression and nPLS proved best suited to handling the nonlinear kinetic data. The degree of kinetic non-linearity was measured as an angle from linearity. This angle was shown to be a good predictor of the accuracy with which a determination could be performed.

Cu(II) and Zn(II) were determined in a real sample with environmental relevance. The accuracy of the determination was within acceptable limits for both analytes. The kinetic and spectral angles and net analyte signals were used to explain the relative accuracy with which the analytes were determined.

**To Melisa and Ceara, and to Mom and Dad**

**With Love**

## ACKNOWLEDGEMENTS

*I use not only all the brains I have, but  
all I can borrow.*

--Woodrow Wilson

There are many people who deserve my thanks and gratitude. Without their help this dissertation would never have been written. First, I should express my heartfelt thanks to Dr. Stan Crouch, under whose guidance the work described in this document was performed. Stan is an exceptional teacher and I've learned more in idle conversation with him than I could ever glean from a thousand textbooks. His scientific guidance and personal support were invaluable.

Others at Michigan State have played large parts in whatever success I've enjoyed. I'm not sure I would have survived my first year if not for the friendship and camaraderie of Dale Lecaptain and Wendy Flory. Together we weathered the storms that are common to the first years of graduate school, and I thank them for their support and friendship. Others whose friendship during those early years is much appreciated include Eric Meyer, Lykourgos Iordanidis, Rhonda Patschke and Matt Prater (who's also appreciated for dragging me back onto the ice after several years of hockey-less existence).

Dana Spence, too, played a large part in my success during those early years. He took a first-year student under his wing and showed him how things worked in the Crouch group, and in the department. The time and sanity saving tips and tricks he



passed on were invaluable, and his companionship during those late nights of data acquisition were much appreciated. We learned much of each other's projects; almost all I know of flow injection I learned from him.

In the latter years of my career I've come to be good friends with several members of the McGuffin group. John Goodpaster and Pete Krouskop are especially appreciated for being supportive during some particularly rough stretches. Sam Howerton is a newcomer who is appreciated for his friendship and for many stimulating intellectual discussions.

Much of the work described in this dissertation was completed with the skilled help of the department's support staff. Russ Geyer, Sam Jackson, and Glenn Wesley of the machine shop are thanked for their assistance with the repair and refurbishing of the machine. The efforts of Ron Haas, Scott Sanderson and especially John Rugis were exceedingly valuable during the design and construction of the diode array interface, and they have earned my gratitude. Scott Bankroff and Manfred Langer lent their glassblowing expertise to the project, and so are thanked for their help. The assistance of Tom Atkinson and Paul Reed with a host of computer-related difficulties is likewise appreciated.

In the course of my work I have on several occasions had the opportunity to interact with scientists whose understanding of chemometrics far outstrips my own. Dr. Pete Wentzell's friendly advice on the subjects of both chemometrics and graduate school was greatly appreciated. Barry Wise and Neal Gallagher provided

tireless assistance to a novice chemometrician, and are owed my humble thanks. Likewise, the patient efforts of Rasmus Bro and Claus Andersson were appreciated.

The assistance of Anthony Cochran with the acquisition of the equilibrium spectrophotometric data described in chapter four is gratefully acknowledged.

Many people's contribution to my success came well before I ever set foot onto MSU's beautiful campus. The love and support showed by my parents, Frank and Eileen Cullen, has sustained me through many trials and tribulations. They instilled in me a love of learning and provided me with the opportunity to pursue my goals. They did this, in part, by allowing me to attend Fenwick High School where Marcus McKinley and Ramzi Farran introduced me to chemistry and so set me on a path that would impact the rest of my life. It was at Fenwick, too, that John Quinn and Fr. John Gambro, O.P. were instrumental as I learned how to learn.

At Illinois Benedictine College my love of chemistry was confirmed. The efforts of Mike Winkler, Dave Sonnenberger and Wayne Wesolowski formed me as a chemist and provided me with the skills necessary for success in graduate school. The Scholars program formed me as a person and endowed me with a global perspective.

Finally, my most heartfelt and sincere thanks must go to my wife, Melisa, and to our daughter Ceara. Without their constant love and support this dissertation could not have been written. Their understanding and acceptance of the long hours necessary are greatly appreciated, and I offer them my love and gratitude.

# TABLE OF CONTENTS

LIST OF TABLES.....	x
LIST OF FIGURES.....	xi
LIST OF ABBREVIATIONS.....	xv
<b>1 INTRODUCTION.....</b>	<b>1</b>
1.1. CHEMOMETRICS.....	2
1.1.1. Nomenclature and Conventions.....	2
1.1.2. Multivariate calibration.....	2
1.1.3. Factor Analysis.....	13
1.1.4. Artificial Neural Networks.....	14
1.1.5. Multiway Methods.....	15
1.2. Kinetic Determinations.....	16
1.2.1. Kinetic Determinations using Hard Modeling Techniques.....	17
1.2.2. Kinetic Determinations using Soft Modeling Techniques.....	19
1.3. REFERENCES.....	23
<b>2 INSTRUMENT DESIGN AND CHARACTERIZATION.....</b>	<b>34</b>
2.1. DESIGN OF DIODE ARRAY INTERFACE.....	34
2.2. REDESIGN OF STOPPED-FLOW OBSERVATION CELL AND OPTICS.....	39
2.3. CHARACTERIZATION OF DATA ACQUISITION SYSTEM.....	40
2.3.1. Determination of Delay Time and Maximum Acquisition Rate.....	40
2.3.2. Determination of Signal/Noise Ratio.....	42
2.3.3. Determination of Linear Range.....	46
2.4. REFERENCES.....	48
<b>3 INITIAL SIMULATION STUDIES: STUDY OF THE EFFECT OF EXPERIMENTAL VARIABLES.....</b>	<b>49</b>
3.1. EXPERIMENTAL.....	50
3.1.1. Generation of Simulated Data.....	50
3.1.2. Data Processing.....	50
3.2. METHODS FOR QUANTIFYING KINETIC AND SPECTRAL DIFFERENCES FOR TWO COMPONENTS.....	51
3.2.1. Methods for Quantifying Kinetic Differences.....	51
3.2.2. Methods for Quantifying Spectral Differences.....	56
3.3. EFFECT OF EXPERIMENTAL VARIABLES.....	58
3.3.1. Effect of Kinetic and Spectral Angles.....	60
3.3.2. Effect of Number of Data Points Acquired (Time Points).....	68
3.3.3. Effect of Instrumental Noise.....	68
3.3.4. Effect of Rate Constant Fluctuations.....	73
3.4. EXPLORATION OF EFFECT OF EXPERIMENTAL VARIABLES ON SIMULATIONS OF THE Ga(III)-Ni(II) SPECTRAL SYSTEM.....	76
3.4.1. Effect of Kinetic Angle.....	77
3.5. References.....	80

4 DETERMINATION OF GALLIUM(III) AND NICKEL (II).....	81
4.1 EXPERIMENTAL.....	82
4.1.1. Solution Preparation.....	82
4.1.2. Spectrophotometric (Equilibrium) Data Collection.....	86
4.1.3. Kinetic-Spectrophotometric Data Collection.....	87
4.1.4. Data Processing.....	87
4.2. DETERMINATION OF RATE CONSTANTS AND ABSORPTION SPECTRA.....	88
4.3. RESULTS OF THE DETERMINATION OF GALLIUM(III) AND NICKEL (II).....	89
4.3.1. Spectrophotometric (Equilibrium) Determination of Gallium (III) and Nickel (II).....	89
4.3.2. Kinetic Determination of Gallium (III) and Nickel (II).....	93
4.3.3. Kinetic-Spectrophotometric Determination of Gallium (III) and Nickel (II).....	94
4.4. REFERENCES.....	97
5 KINETIC-SPECTROPHOTOMETRIC DETERMINATIONS IN SYSTEMS WITH NONLINEAR KINETICS .....	99
5.1. EXPERIMENTAL.....	102
5.1.1. Simulations.....	102
5.1.2. Solution Preparation.....	105
5.1.3. Kinetic-Spectrophotometric Data Collection.....	106
5.1.4. Data Processing.....	107
5.2. SIMULATION STUDIES INVOLVING SYSTEMS WITH NONLINEAR KINETICS.....	107
5.2.1. Systems Where The Reagent Does Not Absorb.....	107
5.2.2. Systems Where The Reagent Does Absorb.....	112
5.3. DETERMINATION OF GALLIUM(III) AND NICKEL(II) IN A SYSTEM WITH NONLINEAR KINETICS.....	114
5.4. REFERENCES.....	118
6 DETERMINATION OF Zn(II) AND Cu(II) IN A DRINKING WATER SAMPLE.....	119
6.1. EXPERIMENTAL.....	120
6.1.1. Solution Preparation.....	120
6.1.2. Kinetic-Spectrophotometric Data Collection.....	122
6.1.3. Data Processing.....	122
6.2. DETERMINATION OF ZINC(II) AND COPPER(II).....	122
6.3. REFERENCES.....	127
7 CONCLUSIONS AND FUTURE PERSPECTIVES.....	130
7.1. CONCLUSIONS AND SUMMARY.....	130
7.2. REFLECTIONS ON FUTURE DIRECTIONS.....	133
7.3. REFERENCES.....	136
APPENDIX:  MATLAB CODE FOR GENERATING SIMULATED KINETIC-SPECTROPHOTOMETRIC DATA .....	138
MULGEN_A.....	140
KINETIC.....	146
VARY_K.....	147

## LIST OF TABLES

Table 4-1	83
Single component calibration and unknown sets for the equilibrium determination of Ni(II)	
Table 4-2	83
Single component calibration and unknown sets for the equilibrium determination of Ga(III)	
Table 4-3	89
Spectrophotometric (equilibrium) determination of Ni(II)	
Table 4-4	90
Spectrophotometric (equilibrium) determination of Ga(III)	
Table 4-5	91
Multicomponent spectrophotometric (equilibrium) determination of Ni(II) and Ga(III)	
Table 4-6	94
Multicomponent kinetic determination of Ni(II) and Ga(III)	
Table 4-7	95
Multicomponent kinetic-spectrophotometric determination of Ni(II) and Ga(III)	
Table 5-1	115
Kinetic-spectrophotometric determination of Ga(III) and Ni(II) with two different values of reagent excess	
Table 6-1	120
Certified concentrations (ppb) of metal cations in a drinking water sample	
Table 6-2	123
Concentrations of analytes and interferents in the unknown samples in $\mu\text{M}$ units	
Table 6-3	123
Results of the determination of Cu(II) and Zn(II) in a series of unknown samples	

## LIST OF FIGURES

Figure 1-1: Multivariate calibration as a “black box”.	4
Figure 1-2: Decomposition of data into principal components.	7
Figure 1-3: Determination of the number of principal components using a scree graph.	9
Figure 1-4: Relationship between principal component regression, partial least squares regression, multiple linear regression and continuum regression.	13
Figure 1-5: Schematic diagram of a neuron.	14
Figure 2-1: Timing diagram of signals sent to and from the diode array.	35
Figure 2-2: Schematic diagram of the peak track-and-hold circuit. $\pm 12\text{V}$ power connections to the LT1363 operational amplifiers and $+5\text{V}$ power connections to the 74LS123 monostable multivibrators are omitted in the interest of clarity.	37
Figure 2-3: Schematic of the observation cell.	39
Figure 2-4: Plot showing dependence of relative error in absorbance to absorbance.	43
Figure 2-5: Dependence of S/N on absorbance.	44
Figure 2-6: Dependence of S/N on intensifier gain.	45
Figure 2-7: Dependence of S/N on integration time.	46
Figure 2-8: Linearity of measured absorbance with the known absorbance of a series of neutral density filters. The linear regression shown was calculated from all absorbances up to and including one absorbance unit.	47
Figure 3-1: Kinetic angle as a function of rate constant ratio. The fraction of the slower reaction observed was held constant at 90%, and the number of data points was held at 100.	54
Figure 3-2: Kinetic net analyte signal for the slower (squares) and the faster (circles) reactants in a two-component mixture. The fraction of the slower reaction observed was held constant at 90%, and the number of data points was held at 100.	55
Figure 3-3: Synthetic spectra used for simulation studies. Spectral angles range between 77.7 and 0.	57

<b>Figure 3-4: Spectral net analyte signal as a function of spectral angle. The spectra used to generate this plot are shown in Figure 3-3.</b>	<b>58</b>
<b>Figure 3-5: Concentrations of calibration (stars) and unknown (open circles) samples.</b>	<b>59</b>
<b>Figure 3-6: Relative standard error of a PLS prediction as a function of the kinetic and spectral angles.</b>	<b>62</b>
<b>Figure 3-7: Relative standard error of a PCR prediction as a function of the kinetic and spectral angles.</b>	<b>62</b>
<b>Figure 3-8: Relative standard error of a CR prediction as a function of the kinetic and spectral angles.</b>	<b>63</b>
<b>Figure 3-9: Relative standard error of an nPLS prediction as a function of the kinetic and spectral angles.</b>	<b>63</b>
<b>Figure 3-10: Relative standard error of an MLR prediction as a function of the kinetic and spectral angles.</b>	<b>64</b>
<b>Figure 3-11: Relative standard error of a PARAFAC prediction as a function of the kinetic and spectral angles.</b>	<b>65</b>
<b>Figure 3-12: Kinetic angle as a function of rate constant ratio and fraction of the slower reaction observed.</b>	<b>67</b>
<b>Figure 3-13: Relative standard error of a CR prediction as a function of the kinetic angle and instrumental noise.</b>	<b>69</b>
<b>Figure 3-14: Relative standard error of an nPLS prediction as a function of the kinetic angle and instrumental noise.</b>	<b>70</b>
<b>Figure 3-15: Relative standard error of a CR prediction as a function of the spectral angle and instrumental noise.</b>	<b>71</b>
<b>Figure 3-16: Relative standard error of an nPLS prediction as a function of the spectral angle and instrumental noise.</b>	<b>72</b>
<b>Figure 3-17: Relative standard error of a CR prediction as a function of the kinetic angle and rate constant fluctuation.</b>	<b>74</b>
<b>Figure 3-18: Relative standard error of an nPLS prediction as a function of the kinetic angle and rate constant fluctuation.</b>	<b>75</b>

Figure 3-19: Absorption spectra of PAR and its Ni(II) and Ga(III) complexes used for simulation studies.	76
Figure 3-20: Relative standard error of a CR prediction as a function of the rate constant ratio and the fraction of the slower reaction observed. The Ga(III)/Ni(II) spectra shown in Figure 3-19 were used. The spectral angle was 6.3.	78
Figure 3-21: Relative standard error of a CR prediction as a function of the rate constant ratio and the fraction of the slower reaction observed. The Ga(III)/Ni(II) spectra shown in Figure 3-19 were used. The spectral angle was 6.3.	79
Figure 4-1: Acid dissociation of PAR.	81
Figure 4-2: Concentrations of calibration (stars) and unknown (open circles) samples used for the two-component equilibrium determinations.	84
Figure 4-3: Concentrations of calibration (stars) and unknown (open circles) samples used for the ph 8.5 kinetic and kinetic-spectrophotometric determinations of Ga(III) and Ni(II).	85
Figure 4-4: Concentrations of calibration (stars) and unknown (open circles) samples used for the ph 7.0 kinetic and kinetic-spectrophotometric determinations of Ga(III) and Ni(II).	86
Figure 4-5: Plot showing the predicted vs. actual concentrations of Ga(III) for a two-component equilibrium determination. The circles show the predicted concentrations. The solid line has a slope of unity and represents a prediction with no error. The dashed lines show $\pm 10\%$ error tolerances.	92
Figure 4-6: Plot showing the predicted vs. actual concentrations of Ni(II) for a two-component equilibrium determination. The circles show the predicted concentrations. The solid line has a slope of unity and represents a prediction with no error. The dashed lines show $\pm 10\%$ error tolerances.	93
Figure 5-1: Example of a linear (pseudo-first-order) kinetic system. This data was generated with a rate constant ratio of 1.7 and a kinetic angle of 10.2. The reagent was in 281 fold excess. The angle from linearity was 0.017.	104
Figure 5-2: Example of a nonlinear kinetic system. This data was generated with a rate constant ratio of 1.7 and a kinetic angle of 10.2. The reagent was in 1.4 fold excess. The angle from linearity was 6.449.	105
Figure 5-3: Concentrations of calibration (stars) and unknown (open circles) samples used for the kinetic-spectrophotometric determinations of Ga(III) and Ni(II) under linear and nonlinear kinetic conditions.	106



Figure 5-4: Relative standard error of a CR prediction as a function of the kinetic angle and angle from linearity.	108
Figure 5-5: Relative standard error of an nPLS prediction as a function of the kinetic angle and angle from linearity.	109
Figure 5-6: Relative standard error of a CR prediction as a function of the spectral angle and angle from linearity. The kinetic angle for this data was $\sim 10^\circ$ .	110
Figure 5-7: Relative standard error of an nPLS prediction as a function of the spectral angle and angle from linearity. The kinetic angle for this data was $\sim 10^\circ$ .	111
Figure 5-8: Relative standard error of a CR prediction as a function of the kinetic angle and reagent excess. The gallium/nickel/PAR spectra (with the PAR absorbing) were used to generate the data. The spectral angle for this data was $\sim 11^\circ$ .	113
Figure 5-9: Relative standard error of an nPLS prediction as a function of the kinetic angle and reagent excess. The gallium/nickel/PAR spectra (with the PAR absorbing) were used to generate the data. The spectral angle for this data was $\sim 11^\circ$ .	114
Figure 5-10: CR determination of Ni(II) by reaction with 1mM PAR (circles) and 40 $\mu$ M PAR (plus signs). At the PAR concentration of 1mM the average excess is 28 fold; at 40 $\mu$ M it is 1.2 fold.	116
Figure 5-11: CR determination of Ga(III) by reaction with 1mM PAR (circles) and 40 $\mu$ M PAR (plus signs). At the PAR concentration of 1mM the average excess is 28 fold; at 40 $\mu$ M it is 1.2 fold.	117
Figure 6-1: Calibration set (stars) used in the determination of Zn(II) and Cu(II). The unknown sample is depicted by an open circle.	121
Figure 6-2: Spectra of the PAR complexes of Zn(II) and Cu(II). The zinc complex is shown as a solid line, the copper complex as a dotted line.	125
Figure 6-3: Kinetic profiles of the formation of the PAR complexes of Zn(II) and Cu(II). The zinc complex is shown as a solid line, the copper complex as a dotted line.	126

## **LIST OF ABBREVIATIONS**

<b>ANN</b>	<b>Artificial Neural Network</b>
<b>CR</b>	<b>Continuum Regression</b>
<b>GRAM</b>	<b>Generalized Rank Annihilation Method</b>
<b>MLR</b>	<b>Multiple Linear Regression</b>
<b>nPLS</b>	<b>N-way Partial Least Squares Regression</b>
<b>PAR</b>	<b>4-(2-Pyridylazo)-resorcinol</b>
<b>PARAFAC</b>	<b>Parallel Factor Analysis</b>
<b>PCR</b>	<b>Principal Component Regression</b>
<b>PLSR</b>	<b>Partial Least Squares Regression</b>
<b>RSEP</b>	<b>Relative Standard Error of Prediction</b>
<b>S/N</b>	<b>Signal to Noise</b>

# CHAPTER 1

## INTRODUCTION

*Beware the man of one book.*

--St. Thomas Aquinas

The subject of this thesis is the application of chemometric methods to kinetic data. It is important, therefore, to understand other work that has been done in both the fields of chemometrics and of kinetic determinations.

First, chemometrics will be discussed and some commonly used chemometric techniques will be described. Particular attention will be paid to multivariate calibration techniques. Kinetic determinations will then be reviewed, and the application of chemometric techniques to kinetic data will be highlighted.

### 1.1. CHEMOMETRICS

Chemometrics has been defined as “the science of relating measurements made on a chemical system to the state of the system via application of mathematical or statistical methods and of designing optimal experiments for investigating chemical systems.”<sup>1</sup> As highlighted by several recent texts,<sup>2,3</sup> chemometrics as a field of study has been steadily growing in recent years.

### **1.1.1. Nomenclature and Conventions**

In this document, matrices, vectors and scalars are written as follows. Matrix  $\mathbf{A}$ , vector  $\mathbf{a}$ , and scalar  $a$  are written as shown. The transpose of matrix  $\mathbf{A}$  and vector  $\mathbf{a}$  are written as  $\mathbf{A}^T$  and  $\mathbf{a}^T$ , respectively. All vectors are assumed to be column vectors unless written as a transpose. In data matrices it is assumed that rows represent samples or observations and that columns represent variables. Often, for simplicity, the examples shown presume that each row is a sample and each column is a measurement at a discrete time point.

### **1.1.2. Multivariate calibration**

To use terminology developed by Booksh and Kowalski in their *Theory of Analytical Chemistry*,<sup>4</sup> zeroth order data is data where only one data point is collected for each sample. Examples of zeroth order data include absorbance at a single wavelength, a single pH measurement, or a single temperature measurement. First order data consists of an array of data for each sample. First order data is extremely common, and examples include absorption spectra, emission spectra, chromatograms, and kinetic profiles. Second order data is made up of a matrix of data for each sample. Many hyphenated chemical analysis techniques produce second order data. Examples include fluorescence excitation-emission spectra, chromatograms with array detection, and kinetic profiles collected with array detectors. When the data consists of an array of absorbance measurements taken at every point in the kinetic profile, we will call the result kinetic-spectrophotometric data.

Calibration is the process of relating the known state of a system to measured data collected from the system. Multivariate calibration, then, is the process of relating the known state of a system to a series of measured variables describing the system. From the above definitions, it is clear that multivariate calibration is calibration performed on first or higher order data. Since much of the data collected by analytical scientists is at least first order, the use of multivariate calibration is becoming routine.

In spite of the above (strict) definition of multivariate calibration, the term is often used to describe the combination of two distinct processes. After multivariate calibration has been performed, the relationship found between the measured variables and the state of the measured system can be used to predict the state of another system, given the values of variables measured on that system. The term multivariate calibration is thus often used to describe the process of performing a calibration and then using the calibration relationship (or model) to perform a prediction. This combined process can be seen graphically in Figure 1. Here the two steps are distinctly separated. In the calibration step, the multivariate calibration algorithm is provided with data for several samples and the system states (in many cases, analyte concentrations) whose relationship to the data is to be discerned. The algorithm finds an empirical relationship (or model). In the second step, data from an unknown system is provided. Using the model built in the calibration step, the state of the unknown system (e.g., the concentration of the analytes in the unknown samples) is predicted.

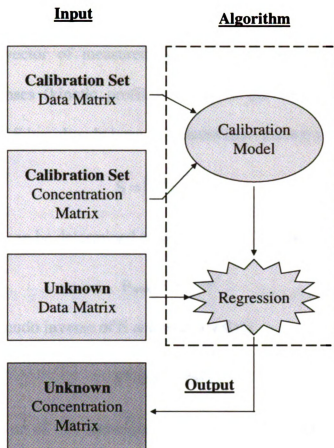


**Figure 1-1: Multivariate calibration as a “black box”.**

#### **1.1.2.1. Multiple Linear Regression**

Multiple linear regression (MLR) is perhaps the simplest and most straightforward of the multivariate calibration techniques. The mathematics have been well described in the literature<sup>1-3,5,6</sup>, and so only a brief discussion will be presented here.

Multiple linear regression assumes a linear relationship between the observed data (e.g., kinetic profiles) and a matrix or vector of weighting factors describing the state of the system (e.g., initial concentrations)

$$\mathbf{x} = \mathbf{pS}$$

where  $\mathbf{x}$  is the vector of measured data,  $\mathbf{S}$  is the matrix of calculated pure component responses (kinetic profiles) and  $\mathbf{p}$  is the vector of weights (initial concentrations). If  $\mathbf{S}$  has already been calculated from known  $\mathbf{x}$  and  $\mathbf{p}$

$$\mathbf{S} = (\mathbf{p}^T \mathbf{p})^{-1} \mathbf{p}^T \mathbf{x}$$

An unknown  $\mathbf{p}_{\text{unk}}$  can be determined from a vector of data  $\mathbf{x}_{\text{unk}}$

$$\mathbf{p}_{\text{unk}} = \mathbf{x}_{\text{unk}} \mathbf{S}^+$$

where  $\mathbf{S}^+$  is the pseudo inverse of  $\mathbf{S}$  and is defined as:

$$\mathbf{S}^+ = \mathbf{S}^T (\mathbf{S} \mathbf{S}^T)^{-1}$$

The major limitation of this technique is that the pure component responses must be linearly independent for  $\mathbf{S}^+$  to be defined.

#### ***1.1.2.2. Principal Component Regression***

Principal component regression (PCR) has also been well described in the literature.<sup>1-3,5-9</sup> PCR is, like other multivariate calibration methods, a two step process. In the first step, principal component analysis (PCA), a data matrix is decomposed into a set of abstract factors (or principal components). These principal components are linear combinations of the measured variables. The variables are combined and weighted such that the first principal component explains the largest fraction of the variance in the data. The manner in which this is accomplished is as follows.

Given a data matrix  $\mathbf{X}$  of size  $m \times n$  ( $m$  samples and  $n$  variables) the covariance matrix can be defined as

$$\text{cov}(\mathbf{X}) = \frac{\mathbf{X}^T \mathbf{X}}{m-1}$$

PCA decomposes  $\mathbf{X}$  as

$$\mathbf{X} = \mathbf{t}_1 \mathbf{p}_1^T + \mathbf{t}_2 \mathbf{p}_2^T + \dots + \mathbf{t}_k \mathbf{p}_k^T + \mathbf{E}$$

where  $k$  is less than or equal to the smaller of the number of variables ( $n$ ) and number of samples ( $m$ ) and  $\mathbf{E}$  is the residuals (error) matrix. The orthogonal  $\mathbf{t}_i$  vectors (the scores) contain information about intersample relationships. The  $\mathbf{p}_i$  vectors (the loadings) are the orthonormal eigenvectors of the covariance matrix,

$$\text{cov}(\mathbf{X}) \mathbf{p}_i = \lambda_i \mathbf{p}_i$$

where  $\lambda_i$  is the eigenvalue corresponding to eigenvector  $\mathbf{p}_i$ . Thus, the scores are the projections of the data matrix onto the loadings vector.

$$\mathbf{X} \mathbf{p}_i = \mathbf{t}_i$$

As already mentioned, the eigenvalues are arranged in order of magnitude. The first eigenvalue,  $\lambda_1$ , is the largest and is associated with the pair  $(\mathbf{t}_1, \mathbf{p}_1)$ . This first principal component contains more information about the system than any other. By examining the eigenvectors it is possible to determine how many principal components must be used to describe the data adequately. Most often, the number of principal components is much smaller than the number of variables. Indeed, one of the main advantages of PCA/PCR is this reduction in dimensionality. In



addition, principal components generated by PCA are often useful as descriptors of a chemical system. They are often more robust than measured experimental variables because of the averaging inherent in PCA. Some artificial neural network applications use PCA scores rather than experimental data as inputs<sup>10</sup>.

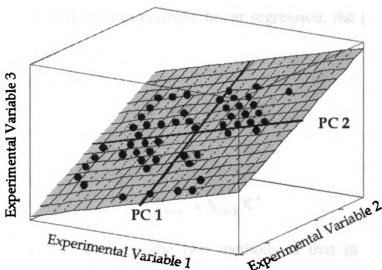


**Figure 1-2: Decomposition of data into principal components.**

Figure 1-2 illustrates the application of PCA to a system described by three experimental measurements. Plotting the data derived from these measurements reveals that all the data points lie in a plane. Using PCA the three variables can be consolidated into two principal components (PCs) that correspond to two axes in this plane and so the dimensionality of the system can be reduced. The first PC describes the main source of variation. The second PC corresponds to the next greatest source of variation in the data. Used in this context, a component that is a major source of variation in the data is one that has a large effect on the measured

data ( $\mathbf{X}$ ). Again, only PCs that have significant effects on the data are used in modeling the system.

The second step of principal component regression involves using the principal components calculated with PCA to create a calibration matrix. In a manner similar to that used in multiple linear regression, the pseudo inverse,  $\mathbf{X}^+$ , can be calculated as

$$\mathbf{X}^+ = \mathbf{P}(\mathbf{T}^T\mathbf{T})^{-1}\mathbf{T}^T$$

such that

$$\mathbf{P}_{\text{unk}} = \mathbf{X}_{\text{unk}}\mathbf{X}^+$$

The major difference between the two methods is that in PCR the data are regressed on the scores of principal components rather than on measured values. This reduction in dimensionality serves to eliminate some noise and provides well conditioned (orthogonal) data for regression. If all the available PCs are used, there is no reduction in dimensionality and PCR converges to MLR. The proper number of PCs to use in the regression can be determined in a variety of ways. The most obvious, and therefore the most common, criterion for choosing the number of principal components is the percentage of the total variation that is described by a set of selected PCs. Generally, the minimum number of PCs that combine to describe a desired fraction (usually 80-90%) of the variation in the data set is chosen.

### Eigenvalue vs. PC Number

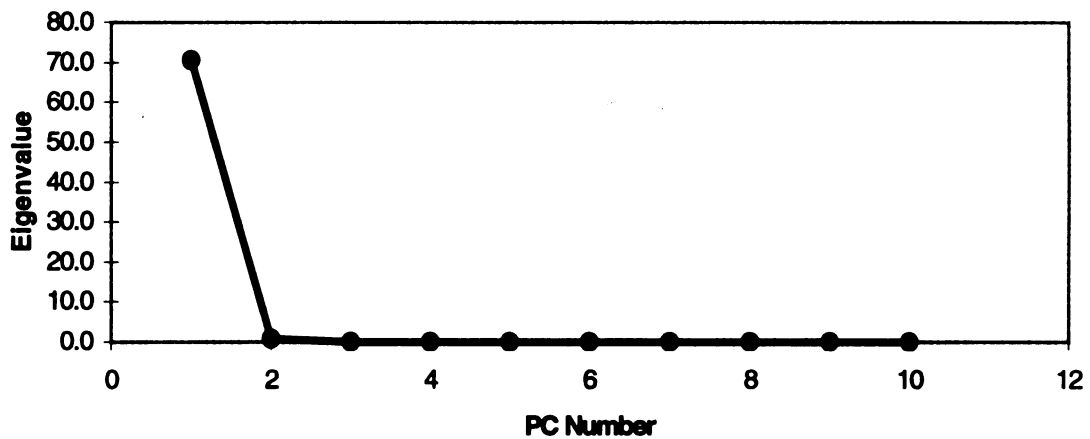


**Figure 1-3: Determination of the number of principal components using a scree graph.**

Graphical methods for determining the number of principal components are also very popular. A scree graph, shown in Figure 1-3, is a plot of the eigenvalue associated with each PC. The reading of a scree graph is not an exact science, but rather relies heavily on the common sense and intuition of the analyst. In general, the “elbow point” where the graph begins to have a nearly zero slope is the last significant PC. In Figure 1-3, it occurs at the second component, and so two PCs should be included in the model of the system. Often, the location of this elbow point is not as clear as that shown and is thus subject to interpretation.

Cross-validation methods for determining the number of PCs can be more computationally intense than the two methods mentioned above. They usually involve splitting the calibration data into two parts. The first is decomposed into PCs. These PCs are then used to perform a prediction on the other set. The number

of PCs that provide the best prediction is then chosen. Most often the process is repeated numerous times so that each sample is used in both a calibration and a validation set. An excellent discussion of various methods for choosing the proper number of PCs can be found in several references.<sup>2,3,6,8</sup>

### ***1.1.2.3. Partial Least Squares Regression***

Partial least squares regression (PLSR)<sup>1-3,6,11,12</sup> can perhaps best be thought of as a compromise between MLR and PCR. Multiple linear regression finds a single factor that correlates data (e.g., kinetic profiles) with weightings (initial concentrations). Principal component regression finds factors that best describe the trends (variance) in the data. PLS attempts to find factors that describe the variance in the data and correlate weightings to the data. PLS is thus less susceptible to error arising from variables that fluctuate significantly, but are unrelated to the weights.

Given a data matrix (e.g., kinetic profiles),  $\mathbf{X}$ , and a matrix of predicted variables (e.g., initial concentrations)  $\mathbf{Y}$ , PLS decomposes  $\mathbf{X}$  and  $\mathbf{Y}$  as:

$$\mathbf{X} = \mathbf{TP}^T$$

$$\mathbf{Y} = \mathbf{UQ}^T$$

where  $\mathbf{T}$  is the matrix of scores for the data,  $\mathbf{P}$  is the matrix containing the loadings for the data,  $\mathbf{U}$  is the matrix of scores for the dependent variables, and  $\mathbf{Q}$  is the matrix containing the loadings for the dependent variables. In addition, a vector of

weights  $\mathbf{w}$  that relate  $\mathbf{U}$  to  $\mathbf{X}$  and a vector  $\mathbf{b}$  that relates  $\mathbf{U}$  and  $\mathbf{T}$  are created. The pseudo inverse used in calibration is then defined as:

$$\mathbf{X}^+ = \mathbf{w}(\mathbf{P}^T \mathbf{w})^{-1} (\mathbf{T}^T \mathbf{T})^{-1} \mathbf{T}^T$$

Then as in MLR and PCR,

$$\mathbf{P}_{\text{unk}} = \mathbf{X}_{\text{unk}} \mathbf{X}^+$$

Again, if all the available latent variables are used in the prediction PLSR converges to MLR. Similar cross validation techniques are used in both PCR and PLSR.

#### ***1.1.2.4. Continuum Regression***

Continuum regression (CR) is a hybrid technique that has been described in several recent publications.<sup>1,13-16</sup> From at least one perspective, it can be argued that MLR, PCR, and PLSR are all special cases of continuum regression. In a manner similar to PLS and PCR, the observed data is decomposed

$$\mathbf{X} = \mathbf{U} \mathbf{S} \mathbf{V}^T$$

where  $\mathbf{U}$  and  $\mathbf{V}$  are orthonormal matrices and  $\mathbf{S}$  is a diagonal matrix. This decomposition is similar to that performed in PCR. In fact, the scores,  $\mathbf{V}$ , are identical to the scores produced by PCR ( $\mathbf{P}$ ). The PCR loadings are related to the other matrices produced by the CR decomposition by

$$\mathbf{U} \mathbf{S} = \mathbf{T}$$

In continuum regression the diagonal matrix  $\mathbf{S}$  is then raised to a power and a new data or  $\mathbf{X}$  matrix is formed as

$$\mathbf{X}^m = \mathbf{U}\mathbf{S}^m\mathbf{V}^T$$

After suitable manipulations and the use of PLSR on the new data matrix, a properly scaled regression vector can be obtained. The value of the exponent  $m$  determines the extent to which the algorithm considers the contribution of variables to the overall variance in the data when forming its set of abstract factors. At high (above unity) powers, the data set is deformed to exaggerate the variance, leading the PLSR algorithm to place inordinate weight on those variables that contribute variance to the data. At extremely high powers (nominally near infinity; practically, above 8) CR converges to PCR.

At low (below unity) powers, the data matrix is deformed to compress the data and to reduce the apparent variance. In this case, with little variance available, the PLSR algorithm places inordinate weight on those variables that are strongly correlated to the concentrations (or the state of the system). At extremely low powers (near zero) CR converges to MLR.

At a power of unity, the data set is undeformed, and CR converges to PLSR. This is summarized in Figure 1-4.

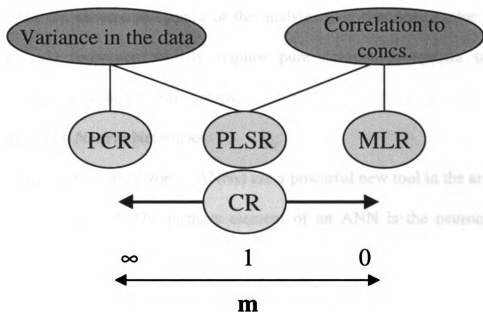


**Figure 1-4: Relationship between principal component regression, partial least squares regression, multiple linear regression and continuum regression.**

#### **1.1.2.5. Nonlinear Partial Least Squares Regression**

Several varieties of nonlinear PLSR exist. The algorithms for these methods are available in the literature.<sup>1</sup> In general, these techniques are functionally identical to PLSR, except that some sort of nonlinear (polynomial or spline, most commonly) fit is used to relate the scores to the concentrations.

#### **1.1.3. Factor Analysis**

Factor analysis is a well established technique that is well represented in the literature<sup>2,3,6-9,17,18</sup>. It, like PCA and PLS, involves decomposing the data into abstract factors. The factors, in this case, are not necessarily aligned to capture maximum variance or covariance, but rather are rotated so as to have physical meaning. In a spectrophotometric application, the abstract factors often are good

estimates of the absorption spectra of the analytes they describe. Factor analysis techniques do, however, usually require pure component spectra or other information to use in target testing steps.

#### 1.1.4. Artificial Neural Networks

Artificial neural networks (ANNs) are a powerful new tool in the arsenal of analytical chemists<sup>19,20</sup>. The primary element of an ANN is the neuron. These neurons are arranged in input and output layers sandwiching one or more “hidden” processing layers. Neurons can be thought of as weighted transfer functions. Neurons can have single or multiple inputs. The processing neurons apply a weighted sum of their inputs and transfer the result to the output. Often the transfer function is non-linear (sigmoidal functions have been most often used).

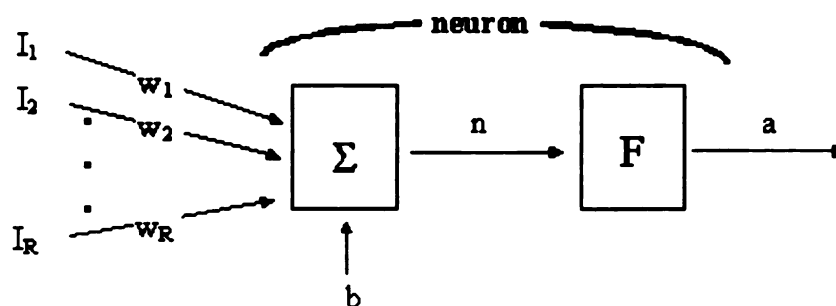


**Figure 1-5: Schematic diagram of a neuron.**

A diagram of a neuron is shown in Figure 1-5. Here  $I_i$  is an input,  $w_i$  is the weighting associated with input  $I$ ,  $b$  is the bias introduced into the summation,  $n$  is the output of the weighted sum and  $a$  is the output of the transfer function ( $F$ ); i.e.,

$$a=F(wI+b)$$



During the training or calibration phase the weightings are adjusted to accurately fit the calibration data. Often PCs are used as inputs to the network instead of experimental variables. This reduces the necessary number of neurons immensely.

#### **1.1.5. Multiway Methods**

All of the aforementioned chemometric techniques are designed to operate on first order data. If second or higher order data is to be used with these algorithms it must first be “unfolded” such that it appears as first order data. This results in a loss of information. Some more recently popular techniques are capable of handling second and higher order data directly without unfolding. These are briefly described below.

##### ***1.1.5.1. GRAM***

Generalized rank annihilation factor analysis, also known as the generalized rank annihilation method (GRAM)<sup>21-24</sup>, is one of the most popular multiway methods used by chemists. In GRAM a single calibration sample is used to predict concentrations in an unknown sample. An advantage of GRAM is that interferences are normally handled well, and that pure component responses of the analytes can be recovered. GRAM’s major weakness, however, is its restriction to only one calibration sample. This makes the algorithm sensitive to collinearity in the data set.

##### ***1.1.5.2. PARAFAC***

Parallel factor analysis (PARAFAC)<sup>25-27</sup> is a technique that is quite powerful, but also quite limited. PARAFAC, unlike GRAM, is not limited to one

calibration sample. It is generally possible to recover pure component responses for each component in each measured dimension. PARAFAC is susceptible, however, to nonlinearity in the data. If the measured data in each dimension is not linearly related to the concentrations being predicted PARAFAC fails to converge to meaningful solutions.

#### ***1.1.5.3. Multiway Partial Least Squares Regression***

A multiway version of the PLSR algorithm has recently been developed.<sup>28</sup> This N-way PLSR (or nPLSR) algorithm has been shown to be superior to PLSR acting on unfolded data. It is known to be quite tolerant of noise.

## **1.2. KINETIC DETERMINATIONS**

In recent years, kinetic methods for multicomponent determinations have become more popular. Several books and reviews covering the principles and applications of kinetic methods can be found<sup>29-36</sup>. Several other papers have reviewed the application of chemometric techniques to kinetic determinations<sup>36-42</sup>.

Multicomponent kinetic methods involve similar species reacting with a common reagent or undergoing a common process. Differences in the reaction or process kinetics are used to distinguish among the components without any physical separation. The major limitation of many conventional techniques for processing kinetic data is their reliance on an accurate model of the kinetics of the system under study. These techniques can, as a group, be referred to as hard modeling techniques. Such techniques require that the analyst have knowledge of

at least the reaction order and usually of the rate constants for each of the reactions in the chemical system.

It is becoming increasingly clear that perhaps the most useful chemometric techniques for handling kinetic data are those that do not assume a kinetic model. In particular, multivariate calibration techniques have shown great promise. Recent publications have demonstrated the use of many of these techniques.

### **1.2.1. Kinetic Determinations using Hard Modeling Techniques**

Hard modeling methods have some inherent advantages. By presuming a model for the chemical system they are often able to perform determinations using small calibration sets, or by not using calibration sets at all (except, perhaps, for determining the parameters of the model).

#### ***1.2.1.1. Kinetic Determinations using Reaction-Rate Methods***

Several workers have reviewed the use of reaction rate based methods for kinetic determinations. The papers by Love and Pardue<sup>43-45</sup> do an excellent job of comparing most of the common (and some more uncommon) techniques. Other excellent reviews of these methods can also be found<sup>37,46</sup>.

#### ***1.2.1.2. Kinetic Determinations using Other Miscellaneous Methods***

A host of techniques are available for effecting kinetic determinations. The H-point standard additions method<sup>47</sup> is an excellent technique that is designed for the simultaneous kinetic determination of the components of a binary mixture. The continuous addition of reagent technique<sup>48</sup> is one that has found some application in systems with complex kinetics<sup>49</sup>. The kinetic wavelength-pair method<sup>50,51</sup>

involves measurements using an array detector or fast-scanning spectrophotometer and relies on measurements at two pre-selected pairs of wavelengths for the determination of the two components in a binary mixture. Both the continuous addition of reagent technique and the wavelength pair method were developed in the laboratory of Professor Dolores Perez-Bendito at the University of Cordoba.

Schechter<sup>52-55</sup> has developed several techniques that are error compensated or error tolerant. One technique that does not require prior knowledge of the rate constants is based upon detecting the intermediate species in a system of consecutive reactions<sup>52</sup>. Other techniques developed in his laboratory include an algorithm that can effect determinations of systems of mixed first and second order reactions ( $A \rightarrow C$  &  $A+B \rightarrow C$ )<sup>53</sup>, a recursive algorithm for extrapolating slow kinetic profiles and instrumental responses<sup>54</sup>, and an error-compensating algorithm capable of determining the reaction order, rate constants, and concentrations of an system of general-order reactions<sup>55</sup>. This latter algorithm, however, requires modification for use with a first order system.

### ***1.2.1.3. Kinetic Determinations using Nonlinear Regression***

In cases where the reaction order and rate constants of a reaction system are well known, nonlinear regression methods can be used to determine the concentration of one or more analytes. These regression methods have been applied to a variety of chemical systems<sup>56-64</sup>. Some workers have also described the use of multidimensional nonlinear least squares fits of kinetic-

spectrophotometric data in cases where both the rate constants and absorptivities of the analytes are known<sup>61,65,66</sup>.

#### **1.2.1.4. Kinetic Determinations using the Kalman Filter**

The Kalman filter<sup>67</sup> is a recursive algorithm well suited to use with kinetic data<sup>68</sup>. Its use for such data has been reviewed<sup>69</sup>. It has also been found to be useful for enzymatic kinetic determinations<sup>70</sup>. Use of the Kalman filter requires knowledge (or at least a good estimate) of the rate constants. It presumes a reaction order.

The application of the extended Kalman filter to kinetic-spectrophotometric data has been described by Quencer and Crouch<sup>71</sup>. It has been used in binary systems with first order kinetics<sup>72</sup> as well as systems of consecutive reactions<sup>73</sup>.

Parallel Kalman filter networks have been applied to kinetic determinations by Wentzell<sup>74</sup>. The Kalman filter and extended Kalman filter have been compared to other data processing techniques in a number of reviews<sup>37,38,41</sup>.

#### **1.2.2. Kinetic Determinations using Soft Modeling Techniques**

Soft modeling techniques have the obvious advantage that they do not presume a model that may not fit the system being studied. They do, however, have the disadvantage that models they generate are often simply empirical and so have no physical meaning beyond their predictive ability. Several of these soft modeling techniques are described below.

### ***1.2.2.1. Kinetic Determinations using Factor Analysis***

While not strictly a soft modeling technique (first order kinetics are usually assumed), factor analysis is closely related to some other multivariate calibration techniques, and so is included in this section. In systems where there is at least a moderate degree of spectral and kinetic resolution between the analytes, factor analysis has been used to determine the rate constants, absorbance spectra, and concentrations of mixtures of analytes<sup>75-81</sup>.

### ***1.2.2.2. Kinetic Determinations using MLR, PCR and PLS***

Multivariate calibration techniques are finding broad application for kinetic determinations. This use has been reviewed in several papers<sup>36,38,39,41,42</sup>. Several of these applications are summarized here.

Gallium and aluminum react with 4-(2-pyridylaxo) resorcinol (PAR) to produce products with very similar spectra. The ratio of the rate constants is  $k_{Al}/k_{Ga} = 3.67$ . Using a stopped-flow, flow injection (FI) system with diode array detection, Blanco, et al.<sup>82</sup> determined mixtures of Ga and Al with an error of less than 10%.

In other work, O-O'-bis-(2-aminoethyl) ethylene glycol-N,N,N',N' tetraacetic acid (EGTA) complexes of Fe(II), Co(II), and Zn(II) were reacted with PAR<sup>10</sup>. These metal ions react with similar kinetics to form products with very similar kinetic profiles. This experiment was performed in a stopped-flow FI system with diode array detection. PCR and PLSR were used to determine Fe, Co and Zn successfully. The kinetics can be complicated by performing the

experiment in two steps in a flow system. If Co, Fe, and Zn are directly injected into the flow system, where they first react with EGTA and then with PAR, the kinetics of the Co and Zn are essentially the same as for the case where the EGTA complexes are directly injected. Iron(II), however, reacts slowly with EGTA and thus the kinetics associated with the formation of the Fe-PAR complex are significantly altered (in a non-linear fashion). Both methods (PCR and PLSR) were used to determine Co, Fe, and Zn using data collected in this second manner. Almost identical results were obtained with PCR and PLSR. They predicted the concentration of Zn and Co with good accuracy, but performed less well in determining Fe.

In other work, Havel and coworkers determined vanadium and cobalt by PLSR using kinetic data<sup>83</sup>. The reaction studied was that of V and Co with the TrAMeR reagent (4-(1'H-1',2',4'-triazolyl-3'-azo)-2-methylresorcinol). The reaction was monitored at 60 s intervals for 30 minutes at five wavelengths between 500 and 540 nm. The average relative percent error was 4%. In the same paper, a stopped FI determination of Zn, Co, and Fe was described. The average error associated with this determination was also about 4%.

Lopez-Cueto and coworkers<sup>84</sup> have described the determination of aminophenol isomers. These authors used PLSR with kinetic-spectrophotometric data that were acquired with a diode array detector. The reaction studied was one that required that the reagent not be present in excess. Also, the concentration of

each isomer influenced the reaction rate of the others. In spite of the inherent kinetic non-linearity, acceptable results were obtained.

Havel and coworkers<sup>85</sup> reported on the kinetic-spectrophotometric determination of europium, terbium and lanthanum using PLSR. Binary mixtures of the metal ions reacted with Xylenol Orange to produce similar spectra. Acceptable errors were obtained (0.2-4%). The authors noted that the PLSR algorithm required at least four latent variables for a satisfactory fit. They also reported that, while excellent results were obtained with binary mixtures, ternary mixtures could not be resolved with acceptable error levels.

A variety of other kinetic determinations have been achieved using multivariate calibration techniques<sup>10,13,41,82-106</sup>.

#### ***1.2.2.3. Kinetic Determinations using Artificial Neural Networks***

Artificial neural networks (ANNs) have been used for a variety of kinetic determinations<sup>10,13,95,99,100,107-110</sup>. In general, it has been found that ANNs are similar to PLSR and PCR in their predictive ability in most cases. Artificial neural networks require more rigorous and lengthy calculations. They also require larger calibration sets. In most cases, the advantage (if any) of using an ANN is more than outweighed by these drawbacks. ANNs do, however, achieve superior results in cases where the data is nonlinear or in other ways ill-behaved<sup>10,13,95</sup>.

#### ***1.2.2.4. Kinetic Determinations using Multiway techniques***

Multiway techniques have been applied to kinetic determinations in only a handful of papers. The use of GRAM for kinetic-spectrophotometric data<sup>111</sup> has



been investigated. Several papers have described initial studies of the application of nPLS to kinetic-spectrophotometric data<sup>112,113</sup>. A number of papers have reported the use of multivariate curve resolution for kinetic-spectrophotometric determinations<sup>114-116</sup>.

### 1.3. REFERENCES

- (1) Wise, B. M.; Gallagher, N. B. *PLS\_Toolbox 2.0 User Manual* ; Eigenvector Research, Inc.: Manson, WA, 1998.
- (2) Kramer, R. *Chemometric Techniques for Quantitative Analysis* ; Marcel Dekker, Inc.: New York, 1998.
- (3) Beebe, K. R.; Pell, R. J.; Seasholtz, M. B. *Chemometrics: A practical guide* ; John Wiley and Sons: New York, 1998.
- (4) Booksh, K. S.; Kowalski, B. R. "Theory of analytical-chemistry" *Anal. Chem.* **1994**, *66*, A782-A791.
- (5) Sanchez, E. S.; Kowalski, B. R. "Tensorial calibration: I. First-order calibration" *J. Chemometr.* **1988**, *2*, 247-264.
- (6) Martens, H.; Naes, T. *Multivariate Calibration* ; Wiley: New York, 1989.
- (7) Malinowski, E. R.; Howery, D. G. *Factor Analysis in Chemistry* ; John Wiley and Sons: New York, 1980.
- (8) Jolliffe, I. T. *Principal Component Analysis* Springer Series in Statistics, ; Springer-Verlag: New York, 1986.
- (9) Brereton, R. G. "Deconvolution of mixtures by factor-analysis" *Analyst* **1995**, *120*, 2313-2336.
- (10) Blanco, M.; Coello, J.; Iturriaga, H.; MasPOCH, S.; Redon, M. "Artificial neural networks for multicomponent kinetic determinations" *Anal. Chem.* **1995**, *67*, 4477-4483.
- (11) Geladi, P.; Kowalski, B. R. "Partial least-squares regression - a tutorial" *Anal. Chim. Acta* **1986**, *185*, 1-17.

- (12) Geladi, P.; Kowalski, B. R. "An example of 2-block predictive partial least-squares regression with simulated data" *Anal. Chim. Acta* **1986**, *185*, 19-32. ✓
- (13) Blanco, M.; Coello, J.; Iturriaga, H.; Maspoch, S.; Redon, M.; Villegas, N. "Artificial neural networks and partial least squares regression for pseudo-first-order with respect to the reagent multicomponent kinetic-spectrophotometric determinations" *Analyst* **1996**, *121*, 395-400.
- (14) Wise, B. M.; Ricker, N. L. "Identification of finite impulse-response models with continuum regression" *J. Chemometr.* **1993**, *7*, 1-14.
- (15) Stone, M.; Brooks, R. J. "Continuum regression - cross-validated sequentially constructed prediction embracing ordinary least-squares, partial least-squares and principal components regression" *J. R. Stat. Soc. Ser. B-Methodol.* **1990**, *52*, 237-269. ↙
- (16) Kalivas, J. H. "Interrelationships of multivariate regression methods using eigenvector basis sets" *J. Chemometr.* **1999**, *13*, 111-132. ✓
- (17) Malinowski, E. R. "Automatic window factor analysis - a more efficient method for determining concentration profiles from evolutionary spectra" *J. Chemometr.* **1996**, *10*, 273-279. ✓
- (18) Harvey, D. T.; Bowman, A. "Factor-analysis of multicomponent samples" *J. Chem. Educ.* **1990**, *67*, 470-472. ✓
- (19) Zupan, J.; Gasteiger, J. "Neural networks: A new method for solving chemical problems or just a passing phase?" *Anal. Chim. Acta* **1991**, *248*, 1-30.
- (20) Despagne, F.; Massart, D. L. "Neural networks in multivariate calibration" *Analyst* **1998**, *123*, 157R-178R. ↙
- (21) Sanchez, E.; Kowalski, B. R. "Generalized rank annihilation factor-analysis" *Anal. Chem.* **1986**, *58*, 496-499. ✓
- (22) Sanchez, E.; Ramos, L. S.; Kowalski, B. R. "Generalized rank annihilation method .1. Application to liquid- chromatography diode-array ultraviolet detection data" *Journal of Chromatography* **1987**, *385*, 151-164. ✓
- (23) Sanchez, E. S.; Kowalski, B. R. "Tensorial calibration: II. Second-order calibration" *J. Chemometr.* **1988**, *2*, 265-280.

- (24) Ramos, L. S.; Sanchez, E.; Kowalski, B. R. "Generalized rank annihilation method .2. Analysis of bimodal chromatographic data" *Journal of Chromatography* **1987**, *385*, 165-180.
- (25) Bro, R. "PARAFAC. Tutorial and applications" *Chemometrics Intell. Lab. Syst.* **1997**, *38*, 149-171.
- (26) Bro, R. "The N-way on-line course on PARAFAC and PLS" <http://newton/foodsci.kvl.dk/n-way> **1998**.
- (27) Harshman, R. A. "Foundations of the PARAFAC procedure: Model and conditions for an 'explanatory' multi-mode factor analysis" *UCLA Working Papers in Phonetics* **1970**, *16*, 1.
- (28) Bro, R. "Multiway calibration. Multilinear PLS" *J. Chemometr.* **1996**, *10*, 47-61.
- (29) Perez-Bendito, D.; Silva, M. *Kinetic Methods in Analytical Chemistry* ; Ellis Horwood: Chichester, 1988.
- (30) Perez-Bendito, D. "Inorganic differential kinetic-analysis - a review" *Analyst* **1984**, *109*, 891-899.
- (31) Perez-Bendito, D. "Approaches to differential reaction-rate methods" *Analyst* **1990**, *115*, 689-698.
- (32) Mottola, H. A. *Some Kinetic Aspects of Analytical Chemistry* ; Wiley: New York, 1988.
- (33) Crouch, S. R. "Kinetic methods for intelligent automation" *Chemometrics Intell. Lab. Syst.* **1990**, *8*, 259-273.
- (34) Crouch, S. R. "Trends in kinetic methods of analysis" *Anal. Chim. Acta* **1993**, *283*, 453-470.
- (35) Crouch, S. R. "Kinetic methods of analysis - how do they rate" *J. Chin. Chem. Soc.* **1994**, *41*, 221-229.
- (36) Crouch, S. R.; Cullen, T. F.; Scheeline, A.; Kirkor, E. S. "Kinetic determinations and some kinetic aspects of analytical chemistry" *Anal. Chem.* **1998**, *70*, 53R-106R.
- (37) Quencer, B. M.; Crouch, S. R. "Multicomponent kinetic methods" *Crit. Rev. Anal. Chem.* **1993**, *24*, 243-262.

- (38) Perez-Bendito, D.; Silva, M. "Recent advances in kinetometrics" *Trac-Trends Anal. Chem.* **1996**, *15*, 232-240.
- (39) Otto, M. "Chemometrics in kinetic-analysis" *Analyst* **1990**, *115*, 685-688.
- (40) Cerda, V.; Cladera, A.; Estela, J. M. "Multicomponent techniques as applied to kinetic analysis" *Quim. Anal.* **1996**, *15*, 341-350.
- (41) Xie, Y. L.; BaezaBaeza, J. J.; RamisRamos, G. "A comparative study of several chemometric methods applied to the treatment of two-way kinetic-spectral data for mixture resolution" *Anal. Chim. Acta* **1996**, *321*, 75-95.
- (42) Cullen, T. F.; Crouch, S. R. "Multicomponent kinetic determinations using multivariate calibration techniques" *Mikrochim. Acta* **1997**, *126*, 1-9.
- (43) Love, M. D.; Pardue, H. L. "Systematic comparison of data-processing options for kinetic- based, single-component determinations of noncatalysts: Effects of random noise" *Anal. Chim. Acta* **1996**, *326*, 95-106.
- (44) Love, M. D.; Pardue, H. L. "Systematic comparison of data-processing options for kinetic- based single-component determinations of non-catalysts .1. Review, systematic classification, mathematical descriptions, performance-characteristics and perspectives" *Anal. Chim. Acta* **1994**, *299*, 195-208.
- (45) Love, M. D.; Pardue, H. L. "Systematic comparison of data-processing options for kinetic- based single-component determinations of non-catalysts .2. One- rate, 2-point/fixed-time, 2-rate, 3-point/fixed-time options" *Anal. Chim. Acta* **1994**, *299*, 209-218.
- (46) Wentzell, P. D.; Crouch, S. R. "Comparison of reaction-rate methods of analysis for systems following 1st-order kinetics" *Anal. Chem.* **1986**, *58*, 2855-2858.
- (47) Boschreig, F.; Campinsfalco, P.; Sevillanocabeza, A.; Herraehernandez, R.; Molinslegua, C. "Development of the h-point standard-additions method for ultraviolet visible spectroscopic kinetic-analysis of 2-component systems" *Anal. Chem.* **1991**, *63*, 2424-2429.
- (48) Marquez, M.; Silva, M.; Perez-Bendito, D. "Continuous addition of reagent technique - a new approach to differential reaction-rate methods" *Anal. Chim. Acta* **1990**, *239*, 221-227.

- (49) Velasco, A.; Silva, M.; Perez-Bendito, D. "Processing analytical data obtained from 2nd-order reactions by using continuous reagent addition" *Anal. Chem.* **1992**, *64*, 2359-2365.
- (50) Carreto, M. L.; Lunar, L.; Rubio, S.; Perez-Bendito, D. "Simultaneous spectrophotometric determination of o-cresol and m-cresol in urine by use of the kinetic wavelength-pair method" *Analyst* **1996**, *121*, 1647-1652.
- (51) Carreto, M. L.; Lunar, L.; Rubio, S.; Perez-Bendito, D. "Simultaneous spectrophotometric determination of chlorpromazine, perphenazine and acetopromazine by use of the kinetic wavelength pair-method" *Anal. Chim. Acta* **1997**, *349*, 33-42.
- (52) Schechter, I. "Error-compensated kinetic determinations by detecting the intermediate product in successive reactions, without prior knowledge of reaction constants" *Anal. Chem.* **1991**, *63*, 1303-1307.
- (53) Schechter, I.; Schroder, H. "Error-compensated kinetic determinations in systems of mixed 1st-order and 2nd-order reactions, without prior knowledge of reaction constants" *Anal. Chem.* **1992**, *64*, 325-329.
- (54) Schechter, I. "Predictive mode of kinetic-analysis and transient detection responses - evaluation of a recursive algorithm" *Anal. Chem.* **1992**, *64*, 2610-2614.
- (55) Schechter, I. "Simultaneous determination of mixtures by kinetic-analysis of general-order reactions" *Anal. Chem.* **1992**, *64*, 729-737.
- (56) Cost, J. R. "Non-linear regression least-squares method for determining relaxation-time spectra for processes with 1st-order kinetics" *J. Appl. Phys.* **1983**, *54*, 2137-2146.
- (57) Gomez, E.; Cladera, A.; Estela, J. M.; Cerda, V. "Multidata treatment applied to the simultaneous resolution of catechol resorcinol mixtures by kinetic enzymatic processes" *Talanta* **1993**, *40*, 1601-1607.
- (58) Diaz, A. N.; Garcia, J. A. G. "Nonlinear multicomponent kinetic-analysis for the simultaneous stopped-flow determination of chemiluminescence enhancers" *Anal. Chem.* **1994**, *66*, 988-993.
- (59) Cai, Q. Y.; Wang, R. G.; Wu, L. Y.; Nie, L. H.; Yao, S. Z. "A nonlinear regression model applied to kinetic studies of ester hydrolysis with a surface acoustic wave sensor" *Talanta* **1996**, *43*, 699-705.

- (60) Gill, A.; Leatherbarrow, R. J.; Hoare, M.; PollardKnight, D. V.; Lowe, P. A.; Fortune, D. H. "Analysis of kinetic data of antibody-antigen interaction from an optical biosensor by exponential curve fitting" *J. Biotechnol.* **1996**, *48*, 117-127.
- (61) Havel, J.; Cuesta, F.; Gonzalez, J. L.; Canedo, M. D. "Multicomponent kinetic analysis and kinetic studies .1. Multipurpose KILET(94) non-linear least squares program" *J. Anal. Chem.* **1996**, *51*, 100-105.
- (62) Kuroda, Y.; Kawashima, A.; Ogoshi, H. "Computer analyses of complex kinetics containing equilibrium processes. Example of application for unusual atropisomerization of a tetraphenylporphyrin derivative" *Chem. Lett.* **1996**, 57-58.
- (63) Roecker, L.; Lee, S. M.; Liu, L. W.; Sun, L. J.; Zaerpoor, K. "Analysis of first-order kinetic data by a differential technique" *Int. J. Chem. Kinet.* **1997**, *29*, 333-338.
- (64) Shultz, L. L.; Nieman, T. A. "Stopped-flow analysis of Ru(bpy)(3)(3+) chemiluminescent reactions" *J. Biolumin. Chemilumin.* **1998**, *13*, 85-90.
- (65) Chau, F. T.; Mok, K. W. "Multiwavelength analysis for a 1st-order consecutive reaction" *Comput. Chem.* **1992**, *16*, 239-242.
- (66) Endo, M.; Sasaki, I.; Abe, S. "Kinetic spectrophotometric determination of iron oxidation- states in geological-materials" *Fresenius J. Anal. Chem.* **1992**, *343*, 366-369.
- (67) Brown, S. D. "The Kalman filter in analytical-chemistry" *Anal. Chim. Acta* **1986**, *181*, 1-29.
- (68) Wentzell, P. D.; Karayannis, M. I.; Crouch, S. R. "Simultaneous kinetic determinations with the Kalman filter" *Anal. Chim. Acta* **1989**, *224*, 263-274.
- (69) Xiong, R.; Velasco, A.; Silva, M.; Perez-Bendito, D. "Performance of the kalman filter algorithm in differential reaction-rate methods" *Anal. Chim. Acta* **1991**, *251*, 313-319.
- (70) Lin, D. Z.; Tan, H. W.; Bao, L. L.; Nie, L. H.; Yao, S. Z. "Study on a modified algorithm - iterative Kalman filter and its application in enzymatic kinetics" *Analyst* **1995**, *120*, 2573-2578.

- (71) Quencer, B. M.; Crouch, S. R. "Extended Kalman filter for multiwavelength, multicomponent kinetic determinations" *Analyst* **1993**, *118*, 695-701.
- (72) Quencer, B. M.; Crouch, S. R. "Multicomponent kinetic determination of lanthanides with stopped-flow, diode-array spectrophotometry and the extended Kalman filter" *Anal. Chem.* **1994**, *66*, 458-463.
- (73) Mok, K. W.; Chau, F. T. "Application of the extended Kalman filter for analysis of a consecutive first-order reaction" *Trac-Trends Anal. Chem.* **1996**, *15*, 170-174.
- (74) Wentzell, P. D.; Vanslyke, S. J. "Parallel Kalman filter networks for kinetic methods of analysis" *Anal. Chim. Acta* **1992**, *257*, 173-181.
- (75) Cladera, A.; Gomez, E.; Estela, J. M.; Cerda, V. "Resolution of simultaneous kinetic spectrophotometric processes by factor-analysis" *Anal. Chem.* **1993**, *65*, 707-715.
- (76) Tam, K. Y.; Chau, F. T. "Simultaneous multiwavelength study of the reduction reaction of chromic-acid with oxalic-acid using a photodiode-array spectrophotometer" *Spectr. Lett.* **1993**, *26*, 1195-1212.
- (77) Tam, K. Y.; Chau, F. T. "Multivariate study of kinetic data for a 2-step consecutive reaction using target factor-analysis" *Chemometrics Intell. Lab. Syst.* **1994**, *25*, 25-42.
- (78) Liang, X. H.; Andrews, J. E.; deHaseth, J. A. "Resolution of mixture components by target transformation factor analysis and determinant analysis for the selection of targets" *Anal. Chem.* **1996**, *68*, 378-385.
- (79) Garland, M.; Visser, E.; Terwiesch, P.; Rippin, D. W. T. "On the number of observable species, observable reactions and observable fluxes in chemometric studies and the role of multichannel integration" *Anal. Chim. Acta* **1997**, *351*, 337-358.
- (80) Fister, J. C.; Harris, J. M. "Resolving component overlap in multiwavelength kinetic spectroscopy: Application to Raman scattering from intermediates in triplet-state photoreactions" *Photochem. Photobiol.* **1997**, *65*, 47-56.
- (81) Amrhein, M.; Srinivasan, B.; Bonvin, D. "Target factor analysis of reaction data: Use of data pre-treatment and reaction-invariant relationships" *Chem. Eng. Sci.* **1999**, *54*, 579-591.

- (82) Blanco, M.; Coello, J.; Iturriaga, H.; Maspoch, S.; Riba, J.; Rovira, E. "Kinetic spectrophotometric determination of Ga(III)-Al(III) mixtures by stopped-flow injection-analysis using principal component regression" *Talanta* **1993**, *40*, 261-267. ✓
- (83) Havel, J.; Jimenez, F.; Bautista, R. D.; Leon, J. J. A. "Evaluation of multicomponent kinetic-analysis data by a partial least-squares calibration method" *Analyst* **1993**, *118*, 1355-1360. ✓
- (84) Lopez-Cueto, G.; Maspoch, S.; Rodriguez-Medina, J. F.; Ubide, C. "Simultaneous kinetic spectrophotometric determination of o-, m- and p-aminophenol using partial least squares calibration" *Analyst* **1996**, *121*, 407-412.
- (85) Fraga, J. M. G.; Abizanda, A. I. J.; Moreno, F. J.; Leon, J. J. A.; Havel, J. "Kinetic spectrophotometric resolution of mixtures of europium, terbium, and lanthanum in a micellar medium using multivariate calibration" *Microchem J.* **1996**, *54*, 32-40.
- (86) Havel, J.; Cuesta, F.; Jancar, L. "PLS self-calibration method for the evaluation of rate constants and or initial concentrations in multicomponent kinetic-analysis" *React. Kinet. Catal. Lett.* **1993**, *49*, 189-195. ✓
- (87) Blanco, M.; Coello, J.; Iturriaga, H.; Maspoch, S.; Riba, J. "Kinetic spectrophotometric method for analyzing mixtures of metal-ions by stopped-flow injection-analysis using partial least-squares regression" *Anal. Chem.* **1994**, *66*, 2905-2911.
- (88) Baxter, P. J.; Christian, G. D.; Ruzicka, J. "Multivariate approach for the simultaneous determination of total biomass and glucose from a yeast fermentation by sequential injection-analysis" *Chem. Anal.* **1995**, *40*, 455-471. ✓
- (89) Blanco, M.; Coello, J.; Iturriaga, H.; Maspoch, S.; Redon, M. "Partial least-squares regression for multicomponent kinetic determinations in linear and nonlinear-systems" *Anal. Chim. Acta* **1995**, *303*, 309-320. ✓
- (90) Garcia, J. M.; Jimenez, A. I.; Arias, J. J.; Khalaf, K. D.; Moralesrubio, A.; Delaguardia, M. "Application of the partial least-squares calibration method to the simultaneous kinetic determination of propoxur, carbaryl, ethiofencarb and formetanate" *Analyst* **1995**, *120*, 313-317.



- (91) Gu, Z. C.; Wang, X. D. "The application of principal component regression on simultaneous multicomponent determinations through a single catalytic kinetic run" *Talanta* **1995**, *42*, 205-210. ↙
- (92) Lupu, M.; Todor, D. "A singular-value decomposition based algorithm for multicomponent exponential fitting of NMR relaxation signals" *Chemometrics Intell. Lab. Syst.* **1995**, *29*, 11-17.
- (93) Meras, I. D.; Mansilla, A. E.; Lopez, F. S. "Simultaneous kinetic spectrophotometric determination of 2-furfuraldehyde and 5-hydroxymethyl-2-furfuraldehyde by application of a modified Winkler's method and partial least-squares calibration" *Analyst* **1995**, *120*, 2567-2571.
- (94) Wang, X. D.; Gu, Z. C. "Generalized-method for simultaneous multicomponent determinations through a single catalytic kinetic run by using the rate spectrum" *Analyst* **1995**, *120*, 1839-1842.
- (95) Blanco, M.; Coello, J.; Iturriaga, H.; Maspoch, S.; Redon, M.; Rodriguez, J. F. "Artificial neural networks and partial least-squares regression for second-order multicomponent kinetic determinations" *Quim. Anal.* **1996**, *15*, 266-275.
- (96) de la Guardia, M.; Khalaf, K. D.; Hasan, B. A.; Morales-Rubio, A.; Arias, J. J.; Garcia-Fraga, J. M.; Jimenez, A. I.; Jemenez, F. "Simultaneous kinetic spectrophotometric determination of five phenolic compounds by reaction with p-aminophenol, using partial least squares data treatment" *Analyst* **1996**, *121*, 1321-1326.
- (97) Khalaf, K. D.; MoralesRubio, A.; DelaGuardia, M.; Garcia, J. M.; Jimenez, F.; Arias, J. J. "Simultaneous kinetic determination of carbamate pesticides after derivatization with p-aminophenol by using partial least squares" *Microchem J.* **1996**, *53*, 461-471.
- (98) Lopez-Cueto, G.; Rodriguez-Medina, J. F.; Ubide, C. "Individual kinetic determinations using partial least squares calibration" *Analyst* **1997**, *122*, 519-523.
- (99) Xing, W. L.; He, X. W. "Kinetic determination of organic vapor mixtures with single piezoelectric quartz crystal sensor using artificial neural networks and partial least squares" *Chem. Lett.* **1996**, 1065-1066.

- (100) Xing, W. L.; He, X. W. "Kinetic determination of organic vapor mixtures with single piezoelectric quartz crystal sensor using artificial neural networks" *Talanta* **1997**, *44*, 959-965.
- (101) Blasco, F.; Medina-Hernandez, M. J.; Sagrado, S. "Use of pH gradients in continuous-flow systems and multivariate regression techniques applied to the determination of methionine and cysteine in pharmaceuticals" *Anal. Chim. Acta* **1997**, *348*, 151-159.
- (102) Blasco, F.; Medina-Hernandez, M. J.; Sagrado, S.; Fernandez, F. M. "Simultaneous spectrophotometric determination of calcium and magnesium in mineral waters by means of multivariate partial least-squares regression" *Analyst* **1997**, *122*, 639-643.
- (103) Sans, D.; Nomen, R.; Sempere, J. "Interactive self-modelling of chemical reaction systems using multivariate data analysis" *Comput. Chem. Eng.* **1997**, *21*, S631-S636.
- (104) Izquierdo, A.; Lopez-Cueto, G.; Medina, J. F. R.; Ubide, C. "Simultaneous determination of niobium and tantalum with 4-(2-pyridylazo) resorcinol using partial least squares regression and artificial neural networks" *Quim. Anal.* **1998**, *17*, 67-74.
- (105) Kappes, T.; Lopez-Cueto, G.; Rodriguez-Medina, J. F.; Ubide, C. "Improved selectivity in multicomponent determinations through interference modelling by applying partial least squares regression to kinetic profiles" *Analyst* **1998**, *123*, 2071-2077.
- (106) Peralta-Zamora, P.; Kunz, A.; Nagata, N.; Poppi, R. J. "Spectrophotometric determination of organic dye mixtures by using multivariate calibration" *Talanta* **1998**, *47*, 77-84.
- (107) Ventura, S.; Silva, M.; Perez-Bendito, D.; Hervas, C. "Multicomponent kinetic determinations using artificial neural networks" *Anal. Chem.* **1995**, *67*, 4458-4461.
- (108) Galvan, I. M.; Zaldivar, J. M.; Hernandez, H.; Molga, E. "The use of neural networks for fitting complex kinetic data" *Comput. Chem. Eng.* **1996**, *20*, 1451-1465.
- (109) Ventura, S.; Silva, M.; Perez-Bendito, D.; Hervas, C. "Estimation of parameters of kinetic compartmental models by use of computational neural networks" *J. Chem. Inf. Comput. Sci.* **1997**, *37*, 517-521.

- (110) Ventura, S.; Silva, M.; Perez-Bendito, D.; Hervas, C. "Computational neural networks in conjunction with principal component analysis for resolving highly nonlinear kinetics" *J. Chem. Inf. Comput. Sci.* **1997**, *37*, 287-291.
- (111) Xie, Y. L.; BaezaBaeza, J. J.; RamisRamos, G. "Second-order tensorial calibration for kinetic spectrophotometric determination" *Chemometrics Intell. Lab. Syst.* **1996**, *32*, 215-232.
- (112) Pettersson, A. K.; Karlberg, B. "Simultaneous determination of orthophosphate and arsenate based on multi-way spectroscopic-kinetic data evaluation" *Anal. Chim. Acta* **1997**, *354*, 241-248.
- (113) Xie, Y. L.; Baezabaeza, J. J.; RamisRamos, G. "Kinetic spectrophotometric resolution of binary-mixtures using 3-way partial least-squares" *Chemometrics Intell. Lab. Syst.* **1995**, *27*, 211-220.
- (114) Tauler, R.; Smilde, A. K.; Henshaw, J. M.; Burgess, L. W.; Kowalski, B. R. "Multicomponent determination of chlorinated hydrocarbons using a reaction-based chemical sensor .2. Chemical speciation using multivariate curve resolution" *Anal. Chem.* **1994**, *66*, 3337-3344.
- (115) Saurina, J.; Hernandez-Cassou, S.; Tauler, R.; Izquierdo-Ridorsa, A. "Multivariate resolution of rank-deficient spectrophotometric data from first-order kinetic decomposition reactions" *J. Chemometr.* **1998**, *12*, 183-203.
- (116) Saurina, J.; Hernandez-Cassou, S.; Tauler, R. "Multivariate curve resolution and trilinear decomposition methods in the analysis of stopped-flow kinetic data for binary amino acid mixtures" *Anal. Chem.* **1997**, *69*, 2329-2336.

## CHAPTER 2

### INSTRUMENT DESIGN AND CHARACTERIZATION

*Never worry about theory as long as the  
machinery does what it's supposed to do.*  
--Robert A. Heinlein

The data acquisition system used to collect the kinetic-spectrophotometric data discussed in this document consisted of a home-built stopped-flow apparatus<sup>1</sup> interfaced to a Tracor Northern (Model TN-6123) 512 element intensified diode array (Tracor Northern, Philadelphia, PA). Both the stopped-flow apparatus and the computerized interface between the stopped-flow and the diode array were modified for this research. These modifications and the subsequent characterization of the entire instrument are the subject of this chapter.

#### **2.1. DESIGN OF DIODE ARRAY INTERFACE**

A new computerized interface between the diode array and the stopped-flow was designed and constructed. This interface controls the diode array and is responsible for sending timing signals to the array and acquiring the array's output. The interface is composed of a peak track-and-hold circuit and a computer program that controls National Instruments LabPC+ and PC-TIO-10 data acquisition and timing boards.

A timing diagram describing the signals sent to and from the array is shown in Figure 2-1.

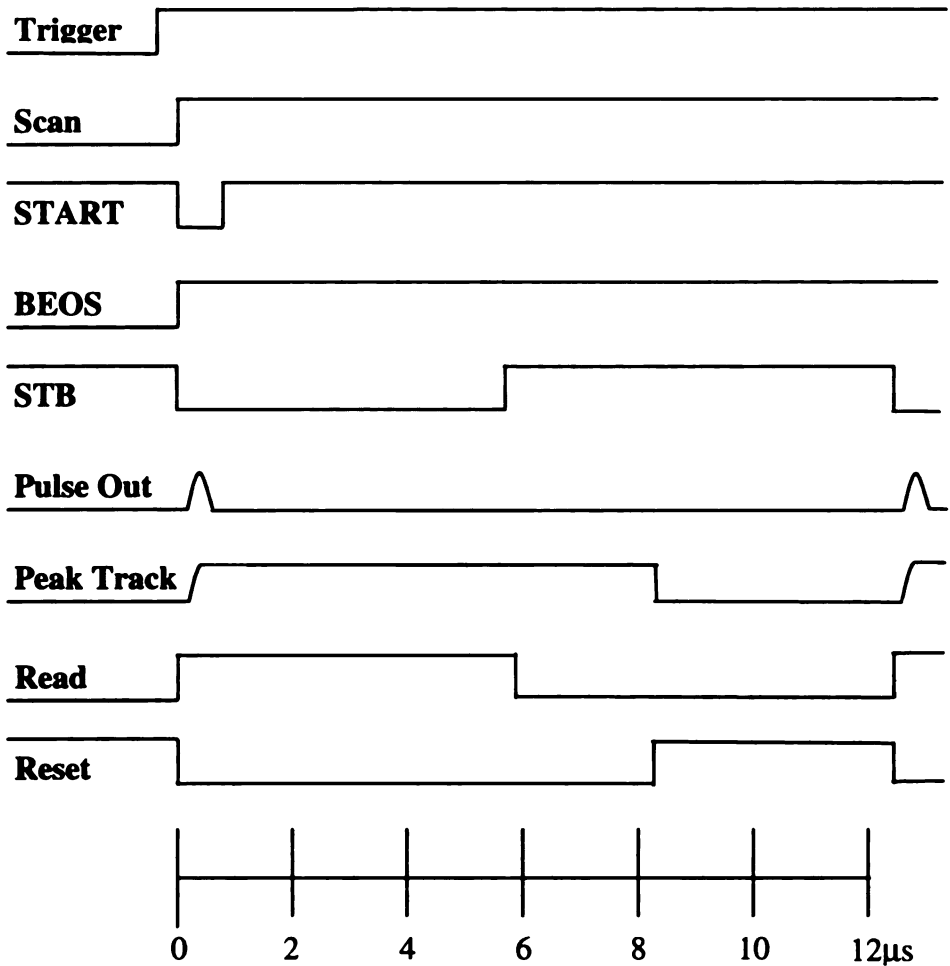


**Figure 2-1: Timing diagram of signals sent to and from the diode array.**

The **Trigger** signal is sent by an opto-interrupter circuit attached to the stopped-flow when a push has occurred and flow is stopped. When the computer sees **Trigger** go high, it sets **Scan** high. The length of time **Scan** stays high is determined by the length of the planned acquisition, i.e., on the number of scans required and on the scan frequency. **START** is gated off of **Scan**, and has a

frequency related to the desired scan rate. Upon receiving the **START** pulse, the diode array sets **BEOS** (Buffered End Of Scan) high. The **STB** (Scan Time Base) timing signal is gated off of **BEOS** and begins to send out pulses when **BEOS** goes high. The frequency of the **STB** pulses is related to the desired integration time for each diode. Each **STB** pulse results, after a short delay, in the appearance of a ~100ns pulse on the **Pulse Out** line. The pulses are the result of each diode's accumulated charge being converted into a voltage pulse in turn. The magnitude of a pulse is related to the number of photons that impacted its diode during the integration time. The **Peak Track** line is the output of a peak track-and-hold circuit which is described in detail later in this section. This circuit tracks the pulse to its maximum and then holds at that level until reset. Six microseconds after an **STB** pulse, the **Read** line goes low, triggering the computer's data acquisition board to initiate an acquisition of the **Peak Track** line. After a short delay, the **Reset** signal goes low and resets the peak track-and-hold circuit into tracking mode. Both the **Read** and the **Reset** signals are initialized by the **START** pulse.

In reality, each scan of the array requires two **START** pulses and two **STB** pulse trains. The first "scan" is not read into memory, but is merely used to clear the array. The **STB** frequency is used to control the period between the clearing and reading of each diode.

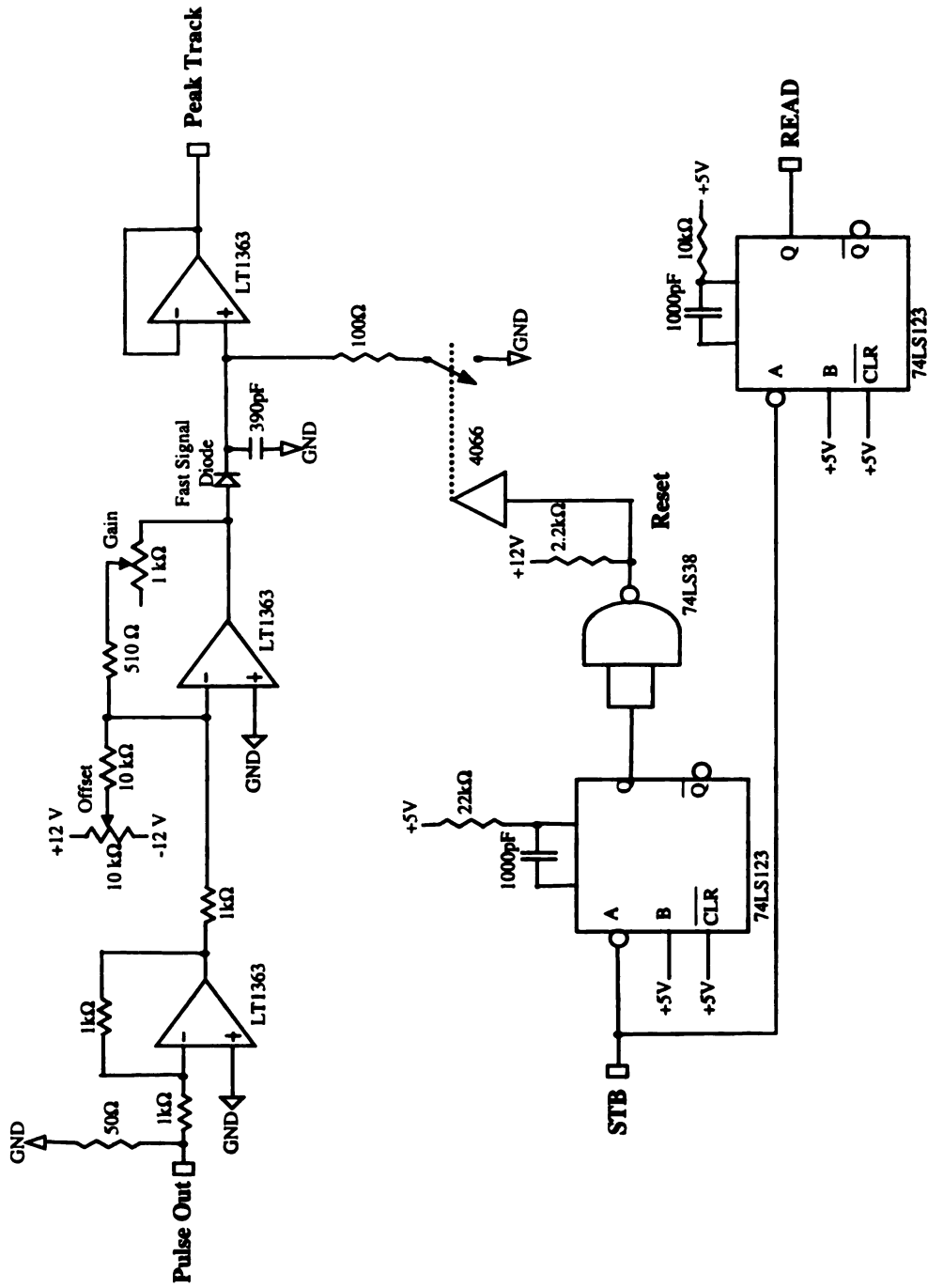


**Figure 2-2: Schematic diagram of the peak track-and-hold circuit.  $\pm 12\text{V}$  power connections to the LT1363 operational amplifiers and  $+5\text{V}$  power connections to the 74LS123 monostable multivibrators are omitted in the interest of clarity.**

Figure 2-2 is a schematic of the peak track-and-hold circuit. The **Pulse Out** signal is inverted by an inverting amplifier. The second op amp has gain and inverts the signal again. The track-and-hold functionality is provided by a fast signal diode, the third op amp, and a high quality capacitor. The capacitor charges as the rising edge of a pulse comes down the **Pulse Out** line. As the pulse hits its maximum and begins to fall, the diode prevents the capacitor from discharging. The input impedance of the voltage follower immediately after the capacitor prevents discharge in that direction. The capacitor thus charges while a pulse is rising and holds at the peak value after the pulse begins to fall. The capacitor is discharged by closing a switch that provides a low resistance path to ground. The switch is closed by a high on the **Reset** line. **Reset** is the output of a monostable multivibrator that clocks off of the **STB** pulse train. Shortly before the **Reset** goes high, a second monostable causes **Read** to go low, triggering the computer's data acquisition board to initiate a sample-and-hold operation on the **Peak Track** signal.

The LT1363 operational amplifiers used for the inverting amplifier, the inverting amplifier with gain, and the voltage follower are 70 MHz amplifiers with slew rates of  $1000\text{V}/\mu\text{s}$  in order to be able to respond to the very short duration pulses on the **Pulse Out** signal. The switching is done with a 4066 high speed quad bilateral switch.



## 2.2. REDESIGN OF STOPPED-FLOW OBSERVATION CELL AND OPTICS

The optical path of the stopped-flow apparatus begins with a fiber optic bundle carrying light from a tungsten lamp to the observation cell. The light passes through the observation cell, where some is absorbed by the sample, and is collected by a second fiber optic bundle which carries it to the diode array detector.

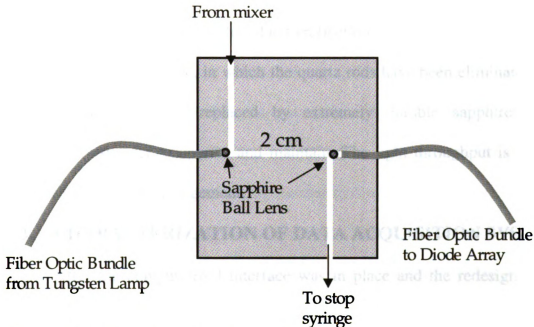


**Figure 2-3: Schematic of the observation cell.**

As seen in Figure 2-3, the fiber optic bundles are inserted into the block containing the observation cell and are butted against spherical sapphire ball lenses. These lenses are fitted against the openings at the ends of the observation cell and serve

both to seal the cell and to collimate and collect the light passed through the observation cell. They are held in place by custom-designed Delrin screws.

In previous incarnations of the instrument, the fiber optic bundles did not extend into the block itself. Rather, a three centimeter quartz rod was inserted into the block and butted against a flat window. The rod was screwed into place with sufficient pressure to force the window to seal the cell. The fiber optics were touched to the quartz rod. Thus, the light had to pass from the fiber optic bundle, through the rod, through the window, and into the cell. This resulted in several interfaces where light could be lost due to reflection.

The current scheme, in which the quartz rods have been eliminated and the fragile quartz windows replaced by extremely durable sapphire balls, is significantly simpler to operate and maintain. The light throughput is at least as good as the previous arrangement.

## **2.3. CHARACTERIZATION OF DATA ACQUISITION SYSTEM**

After the computerized interface was in place and the redesigned optical path had been implemented, a detailed characterization study of the instrument as a whole was performed. The delay time and maximum scan rate were determined. The mixing time was not determined for reasons discussed below. The signal-to-noise ratio of the instrument was measured, and the linear range was found.

### **2.3.1. Determination of Delay Time and Maximum Acquisition Rate**

Literature procedures<sup>2</sup> were used in an attempt to determine the dead and mixing times of the instrument. An attempt was made to experimentally determine

the dead time of the stopped flow by observing the reaction of iron (III) with thiocyanate to form a colored product<sup>2</sup>. Due to instrumental and electronic limitations, the dead time was not determined; rather another parameter we shall call the delay time was calculated by extrapolating the reaction curve back to the initial absorbance of the reactant mixture. Delay time, then, is defined as the time for which the reactants are mixing in the observation cell but are unobserved, i.e., the time between the mixing of the sample and reagent and the collection of the first data point.

If the first data point is defined to be acquired at time zero, the delay time is the negative of the time at which the extrapolated reaction curve reaches the absorbance of the reactants. For this system, the delay time was determined to be 75 ms. Previous work using this same stopped-flow apparatus<sup>1</sup> had found the dead time of the stopped-flow itself be approximately 5 ms. The difference between the two values can be attributed to several factors. Those that contribute most to the difference are the delay between stoppage of flow and the triggering of the opto-interrupter circuit, the delay between the arrival of the **Trigger** signal and the generation of the first **START** pulse, and the need for one complete scan of all 512 diodes (to clear the array) before any data can be acquired.

The mixing time of the stopped-flow apparatus was not accurately determined because it was shorter than the delay time of the instrument as a whole, and so not measurable using the experimental setup used for the other experiments.

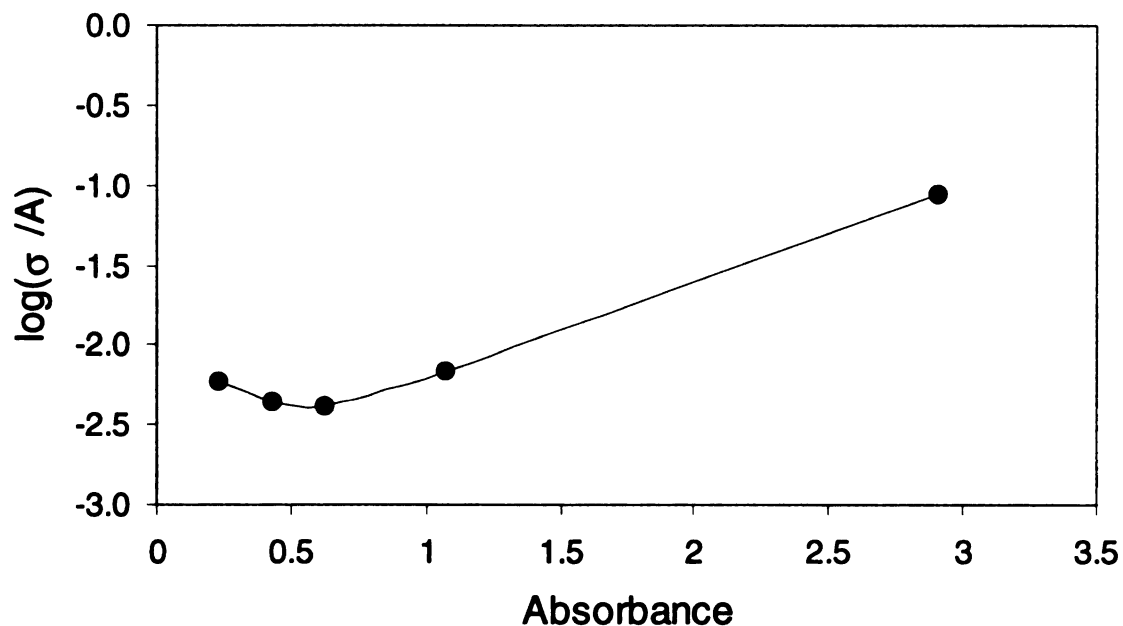
The maximum rate at which spectra could be collected was determined, and found to be a function of the desired integration time. The integration time determines the frequency of the **STB** pulse train, and therefore the length of time necessary to complete one full scan of the array. Due to the maximum **STB** frequency (80 kHz) supported by the track-and-hold circuit and the lag between the end of the clearing scan of the array and the beginning of the data acquisition scan (determined in part by the speed of the PC running the interface program, in our case a 33 MHz 486SX), the minimum practical integration time is 13 ms. At this minimum integration time spectra can be acquired at 10.5 Hz. Many studies described in this work were performed with 35 ms integration times. At that integration time, 5.5 spectra can be acquired per second..

### **2.3.2. Determination of signal/noise ratio**

The signal/noise ratio (S/N) for each wavelength was measured as the range of recorded intensity measurements for a series of spectra acquired from a static system. The average S/N was computed as the average of the S/Ns of all wavelengths between 500 and 700 nm (the range used in these experiments). These S/N measurements were carried out under a variety of circumstances. The S/N was found to be a function of percent of the radiation transmitted through the observation cell, intensifier gain, and integration time.

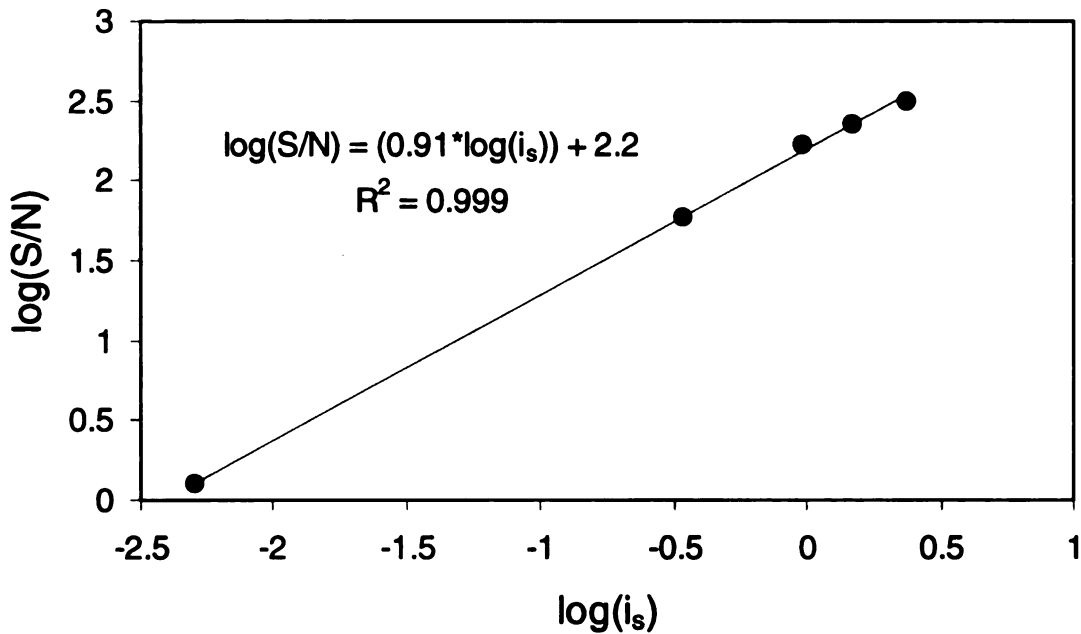
The dark noise (the range of intensities measured when no light impinges on the array) is a major source of noise. Accordingly, attempts were made to minimize it by cooling the array. A Peltier thermoelectric cooler was used to bring

the array temperature to  $-5.9^{\circ}\text{C}$ . The cooler decreased the dark signal by only 2%, but decreased the amplitude of the dark noise by 30%. For all measurements, the average dark signal at each wavelength was removed in a background subtraction step.



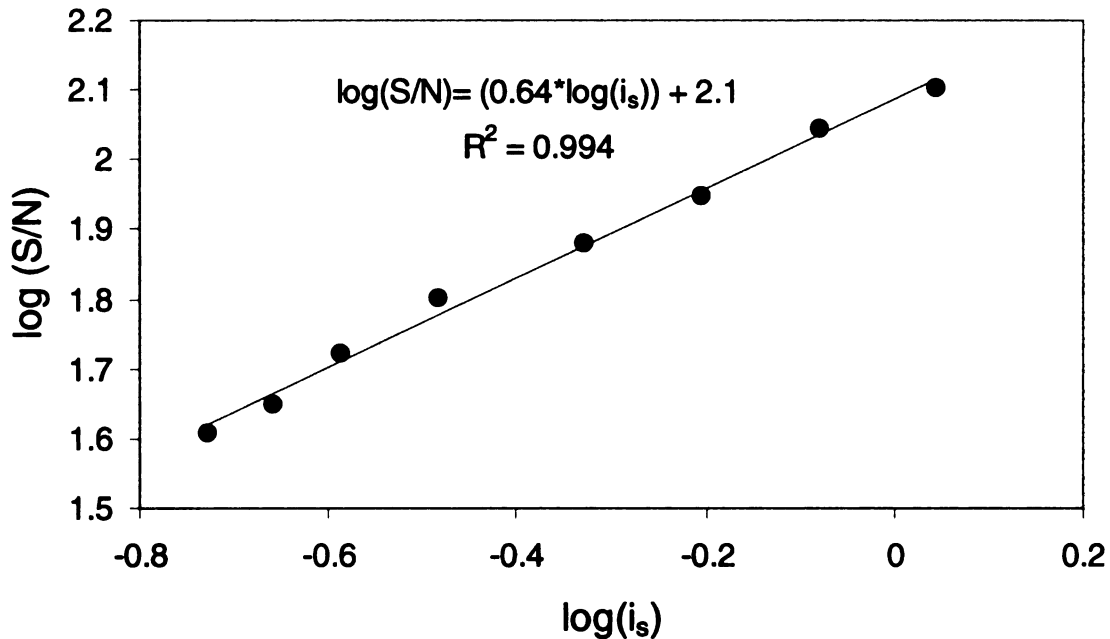
**Figure 2-4: Plot showing dependence of relative error in absorbance to absorbance.**

Figure 2-4 shows the relationship between absorbance (in this case the absorber was a neutral density filter that attenuates the light) and the relative error in absorbance. As is expected,  $\log(\sigma_A/A)$  goes through a minimum at an absorbance of  $\sim 0.5$ . It can also be seen that  $\log(\sigma_A/A)$  is fairly constant between absorbances of 0.2 and 1.0. For this reason all experiments were run under conditions where no absorbances greater than 1.0 were measured.



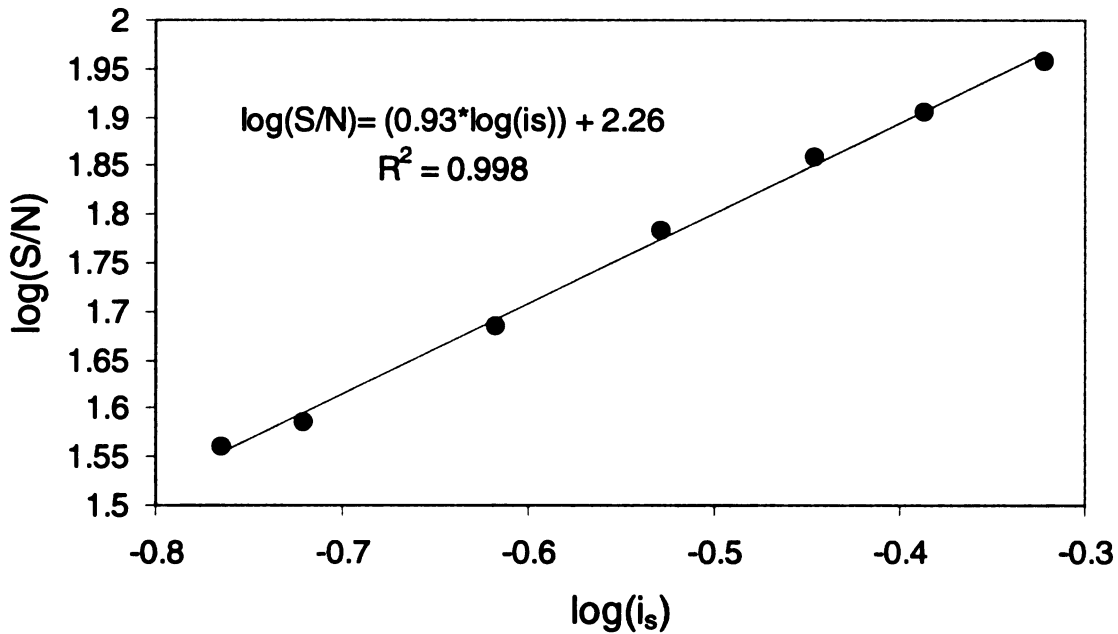
**Figure 2-5: Dependence of S/N on absorbance.**

Figure 2-5 shows a linear relationship between the logarithm of the signal to noise ratio and the logarithm of the measured signal ( $i_s$ ), where the signal level was varied by varying the light intensity. The different measured intensities are due to the attenuation of the light with a series of neutral density filters. The measured slope was 0.91. For a shot noise limited system a slope of 0.5 is anticipated; when blank noise dominates a slope of unity is expected<sup>3</sup>. It can thus be inferred that the measurement is not shot noise limited, but over this region a mixture of shot noise and blank noise predominates. We can speculate that blank noise is dominant at the low end of the region and shot noise is dominant when light levels are at the high end of the region shown in Figure 2-5<sup>3</sup>.



**Figure 2-6: Dependence of S/N on intensifier gain.**

Figure 2-6 shows a linear relationship between the logarithm of the signal to noise ratio and the logarithm of the measured signal ( $i_s$ ) where the measured signal was varied by changing the intensifier gain at a constant integration time (13 ms, the minimum integration time) and constant light intensity. As gain increases, so does the measured signal amplitude. At this minimum integration time, the slope of the linear plot is 0.64. Blank noise contributes less and the system is more nearly shot noise limited when intensifier gain is increased.



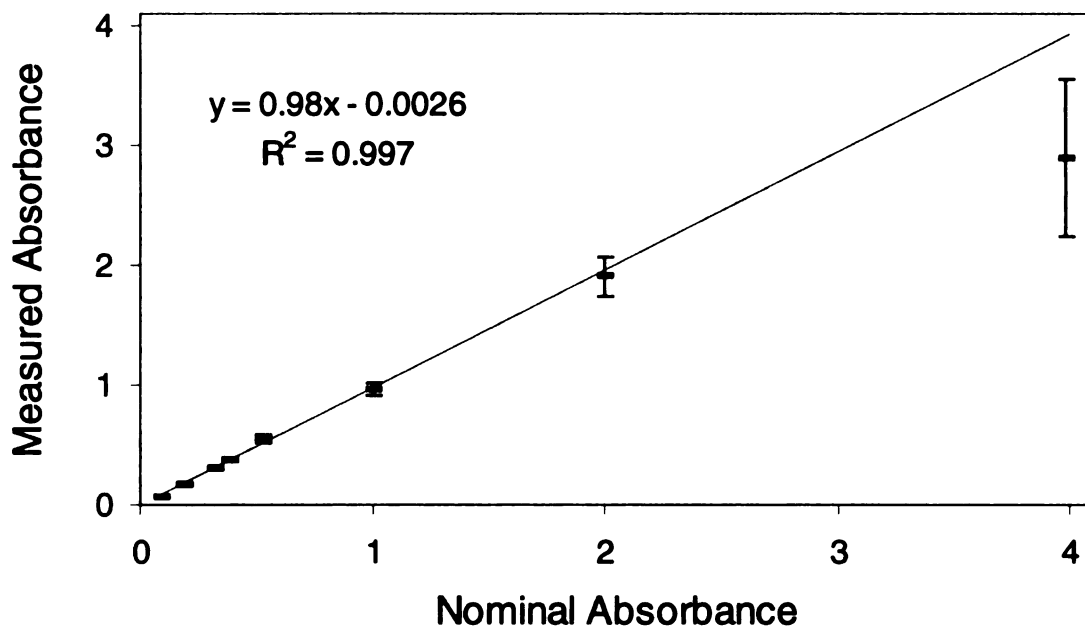
**Figure 2-7: Dependence of S/N on integration time.**

Figure 2-7 shows the relationship between the logarithm of the signal to noise ratio and the logarithm of the measured signal ( $i_s$ ) where the measured signal is a function of integration time at a constant intensifier gain (0.2, a very low gain) and constant light intensity. As integration time increases, so does the signal. Here the measured slope is close (0.93) to unity. At low gains blank noise is important.

### **2.3.3. Determination of linear range**

The range over which absorbance measurements are linearly related to the absorption properties of samples in the optical path was determined in two ways. First, a series of neutral density filters with known absorbances across a broad region of the spectrum were inserted into the optical path. Absorbance as measured by the diode array at all wavelengths between 500 and 700 nm was compared to the known absorbance of the filters.





**Figure 2-8: Linearity of measured absorbance with the known absorbance of a series of neutral density filters. The linear regression shown was calculated from all absorbances up to and including one absorbance unit.**

As shown in Figure 2-8, the array shows linearity for absorbances at least up to one absorbance unit. Above this point stray light causes a negative deviation from Beers law. As a second check of linearity, a series of chromium (III) solutions were passed through the observation cell of the stopped-flow and their spectra recorded. A calibration plot of absorbance at 569 nm versus concentration was generated and found to be linear to absorbances of greater than 1.50 (the absorbance of the solution with the highest concentration).

## 2.4. REFERENCES

- (1) Beckwith, P. M.; Crouch, S. R. "An automated stopped-flow spectrophotometer with digital sequencing for millisecond analyses" *Anal. Chem.* **1972**, *44*, 221-227.
- (2) Stewart, J. E. "Flow deadtime in stopped-flow measurements" *Dionex Application Notes* , 1-4.
- (3) Ingle, J. D., Jr.; Crouch, S. R. *Spectrochemical Analysis* ; Prentice Hall: Englewood Cliffs, NJ, 1988.

## CHAPTER 3

### INITIAL SIMULATION STUDIES:

#### STUDY OF THE EFFECT OF EXPERIMENTAL VARIABLES

*The sciences do not try to explain, they hardly even try to interpret, they mainly make models. By a model is meant a mathematical construct which, with the addition of certain verbal instructions, describes observed phenomena. The justification of such a mathematical construct is solely and precisely that it is expected to work.*

--John Von Neumann

*I do not fear computers. I fear the lack of them.*

--Isaac Asimov

In order to understand the factors that limit the accuracy with which an analyte can be determined in a sample using kinetic-spectrophotometric data, a systematic study of the effect of an array of experimental parameters on the accuracy of a kinetic-spectrophotometric determination was performed. Because of the impracticality of performing the number of experiments needed to complete the study, simulated experiments were used. In these simulations experimental parameters were varied and the effect of these variations on the accuracy of a multicomponent (in this case, a two-component) kinetic-spectrophotometric determination was noted.

### **3.1. EXPERIMENTAL**

#### **3.1.1. Generation of Simulated Data**

Multicomponent kinetic-spectrophotometric data were simulated using a program written in MATLAB (The Math Works, Natick, Mass.). The algorithm generates kinetic profiles for parallel second order reactions (first order in analyte and first order in reagent) by numerically solving the appropriate differential equations. The program *mulgen\_a* which was used for this purpose is given in the appendix.

For most of the simulation studies, synthetic spectra and rate constants were used to generate kinetic-spectrophotometric data. The absorbance data were generated by assuming that the analytes and reagent do not absorb in the spectral region of interest and that the absorption spectra of the reaction products can be modeled as overlapped Gaussian-shaped profiles. These synthetic spectra are shown later in this chapter.

In all cases, adherence to Beer's law was presumed for each component, and the total absorbance at each wavelength was assumed to be the sum of the absorbances of the components.

#### **3.1.2. Data processing**

Time dependent spectra were collected in triplicate and averaged, i.e., each metal ion solution was reacted with PAR three times. The resulting three sets of kinetic-spectrophotometric data were averaged. Data were mean-centered (i.e., the mean of each variable vector was subtracted from each of its elements) before being

input to the appropriate algorithms. Multivariate calibration algorithms provided in the PLS\_TOOLBOX (Eigenvector Technologies, Manson, WA.) and run in MATLAB were used to perform determinations.

### **3.2. METHODS FOR QUANTIFYING KINETIC AND SPECTRAL DIFFERENCES FOR TWO COMPONENTS**

In a kinetic-spectrophotometric determination, the accuracy with which an analyte can be determined in unknown samples depends on the degree of kinetic and spectral differentiation between the analyte and the other components of the sample. In order to examine the effect of an array of experimental parameters on both degree of kinetic and spectral differentiation and on the accuracy of a kinetic-spectrophotometric determination, it was necessary to develop means for quantifying the degree of kinetic and spectral differentiation between the analytes in a mixture.

#### **3.2.1. Methods for quantifying kinetic differences**

In the following discussion, and indeed in most of this document, it is assumed that in kinetic or kinetic-spectrophotometric determinations analytes react with a common reagent to form different products at different rates. The plot of concentration of product vs. time (or of absorbance vs. time, if either the analyte or its product absorbs in the wavelength region of interest) is referred to as a kinetic profile.

The amount of kinetic differentiation between two components can be described by the ratio of the rate constants for the reactions of the analytes with the reagent. As the ratio of the rate constants increases, so does the difference between the rate constants and thus the difference in the kinetic profiles of the reactions of the analytes.

The angle ( $\theta_K$ ) between the kinetic profiles of the two reaction products was used as a measure of the degree of kinetic differentiation between the analytes, and was calculated as the arccosine of the correlation between the kinetic concentration profiles of the reaction products.

$$\theta_K = \arccos\left(\frac{\sigma_{K_1 K_2}}{\sigma_{K_1} \cdot \sigma_{K_2}}\right)$$

where  $K_1$  and  $K_2$  are the two kinetic profiles,  $\sigma_{K_1}$  and  $\sigma_{K_2}$  are their standard deviations, and  $\sigma_{K_1 K_2}$  is the covariance of  $K_1$  and  $K_2$ . A kinetic angle of  $0^\circ$  indicates that the kinetic profiles are completely correlated, while an angle of  $90^\circ$  indicates complete independence. Practically, as the kinetic angle decreases, the degree of kinetic differentiation decreases and so does the amount of kinetic information that can be used to differentiate the analytes.

The calculation of figures of merit for multivariate data has been described<sup>1-3</sup>. Using these methods, which state that the net analyte signal for the  $k$ th analyte in a mixture can be calculated as the portion of the data orthogonal to the data due to all of the other components of the mixture, net analyte signal and

selectivity can be easily calculated from the mixture data if the pure component response of the components of the mixture are known:

$$\mathbf{v} = (\mathbf{I} - \mathbf{X}\mathbf{X}^+) \mathbf{u}$$

where  $\mathbf{v}$  is the portion of data vector (pure component response)  $\mathbf{u}$  that is orthogonal to data matrix  $\mathbf{X}$  (which consists of the pure component responses of all of the other components), and  $\mathbf{X}^+$  is the pseudoinverse of  $\mathbf{X}$ . The norm of  $\mathbf{v}$ ,  $\|\mathbf{v}\|$ , is the net analyte signal of the analyte. The selectivity,  $s$ , is calculated as the ratio of the norms of the orthogonal part of the pure component response and the pure component response,

$$s = \frac{\|\mathbf{v}\|}{\|\mathbf{u}\|}$$

The kinetic net analyte signal and kinetic selectivity for each analyte were calculated from the concentration kinetic profile for the analyte and the sum of the concentration kinetic profiles of all components of the mixture.

The rate constant ratio is a measure of the similarity of the reaction rates, and is insensitive to factors other than the rate constant which affect the kinetic profile. The kinetic angle is sensitive to factors other than the rate constant; indeed the length of time for which the reaction is observed has a large effect on the kinetic angle. A plot of kinetic angle vs. rate constant ratio (with other factors that contribute to the kinetic angle held constant) is shown in Figure 3-1.

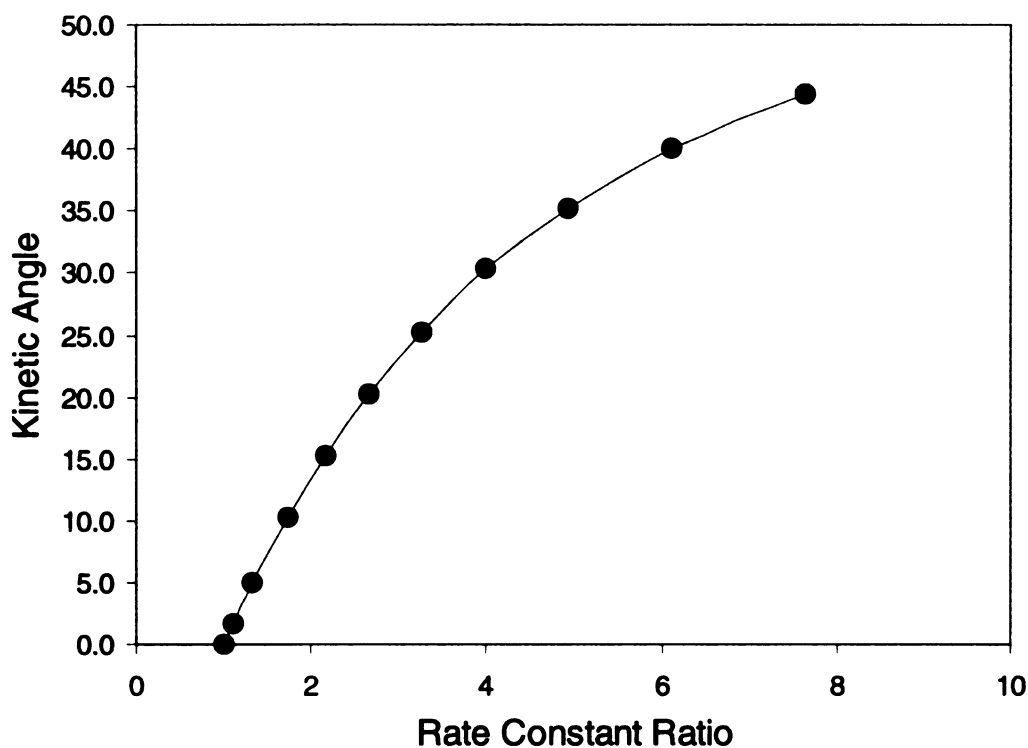


**Figure 3-1: Kinetic angle as a function of rate constant ratio. The fraction of the slower reaction observed was held constant at 90%, and the number of data points was held at 100.**

Neither the rate constant ratio nor the kinetic angle provide information about which analyte is more resolved. The kinetic net analyte signal does provide this information. For the case where the rate constant ratio is varied (by varying the faster rate constant) and the length of time the reaction is observed is held constant (at the time at which the slower reaction has reached 90% completion), the plot of kinetic net analyte signal vs. rate constant ratio is as shown in Figure 3-2.



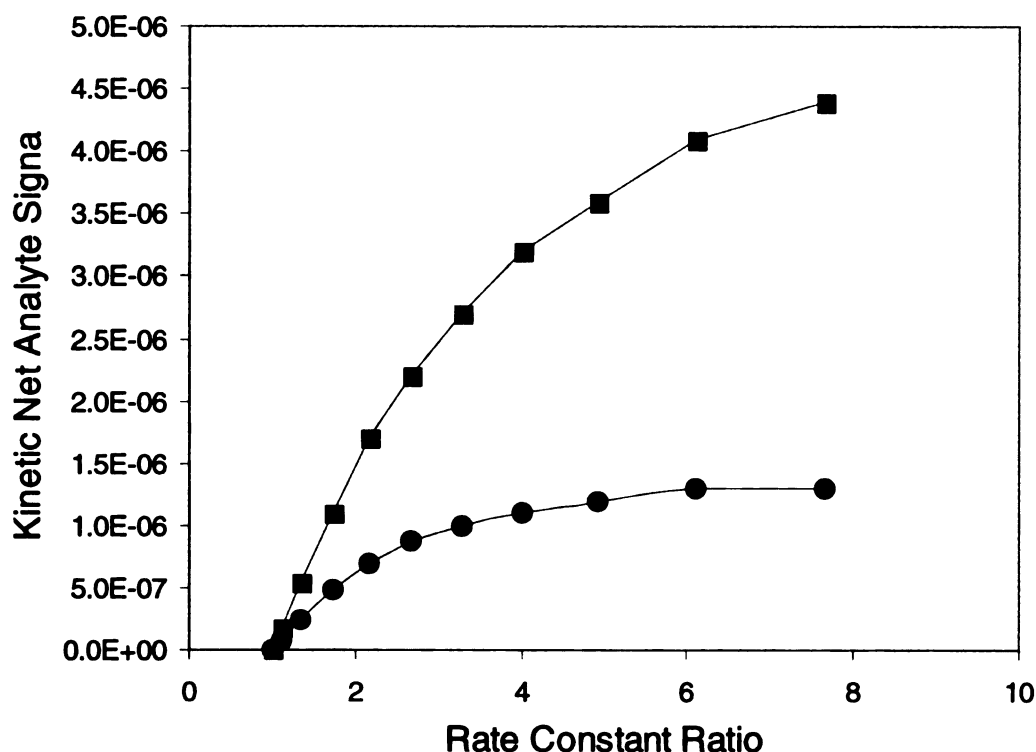


**Figure 3-2: Kinetic net analyte signal for the slower (squares) and the faster (circles) reactants in a two-component mixture. The fraction of the slower reaction observed was held constant at 90%, and the number of data points was held at 100.**

More information is available for the slower analyte than the faster analyte. The analytical signal of the slower component is larger than that of the faster component since it reaches a higher equilibrium concentration. When all other variables are equal and the concentration sets shown later in Figure 3-3 are used, the slower analyte can be more accurately determined than the faster analyte because of its higher net analyte signal.

### 3.2.2. Methods for quantifying spectral differences

The degree of spectral overlap (or more precisely, the amount of spectral differentiation) between the analytes was quantified by calculating the angle between the two spectra. This angle, referred to in this work as the spectral angle ( $\theta_S$ ), is defined as the arccosine of the correlation between the spectra (represented by their respective molar absorptivities ( $\epsilon_\lambda$ )) so that the spectral angle is independent of concentration, and so therefore also of time):

$$\theta_S = \arccos\left(\frac{\sigma_{S_1 S_2}}{\sigma_{S_1} \cdot \sigma_{S_2}}\right)$$

where  $S_1$  and  $S_2$  are the two spectral profiles,  $\sigma_{S_1}$  and  $\sigma_{S_2}$  are their standard deviations, and  $\sigma_{S_1 S_2}$  is the covariance of  $S_1$  and  $S_2$ . A spectral angle of  $0^\circ$  indicates that the spectra are completely correlated, while an angle of  $90^\circ$  indicates complete independence. Practically, as the spectral angle decreases, the degree of spectral differentiation decreases and so does the amount of spectral information that can be used to differentiate the analytes. The synthetic spectra used in the simulations are shown with their spectral angles in Figure 3-3.

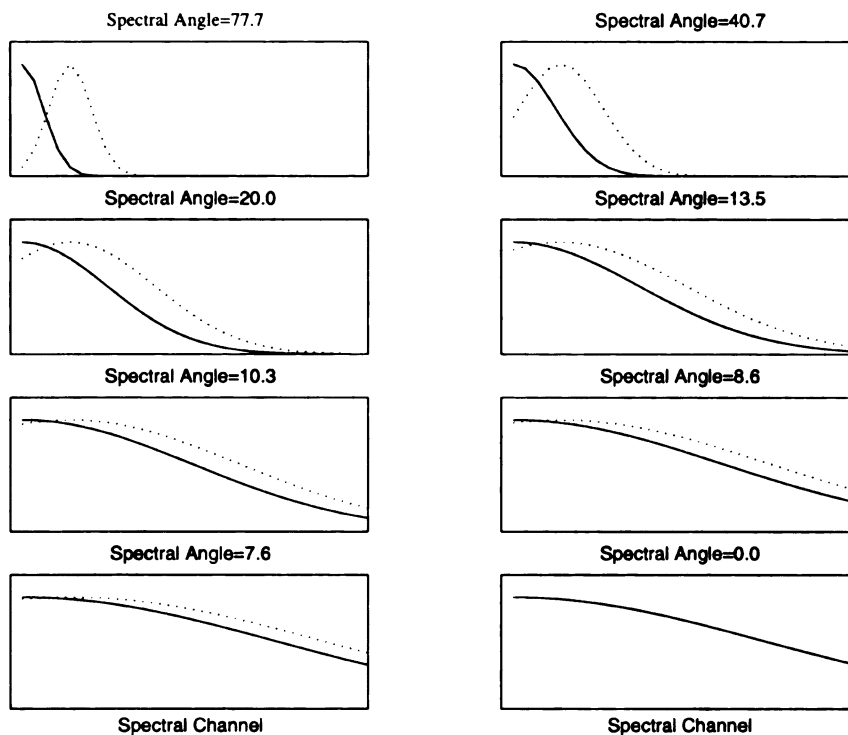


**Figure 3-3: Synthetic spectra used for simulation studies. Spectral angles range between 77.7 and 0.**

A spectral net analyte signal can be calculated in a manner similar to the method for calculating the kinetic net analyte signal. It, like the kinetic net analyte signal, has the advantage of providing information that reveals which analyte is more resolved, and so should be more accurately determined. Figure 3-4, the spectral net analyte signal for each analyte is plotted vs. the spectral analytes between the analytes. The dashed line corresponds to the analyte whose spectrum is depicted with a dashed line in Figure 3-3.

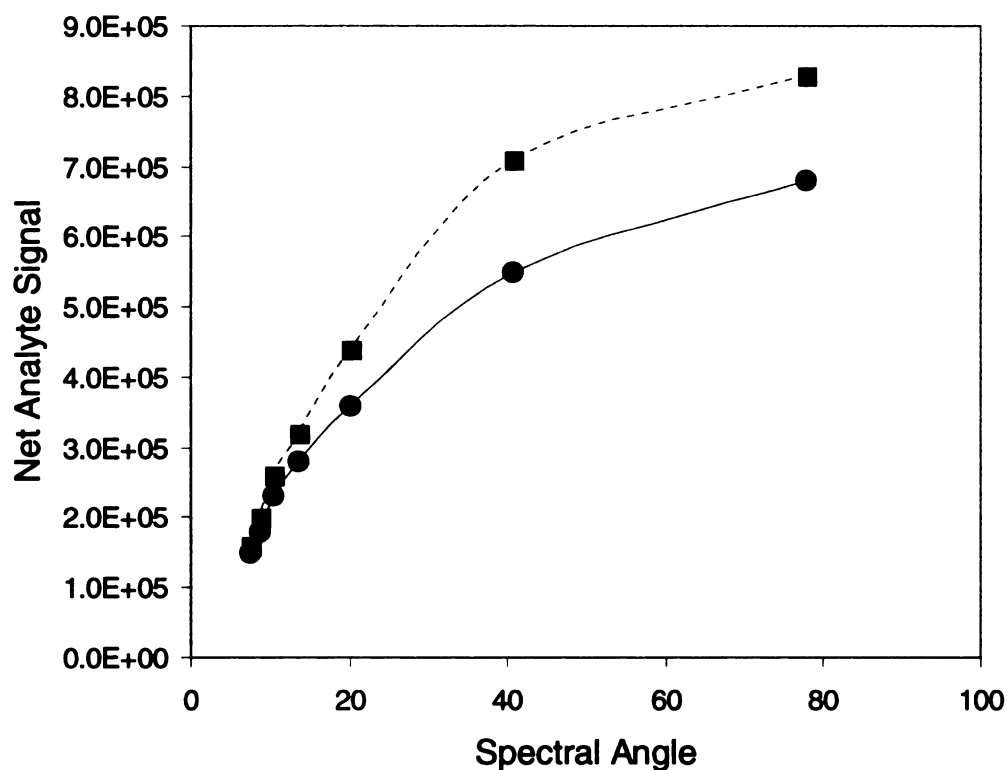


**Figure 3-4: Spectral net analyte signal as a function of spectral angle. The spectra used to generate this plot are shown in Figure 3-3.**

The more strongly absorbing analyte (depicted with the dashed line) has a higher net analyte signal. As the spectra become more similar, the difference between the net analyte signals decreases as well. We would thus expect the more strongly absorbing analyte to be determined with greater accuracy.

### **3.3. EFFECT OF EXPERIMENTAL VARIABLES**

Data were generated for a collection of 12 standard calibration mixtures and four unknown mixtures. The arrangement of these mixtures in the concentration space of the two analytes is shown below. In all cases, the simulated data were

generated using 30 spectral channels (wavelengths); in most cases 100 time points were generated (unless the number of time points was being varied).

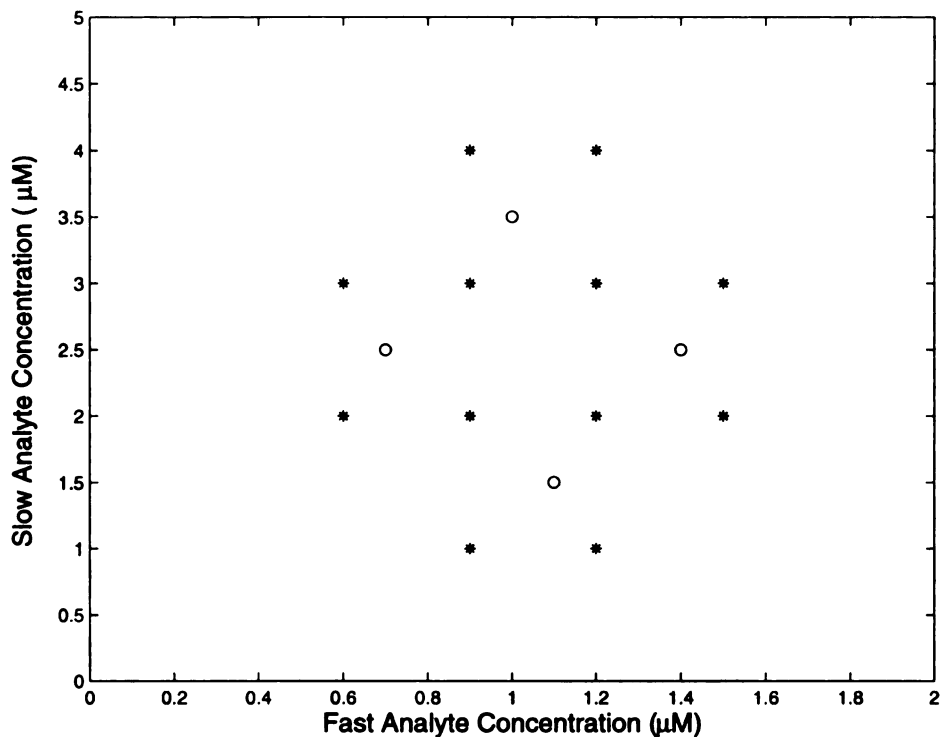


**Figure 3-5: Concentrations of calibration (stars) and unknown (open circles) samples.**

These data were used to generate calibration models with each of the multivariate calibration techniques being investigated. These models were applied to data from the four unknown mixtures, and the error of prediction for each analyte was calculated as the relative standard error of prediction (RSEP)

$$\% \text{ RSEP} = \sqrt{\frac{\sum_{i=1}^h (C_i - \hat{C}_i)^2}{\sum_{i=1}^h C_i^2}} \cdot 100$$

where  $C_i$  is the true concentration of the analyte in sample  $i$ ,  $\hat{C}_i$  is the predicted concentration of the analyte in sample  $i$ , and  $h$  is the number of samples.

### 3.3.1. Effect of kinetic and spectral angles

The kinetic resolution of the analytes was varied by changing the rate constant of the slower analyte and by varying the nearness to completion of the slower reacting analyte at the end of data collection (fraction of the reaction observed). These two experimental parameters were found to influence the accuracy of the determinations through their influence on the kinetic angle, and so on the amount of kinetic differentiation observed between the analytes.

In all cases, the slower analyte was more accurately determined. Examining the kinetic net analyte signal (Figure 3-2) reveals that this is expected. The slower reacting analyte was also the more strongly absorbing analyte, and so it has a higher spectral net analyte signal.

For all cases studied, principal component regression and partial least squares regression produced predicted concentrations of similar accuracy. Determinations using continuum regression were slightly more accurate. In every case, multiple linear regression produced inferior predictions. PARAFAC generally produced poor predictions, and multiway PLS (nPLS) in most cases produced the most accurate predictions. The following plots illustrate the accuracy

of the predicted concentrations produced by each algorithm (expressed as the %RSEP) as a function of kinetic and spectral angles.

Figures 3-6 through 3-9 shows the effect of varying kinetic and spectral angles on the accuracy of a PLS, PCR, CR, and nPLS prediction, respectively. PLS, PCR and CR all behave similarly. The accuracy of the nPLS prediction is generally higher, but has the same dependence on the kinetic and spectral angles as do the PLS, PCR and CR determinations.

The accuracy with which the faster analyte can be predicted decreases as the spectral angle decreases. The slower analyte is mostly unaffected by a decrease in spectral angle. At any given kinetic angle, the slower analyte has a larger kinetic net analyte signal (Figure 3-2) and so its prediction is less affected by a decrease in spectral differentiation because it can rely more on kinetic information than can the prediction of the faster analyte. Changes in the kinetic angle have little effect at all but the lowest spectral angles, revealing that the regression algorithms rely more heavily on spectral than kinetic differences. At very low spectral angles ( $<10^\circ$ ), the amount of spectral information available becomes negligibly small, and the prediction of both analytes depend on the kinetic information. In this case decreasing kinetic angle produces marked increases in the error of both predictions. The error of the prediction of the faster analyte increases more quickly since less kinetic information about it is available. At very low spectral and kinetic angles an accurate determination can not be performed.

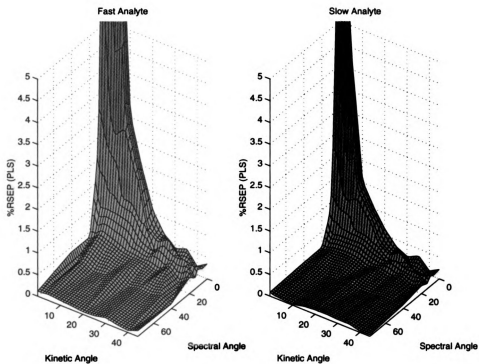


**Figure 3-6: Relative standard error of a PLS prediction as a function of the kinetic and spectral angles.**

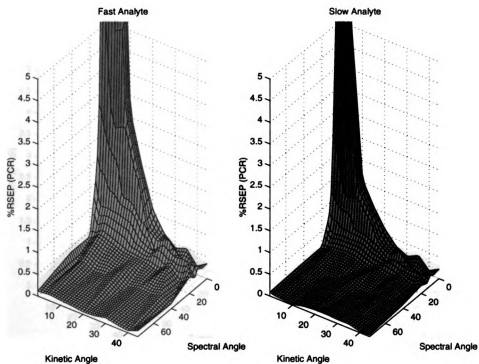


**Figure 3-7: Relative standard error of a PCR prediction as a function of the kinetic and spectral angles.**



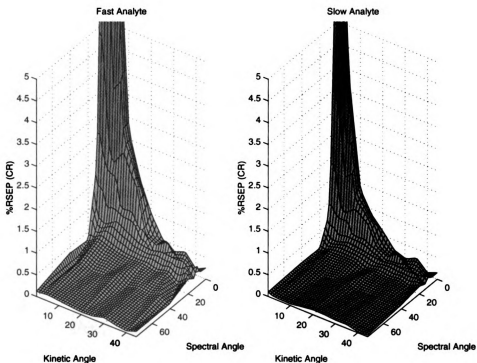


**Figure 3-8: Relative standard error of a CR prediction as a function of the kinetic and spectral angles.**

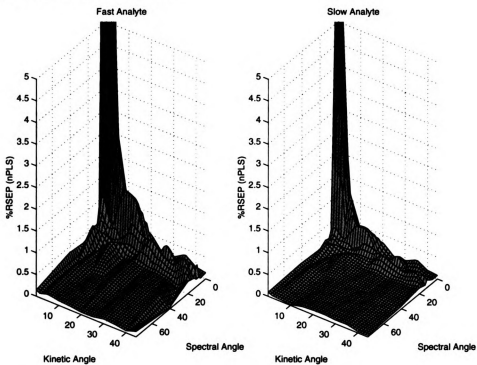


**Figure 3-9: Relative standard error of an nPLS prediction as a function of the kinetic and spectral angles.**

The effects of varying kinetic and spectral angles on an MLR determination are shown in Figure 3-10. The same general trends observed for PLS, PCR, CR, and nPLS can be seen here as well, though the magnitude of the errors is much larger.

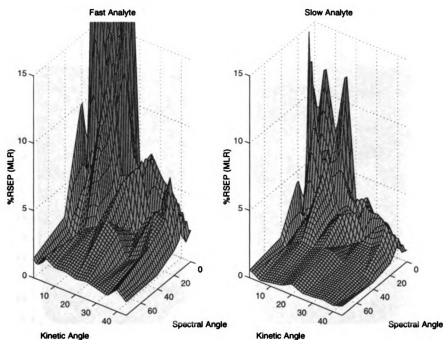


**Figure 3-10: Relative standard error of an MLR prediction as a function of the kinetic and spectral angles.**

Figure 3-11 shows the effect of varying kinetic and spectral angles on the accuracy of a PARAFAC determination. At kinetic or spectral angles of less than  $10^\circ$  neither analyte can be accurately determined, though when both angles are high the accuracy of the predictions rivals that of CR and nPLS. PARAFAC's flaw, then, is its need for resolution in both, rather than one, dimension.

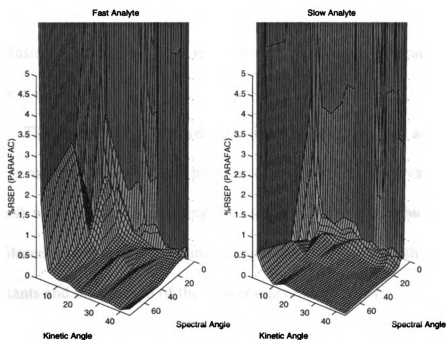


**Figure 3-11: Relative standard error of a PARAFAC prediction as a function of the kinetic and spectral angles.**

In the following sections, the results shown will be those produced by continuum regression and multiway partial least squares regression.

### **3.3.1.1. Contributors to kinetic angle**

The effect of decreasing kinetic information is not evenly distributed over the two analytes. As already mentioned and seen in Figures 3-6 to 3-11, the

prediction of the faster-reacting of the two components is affected to a much larger degree than is the prediction of the slower-reacting analyte. Using CR or nPLS (the techniques to which it can be assumed that most assertions in the next several sections refer) the slower-reacting analyte can be successfully determined in a two-component mixture if either angle is greater than  $8^\circ$ ; the faster-reacting component requires that at least one angle be  $15^\circ$  for a determination to succeed. The faster component is also more sensitive to small spectral angles than is the slower component.

The fraction of the slowest reaction observed (defined as the fraction of the slower analyte molecules that have reacted at the time observation of the reaction ceases) was changed by varying the length of time over which the reaction was monitored. It was found that kinetic angle is a function of both the ratio of the rate constants and the fraction of the slower reaction observed.

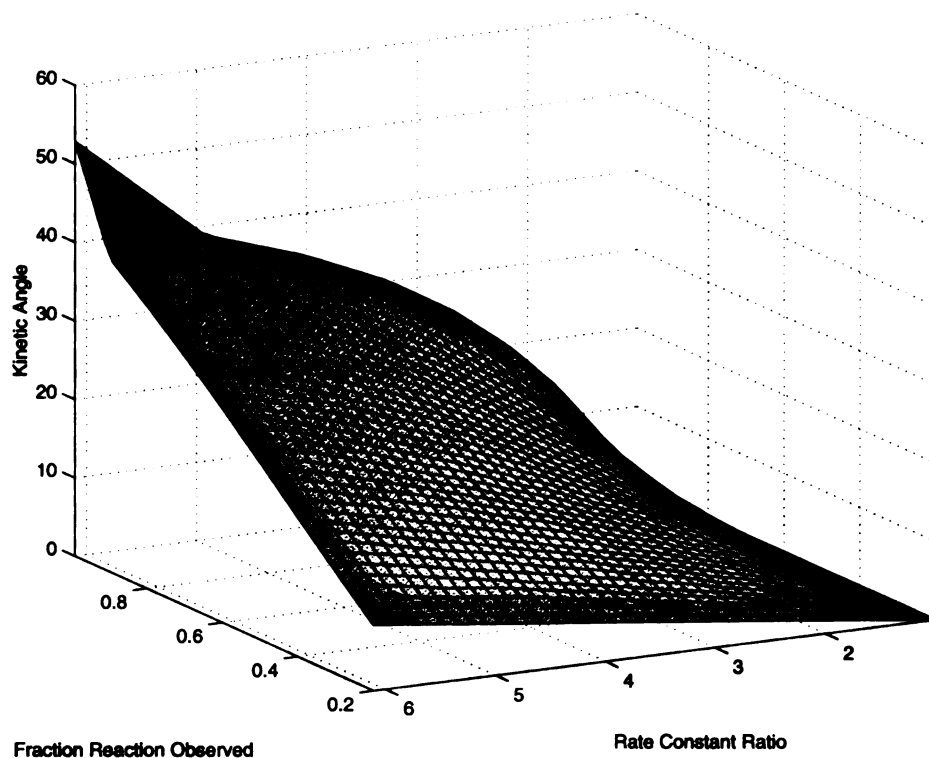


**Figure 3-12: Kinetic angle as a function of rate constant ratio and fraction of the slower reaction observed.**

The relationship between kinetic angle and these two parameters is shown in Figure 3-12. Generally, kinetic angle increases as either the fraction of the slower reaction observed increases or the ratio of the rate constants increases. The effect of increasing rate constant ratio at a constant 90% reaction observed was shown in Figure 3-1. The same relationship observed there can be seen in Figure 3-12. At low fractions of the reaction observed, the relationship is much the same, though the total change in kinetic angle is smaller. At any constant rate constant ratio, an increase in the fraction of the slower reaction observed results in a fairly linear increase in kinetic angle.

### **3.3.2. Effect of number of data points acquired (time points)**

The number of time points acquired was varied while the time for which data was taken was held constant (i.e., the rate at which spectra were acquired was varied). In general it was found that varying the number of spectra between 10 and 100 produced no appreciable change in the accuracy of the determination.

### **3.3.3. Effect of instrumental noise**

Heteroschedastic (i.e., not uniform across the spectrum) instrumental noise proportional to absorbance at each wavelength was added to all simulated data. In most cases, 1% noise was added; in a few cases this value was varied, and the effect of varying levels of noise on the accuracy of kinetic-spectrophotometric determinations was explored. It was found that as the instrumental noise was varied with kinetic angle (at a low spectral angle) the accuracy of the determination using the multivariate calibration techniques decreased uniformly at all kinetic angles as the noise level increased (see Figure 3-13).

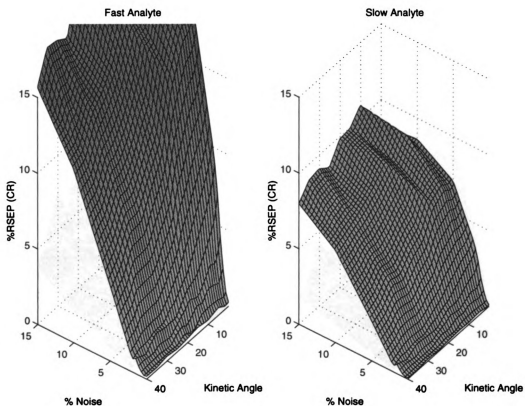


**Figure 3-13: Relative standard error of a CR prediction as a function of the kinetic angle and instrumental noise.**

Determinations using multiway PLS were more tolerant of instrumental noise at high kinetic angles as can be seen from Figure 3-14 below.

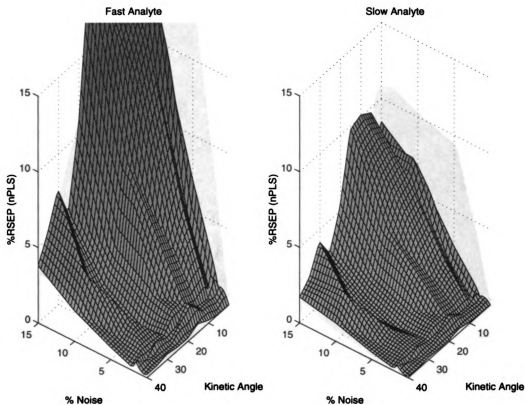


**Figure 3-14: Relative standard error of an nPLS prediction as a function of the kinetic angle and instrumental noise.**

When the level of the instrumental noise was varied concurrently with the spectral angle (at a constant low kinetic angle), it was found that the effect of the instrumental noise was less pronounced at high spectral angles. Figure 3-15 shows this effect.



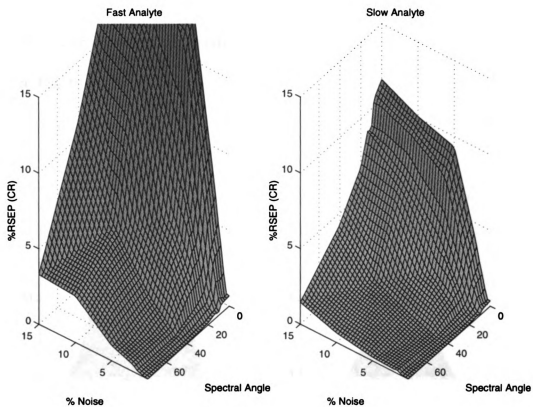


**Figure 3-15: Relative standard error of a CR prediction as a function of the spectral angle and instrumental noise.**

This same phenomenon was observed with nPLS, though the magnitude of the errors was lower. One can see from Figure 3-16 that errors are somewhat lower than from Figure 3-15.

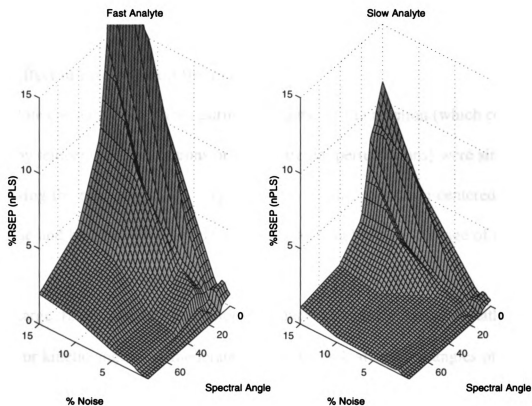


**Figure 3-16: Relative standard error of an nPLS prediction as a function of the spectral angle and instrumental noise.**

It is apparent that instrumental noise (as defined and added to the data) has more influence on the spectral differentiation between the analytes than on the kinetic differentiation, i.e., noise tends to blur spectral differences, especially when the spectra are similar. Techniques that use unfolded data are unable to ignore the spectral data and simply focus on the kinetic data; they are thus

unaffected by increased kinetic differentiation. Multiway PLS is able to more exclusively use the kinetic data and so is able to take advantage of increasing angles. At constant kinetic angles, all techniques perform better with high noise levels if the spectral angle is large, though multiway PLS is (as usual) more accurate.

#### **3.3.4. Effect of rate constant fluctuations**

Rate constant fluctuations during the course of the reaction (which could be caused by temperature fluctuations or other external perturbations) were simulated by allowing the rate constant to vary with a Gaussian distribution centered on the true value and having a standard deviation proportional to a percentage of the rate constant.

Large rate constant fluctuations produce acceptable errors if either the spectral or kinetic angles are moderately large. Indeed, at spectral angles of  $20^\circ$  or larger, rate constant fluctuations up to 15% had no noticeable effects, as can be seen from Figures 3-17 and 3-18.

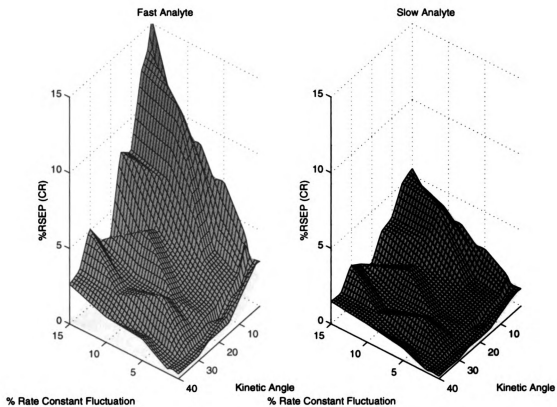


**Figure 3-17: Relative standard error of a CR prediction as a function of the kinetic angle and rate constant fluctuation.**

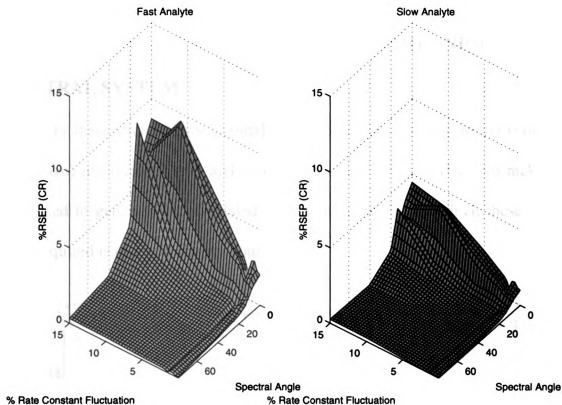


**Figure 3-18: Relative standard error of an nPLS prediction as a function of the kinetic angle and rate constant fluctuation.**

From comparing Figures 3-13 through 3-16 with Figures 3-17 and 3-18, we can see that the addition of instrumental noise (as defined above) has a much larger effect on the accuracy of determinations than do rate constant fluctuations. For this reason, it was decided to focus more effort on decreasing the instrumental noise level of the experimental system than on controlling factors that could lead to rate constant fluctuations.

### 3.4. EXPLORATION OF EFFECT OF EXPERIMENTAL VARIABLES ON SIMULATIONS OF THE GA(III) -- NI(II) SPECTRAL SYSTEM

For these studies, experimentally determined spectra (Figure 3-19) of 4-(2-pyridylazo)-resorcinol (PAR) and its complexes with gallium (III) and nickel (II) were used to generate the simulated data. The procedure by which these spectra were acquired is given in chapter four.

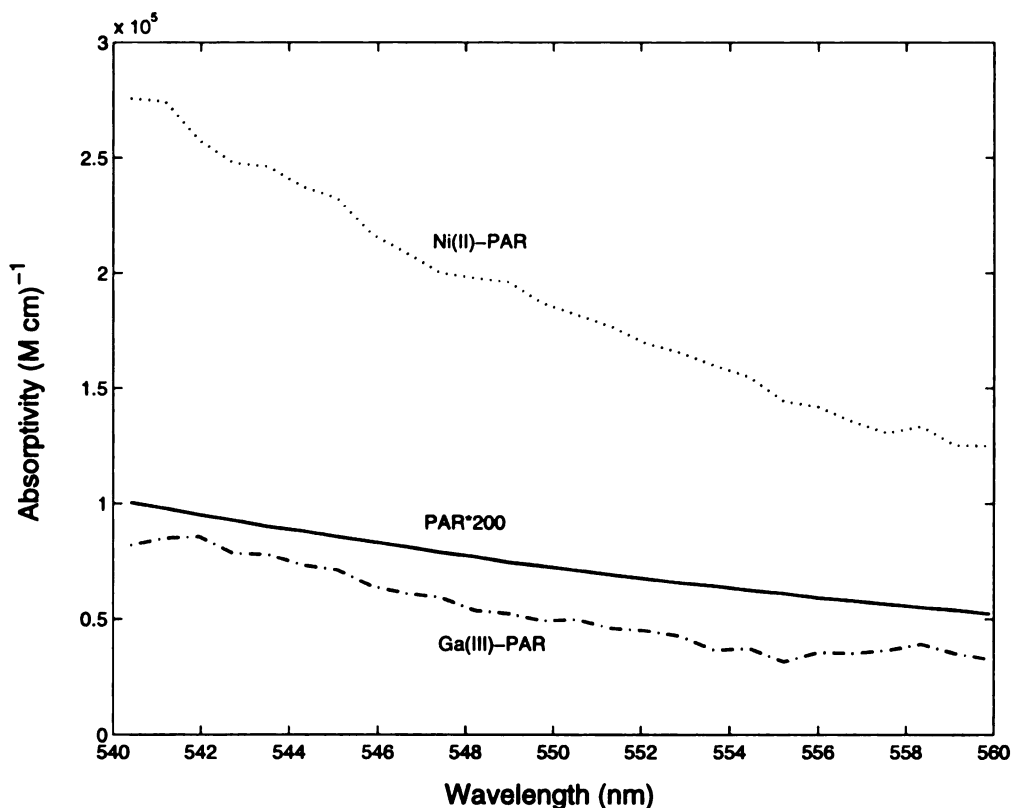


**Figure 3-19: Absorption spectra of PAR and its Ni(II) and Ga(III) complexes used for simulation studies.**

The spectral angle between the analytes is 6.3; the spectral net analyte signal for the Ni(II)-PAR complex is 26% higher than that for the Ga(III)-PAR complex. This indicates that it should be much more accurately predicted. Ni(II) is the faster reacting analyte, and so always has a lower kinetic net analyte signal. In practice, the much higher spectral net analyte signal overwhelms the slightly lower kinetic net analyte signal. It is thus expected that Ni(II) should be determined more accurately than Ga(III).

Using the measured spectra, the remaining experimental parameters were varied. The simulations were carried out in the same manner as the previously described studies.

#### **3.4.1. Effect of Kinetic Angle**

In this highly spectrally overlapped system, it is not unexpected that the kinetic angle should affect the accuracy of kinetic-spectrophotometric determinations (see Figures 3-6 through 3-11). The multivariate calibration techniques are adversely affected by factors that lower the kinetic angle. This is seen in Figure 3-20 which shows that errors below 5% can be achieved for the faster (less spectrally overlapped) analyte under most kinetic conditions, i.e., with all but the lowest kinetic angles (or as shown here, with all combinations of rate constant ratios and fractions of the slower reaction observed save those with low (<3) rate constant ratios and less than 40% of the slower reaction observed). The slower (more spectrally overlapped) analyte is less accurately determined; errors

near 5% can be determined only when at least 50% of the slower reaction is observed.

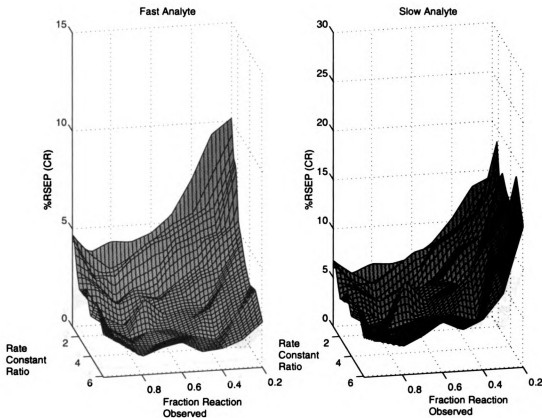


**Figure 3-20: Relative standard error of a CR prediction as a function of the rate constant ratio and the fraction of the slower reaction observed. The Ga(III)/Ni(II) spectra shown in Figure 3-19 were used. The spectral angle was 6.3.**

Multiway PLS is more able to use the limited kinetic and spectral information available in this system. As such, the accuracy of its predictions is largely unaffected by the parameters that affect the kinetic angle. Looking back at Figure 3-11, it can be seen that a spectral angle of  $\sim 6$ , the kinetic angle has little effect. Figure 3-21 shows that neither the rate constant ratio nor the fraction of the slower



reaction observed had an appreciable effect on the prediction of either analyte. The faster (less spectrally overlapped) analyte is predicted with greater accuracy.

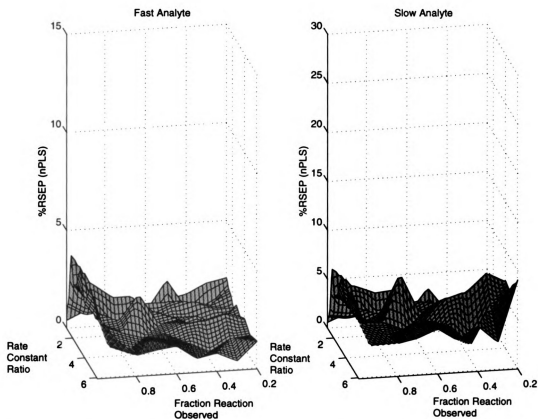


**Figure 3-21:** Relative standard error of a CR prediction as a function of the rate constant ratio and the fraction of the slower reaction observed. The Ga(III)/Ni(II) spectra shown in Figure 3-19 were used. The spectral angle was 6.3.

### **3.5. REFERENCES**

- (1) Faber, K.; Lorber, A.; Kowalski, B. R. "Analytical figures of merit for tensorial calibration" *J. Chemometr.* **1997**, *11*, 419-461.
- (2) Lorber, A.; Faber, K.; Kowalski, B. R. "Net analyte signal calculation in multivariate calibration" *Anal. Chem.* **1997**, *69*, 1620-1626.
- (3) Messick, N. J.; Kalivas, J. H.; Lang, P. M. "Selectivity and related measures for nth order data" *Anal. Chem.* **1996**, *68*, 1572-1579.

## CHAPTER 4

### DETERMINATION OF GALLIUM (III) AND NICKEL (II)

*No man's knowledge here can go beyond  
his experience.*

--John A. Locke

The determination of nickel (II) and gallium (III) using their reaction with 4-(2-Pyridylazo)-resorcinol (PAR) was carried out under a variety of experimental conditions. Kinetic, spectrophotometric, and kinetic-spectrophotometric determinations were performed. Several of chemometric methods were used in the determinations.

PAR is a highly sensitive photometric reagent that reacts with a variety of metal ions<sup>1</sup>. It is a triprotic weak acid whose dissociation progresses as<sup>1</sup>:

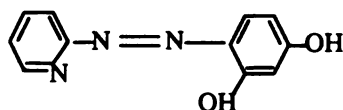
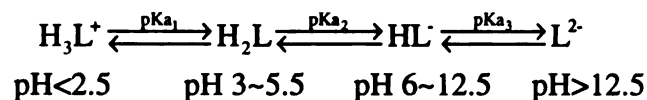
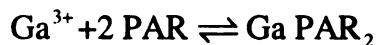
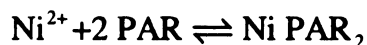


**Figure 4-1: Acid dissociation of PAR**

In all of the work described in this document, PAR exists in its singly protonated form. PAR complexes with metal ions as either a bi- or tridentate ligand. The two

metal ions whose determination is discussed in this chapter, Ga(III) and Ni(II), both form complexes where two PAR molecules react with one metal ion<sup>1</sup>.



Gallium (III) and nickel (II) were chosen for several reasons. Both react with PAR, and both are soluble in the buffer solutions used in these studies. They also present a highly challenging system. The rates at which they react with PAR are very close together, and the absorption spectra of their reaction products with PAR are quite similar.

The use of PAR as a spectrophotometric reagent for the determination of gallium and especially of nickel has been reported in the literature<sup>2-9</sup>. Other workers have described the determination of nickel or gallium using a chromatographic separation and either a pre-concentration step involving PAR or a post-column reaction with PAR<sup>10-13</sup>. There have been a few reports of kinetic determinations of nickel or gallium using PAR as a reagent<sup>14,15</sup>.

## **4.1. EXPERIMENTAL**

### **4.1.1. Solution Preparation.**

All solutions were prepared with distilled water and reagent grade chemicals. Buffers of pH 8.5 and 7.0 were prepared from sodium borate and sodium phosphate, respectively, and adjusted with nitric acid. All working solutions were prepared in one of these buffers.

The equilibrium studies were performed using a set of three calibration sets. The single component calibration and unknown solution sets contained six and four solutions, respectively, and are described by Tables 4-1 and 4-2.

**Table 4-1**  
**Single component calibration and unknown sets for**  
**the equilibrium determination of Ni(II)**

Ni(II) concentration ( $\mu\text{M}$ )		
Solution #	Calibration Set	Unknown Set
1	0.06	2.00
2	1.60	4.00
3	2.60	
4	3.60	
5	4.60	
6	5.60	

**Table 4-2**  
**Single component calibration and unknown sets for**  
**the equilibrium determination of Ga(III)**

Ga(III) concentration ( $\mu\text{M}$ )		
Solution #	Calibration Set	Unknown Set
1	1.60	2.00
2	2.60	4.00
3	3.60	
4	4.60	
5	5.60	
6	6.60	

The equilibrium multicomponent determinations were performed using a solution set containing eight calibration solutions and two unknown solutions. These samples were reacted with 1mM PAR at a pH of 7.0. The position of these samples in concentration space is shown in Figure 4-2.

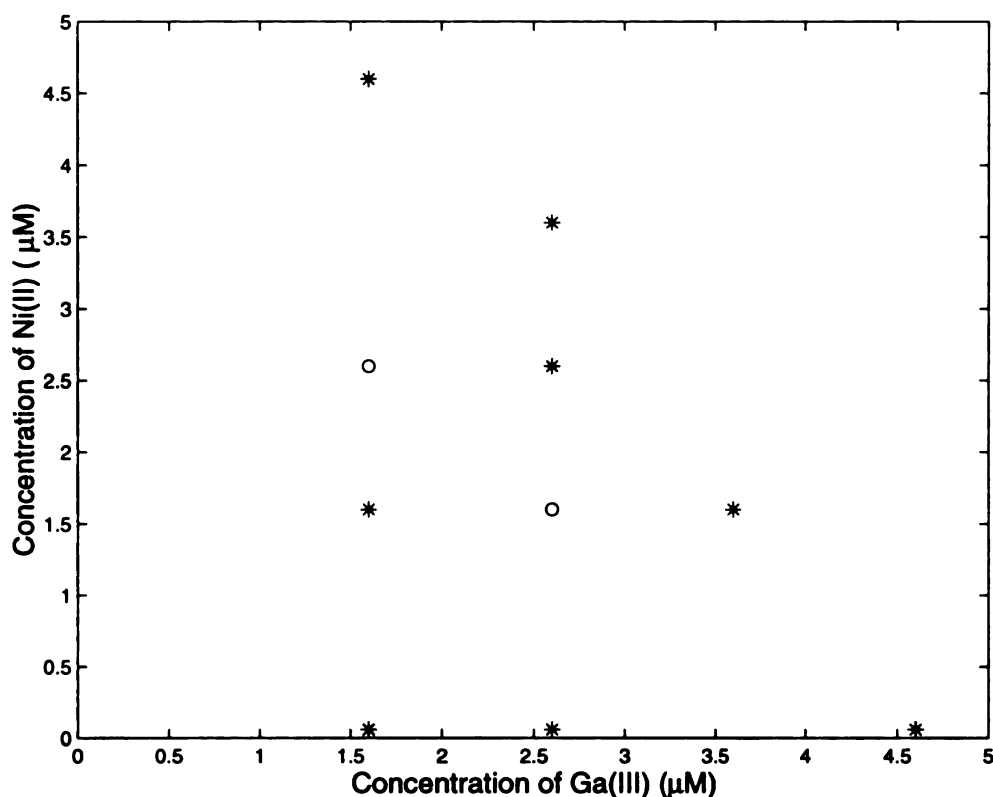


**Figure 4-2: Concentrations of calibration (stars) and unknown (open circles) samples used for the two-component equilibrium determinations.**

For the pH 8.5 kinetics studies, thirteen calibration mixtures and four unknown mixtures were made. These were mixed and reacted in the stopped flow system with a solution of  $10^{-3}$  M PAR. The calibration and unknown sets used for the pH 8.5 kinetics studies are can be seen in Figure 4-3.

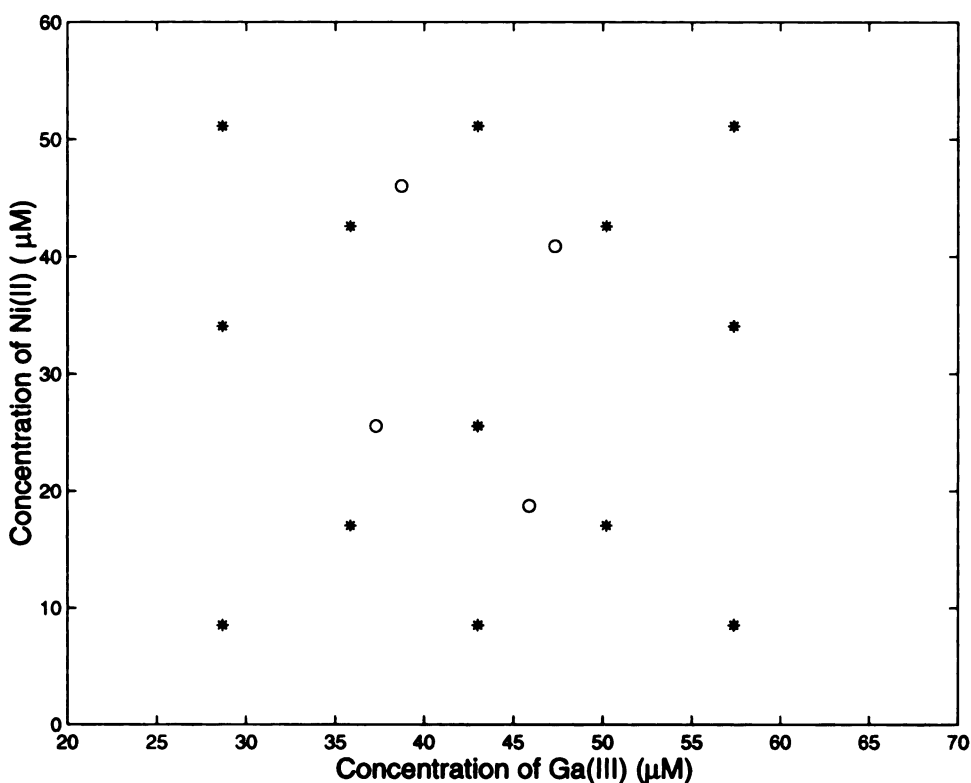


**Figure 4-3: Concentrations of calibration (stars) and unknown (open circles) samples used for the pH 8.5 kinetic and kinetic-spectrophotometric determinations of Ga(III) and Ni(II).**

The pH 7.0 studies were performed using a similar, but slightly different set of solutions. Sixteen calibration and four unknown solutions were mixed and reacted in the stopped flow system with a solution of  $10^{-3}$  M PAR. The location of the mixtures in the concentration space of the analytes is given in Figure 4-4.

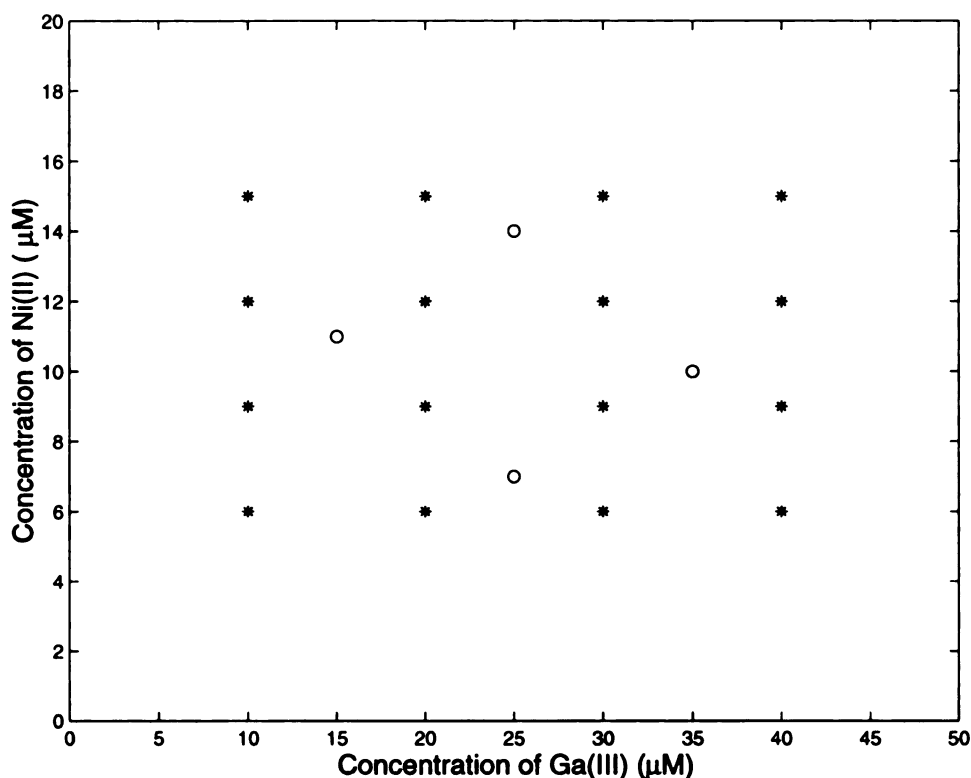


**Figure 4-4: Concentrations of calibration (stars) and unknown (open circles) samples used for the pH 7.0 kinetic and kinetic-spectrophotometric determinations of Ga(III) and Ni(II).**

#### 4.1.2. Spectrophotometric (Equilibrium) Data Collection

Gallium (III) and Nickel (II) were reacted with PAR in a pH 7.0 phosphate buffer. The reactions were allowed to proceed to equilibrium, and spectra were obtained. Data were collected in two wavelength ranges (500-550nm and 500-600nm) using a Hitachi U-4001 UV-visible spectrophotometer. A one centimeter quartz cuvette was employed as a sample holder. A pH 7.0 phosphate buffer was used as a blank. Spectra were collected at 201 wavelengths between 500 and 600 nm, and 101 wavelengths between 500 and 550 nm..



### **4.1.3. Kinetic-spectrophotometric Data Collection**

Data were collected using a home-built stopped-flow apparatus interfaced to a thermoelectrically cooled Tracor Northern (Model TN-6123) 512 element intensified diode array (Tracor Northern, Philadelphia, PA) configured to acquire spectra in the 400-800 nm range as described in chapter 2.

In the wavelength range of interest (520-560 nm), absorbance was measured at 52 equally-spaced wavelengths. In cases where the entire 520-560 nm spectral region was not used, a subset of the 52 wavelengths was employed. Specifically, in the range 540-560 nm, 26 wavelengths were used.

At pH 8.5, kinetic information was obtained by acquiring 26 spectra at a rate of 5.0 scans per second for a total acquisition time of 5.2 seconds. At pH 7.0, 100 spectra were acquired at a rate of 7.575 scans per second over a total acquisition time of 13.07 seconds..

### **4.1.4. Data processing**

Time dependent spectra were collected in triplicate and averaged, i.e., each metal ion solution was reacted with PAR three times. The resulting three sets of kinetic-spectrophotometric data were averaged. Data were mean-centered (i.e., the mean of each variable vector was subtracted from each of its elements) before being input to the appropriate algorithms. Multivariate calibration algorithms provided in the PLS\_TOOLBOX (Eigenvector Technologies, Manson, WA.) and run in MATLAB were used to perform determinations.

## 4.2. DETERMINATION OF RATE CONSTANTS AND ABSORPTION SPECTRA

Experiments were performed to determine pure component spectra and rate constants for the reaction products of the reaction of Ni(II) and Ga(III) with PAR. The pure spectrum of PAR was subtracted from observed absorbance versus time data resulting from the reaction of PAR with a single metal ion. These subtracted data were fit to the equation<sup>16,17</sup>:

$$A_t = A_\infty - (A_\infty - A_0) \cdot e^{-k' \cdot t}$$

The pseudo-first order rate constant,  $k'$ , was calculated from data at several wavelengths, and an average value was computed. The second-order rate constant was calculated from this average  $k'$  and the known excess concentration of PAR as

$$k = k'[\text{PAR}]$$

From the fit values of  $A_\infty$ ,  $A_0$ , and  $k'$ , the initial rate of the reaction was calculated at each wavelength:

$$\frac{\partial A_t}{\partial t} = k'(A_\infty - A_0)$$

The initial rate was plotted versus concentration. The molar absorptivities of the reaction product at each wavelength were computed from the slope of this plot:

$$\varepsilon = \frac{\text{slope}}{k'}$$

These values were then used in the simulations described in other chapters.

### **4.3. RESULTS OF THE DETERMINATION OF GALLIUM (III) AND NICKEL (II)**

A spectrophotometric (equilibrium) determination of Ga(III) and Ni(II) was performed, and the ability of the various chemometric algorithms to accurately predict the concentration of the analytes in unknown mixtures was examined. Rate constants and pure component spectra were obtained experimentally for the reactants and products of the reactions of Ni(II) and Ga(III) with PAR. Kinetic-spectrophotometric determinations of Ga(III) and Ni(II) were performed. These determinations were then compared to the spectrophotometric (equilibrium) determination and to a kinetic determination carried out at a single wavelength.

#### **4.3.1. Spectrophotometric (Equilibrium) Determination of Gallium (III) and Nickel (II)**

Continuum regression and partial least squares regression both produced acceptable results for single-component equilibrium determinations. The relative standard errors of prediction (as defined in chapter two) for each determination are shown in tables 4-3 and 4-4.

**Table 4-3**  
**Spectrophotometric (equilibrium) determination of Ni(II)**

<b>Method</b>	<b>% RSEP (500-550 nm)</b>	<b>% RSEP (500-600 nm)</b>
CR	1.2	1.2
PCR	20.4	20.4
PLS	1.2	1.2
MLR	1.6	1.9

**Table 4-4**  
**Spectrophotometric (equilibrium) determination of Ga(III)**

<b>Method</b>	<b>% RSEP (500-550 nm)</b>	<b>% RSEP (500-600 nm)</b>
CR	8.6	8.3
PCR	30.6	36.8
PLS	8.6	8.3
MLR	19.6	21.0

The determination of Ni(II) produced relative standard errors of prediction of approximately 1.2% for both wavelength ranges when CR and PLS were used. PCR produced inaccurate predictions for reasons which are not altogether clear. Ga(III) was less accurately predicted than was Ni(II). Because the molar absorptivity of the Ni-PAR complex is much higher than that of the Ga-PAR complex (see chapter 3), more accurate predictions of Ni(II) were expected.

The determination of Ga(III) produced slightly lower errors for the larger wavelength range (8.3%) than for the smaller wavelength range (8.6%) when CR and PLS were used. The addition of more wavelengths decreases the error of the Ga(III) determination more than it does the error of the Ni(II) determination because although the additional wavelengths add much more noise than information about the analytes, the algorithms used (CR and PLS) are able to extract the small additional amount of information present in the added wavelengths from the background noise. It is interesting to note that the same effect is not seen when principal component regression or multiple linear regression is employed. It is probable that the ability of continuum regression and partial least squares regression to place lower weights on variables (wavelengths)

that vary substantially but are not correlated to the concentrations of the analytes is responsible for their more accurate predictions. The Ga(III) determination is most strongly impacted by this phenomenon, as the lower absorptivity of the Ga-PAR complex results in smaller observed absorbances (and thus less information related to the concentrations being determined).

The multicomponent equilibrium determination of Ga(III) and Ni(II) showed significantly higher errors than the single-component determinations. These results are summarized in table 4-5.

**Table 4-5**  
**Multicomponent spectrophotometric (equilibrium)**  
**determination of Ni(II) and Ga(III)**

<b>Method</b>	<b>500-550 nm</b>		<b>500-600 nm</b>	
	<b>% RSEP (Ga)</b>	<b>% RSEP (Ni)</b>	<b>% RSEP (Ga)</b>	<b>% RSEP (Ni)</b>
CR	26	6	21	6
PCR	22	6	21	8
PLS	21	6	21	7
MLR	23	4	24	5

As expected, Ni(II) was determined with greater accuracy than was Ga(III). The spectra are highly overlapped, and so there is little information present that can be used to differentiate the two analytes. Thus, it is not surprising that the additional information that is present in the larger wavelength range results in lowered error for determinations using all algorithms. Figures 4-5 and 4-6 are plots of the predicted vs. actual concentrations.

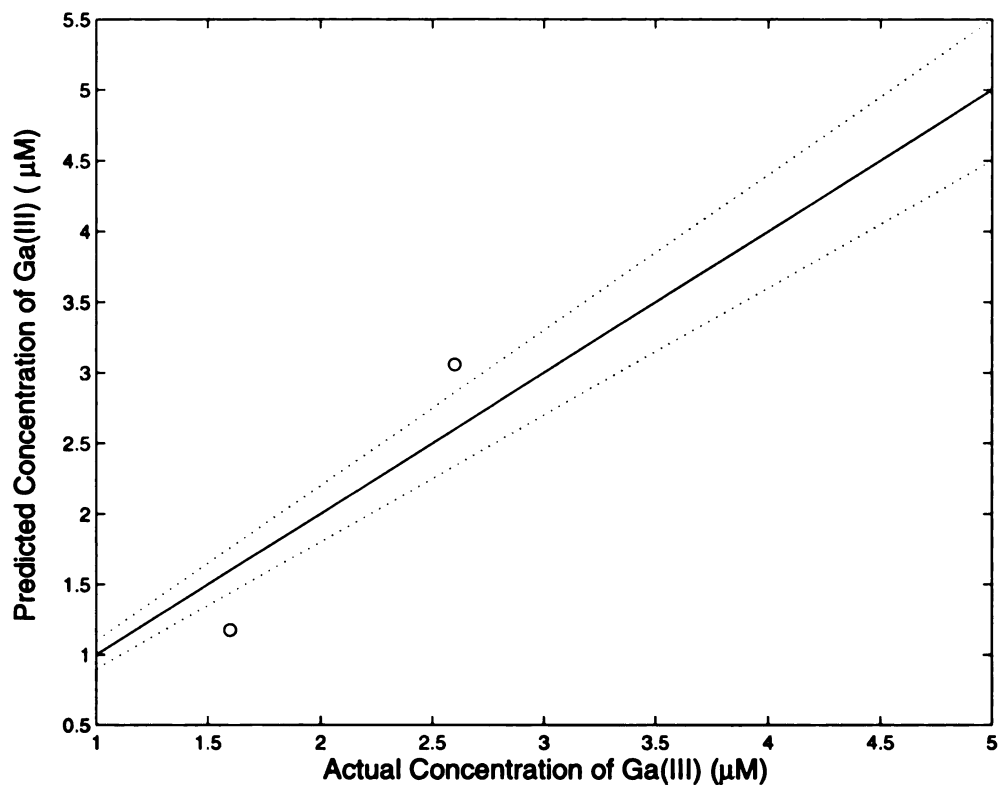


**Figure 4-5: Plot showing the predicted vs. actual concentrations of Ga(III) for a two-component equilibrium determination. The circles show the predicted concentrations. The solid line has a slope of unity and represents a prediction with no error. The dashed lines show  $\pm 10\%$  error tolerances.**

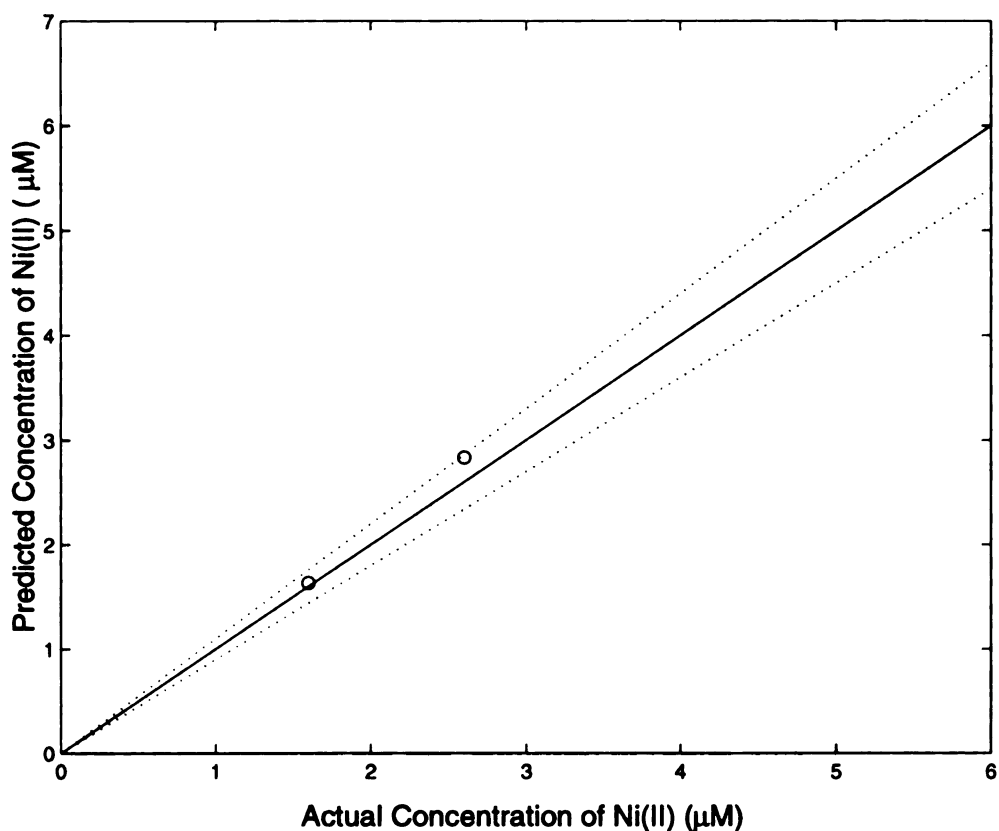


**Figure 4-6: Plot showing the predicted vs. actual concentrations of Ni(II) for a two-component equilibrium determination. The circles show the predicted concentrations. The solid line has a slope of unity and represents a prediction with no error. The dashed lines show  $\pm 10\%$  error tolerances.**

#### **4.3.2. Kinetic Determination of Gallium (III) and Nickel (II)**

Using the data collected during the kinetic-spectrophotometric determinations, a single-wavelength (550 nm) kinetic determination of Ga(III) and Ni(II) was performed at both pH 7.0 and pH 8.5. The results of these determinations are summarized in table 4-6.

**Table 4-6**  
**Multicomponent kinetic determination of Ni(II) and Ga(III)**

Method	pH=7.0		pH=8.5	
	% RSEP (Ga)	% RSEP (Ni)	% RSEP (Ga)	% RSEP (Ni)
CR	35	26	10	6
PCR	30	20	10	6
PLS	35	19	10	4
MLR	47	31	12	9

The results at pH 8.5 (where a good deal of kinetic differentiation exists between the analytes) are quite comparable with those from the kinetic-spectrophotometric determination (table 4-7). There is little spectral differentiation present in this system, and so the addition of more wavelengths adds little additional information about the analytes. At pH 7.0 (where much less kinetic differentiation exists) the kinetic determination is clearly inferior to the kinetic-spectrophotometric determination. The additional differentiation between the analytes afforded by the spectral information is, in this case, necessary.

#### **4.3.3. Kinetic-spectrophotometric determination of Gallium(III) and Nickel(II)**

Two different pH values and two wavelength ranges were used to determine Ga(III) and Ni(II). The results of these determinations are presented in table 4-7. As can be seen, errors of prediction at pH 8.5 were generally half those at pH 7.0. This can be rationalized in several ways. First, the kinetic angle at pH 8.5 (40.1) is much larger than the angle at pH 7.0 (12.6). This represents a large



increase in the amount of kinetic differentiation between the analytes. The spectral angles at pH 8.5 and pH 7.0 are similar, but since both are small (~6.3), kinetic differentiation is the major source of selectivity; it is thus expected that a larger kinetic angle will result in a smaller error of prediction. Indeed, this is what is observed.

**Table 4-7**  
**Multicomponent kinetic-spectrophotometric determination of Ni(II) and Ga(III)**

pH	Method	540-560 nm		520-560 nm	
		% RSEP (Ga)	% RSEP (Ni)	% RSEP (Ga)	% RSEP (Ni)
7.0	CR	19	17	17	18
	PCR	18	18	20	19
	PLS	20	17	19	17
	MLR	50	12	11	20
	nPLS	21	15	29	16
8.5	CR	11	6	14	8
	PCR	9	5	11	6
	PLS	9	6	14	6
	MLR	31	5	29	8
	nPLS	9	5	11	6

The results of these determinations can be compared to the results of the equilibrium spectrophotometric determination described previously (table 4-5). The results of the kinetic-spectrophotometric determination performed at pH 8.5 show a marked improvement over the equilibrium results for all techniques except multiple linear regression.

In comparing the multivariate calibration techniques, continuum regression, partial least squares regression, principal component regression and multiway partial least squares regression all produce predictions of similar accuracy.

Multiple linear regression sometimes produced slightly more accurate predictions, but, more often, was clearly inferior. For the type of data studied, continuum regression and principal component regression proved the most stable of the multivariate calibration techniques. While not always the best choice, they were rarely worse than any others and often significantly better. Multiway PLS (nPLS) was often superior to the one way techniques, but also performed poorly on occasion. The reasons for these failures are not clear.

The spectral region between 540-560 nm was found to contain the majority of the spectral differentiation between the analytes. Increasing the spectral window greatly increased the data processing time, but did not appreciably affect the error of prediction.

The results are similar to what is expected based on the simulation studies done using the Ga(III) and Ni(II) spectra and on the relative kinetic and spectral net analyte signals (as discussed in chapter 3). Ni(II) was more accurately predicted, as expected.

#### 4.4. REFERENCES

- (1) Shibata, S., "2-Pyridylazo compounds in analytical chemistry", in *Chelates in Analytical Chemistry*; Flaschka, H. A., Barnard, A. J., Jr, Eds.; Marcel Dekker: New York, 1972; Vol. 4.
- (2) Bobrowska Grzesik, E.; Grossman, A. M. "Derivative spectrophotometry in the determination of metal ions with 4-(pyridyl-2-azo) resorcinol (PAR)" *Fresenius J. Anal. Chem.* **1996**, *354*, 498-502.
- (3) Cladera, A.; Gomez, E.; Estela, J. M.; Cerda, V.; Cerda, J. L. "Computer method for the simultaneous kinetic determination of compounds in mixtures based on the use of diode-array spectrophotometry" *Anal. Chim. Acta* **1993**, *272*, 339-344.
- (4) Gomez, E.; Estela, J. M.; Cerda, V.; Blanco, M. "Simultaneous spectrophotometric determination of metal-ions with 4-(Pyridyl-2-Azo)Resorcinol (PAR)" *Fresenius J. Anal. Chem.* **1992**, *342*, 318-321.
- (5) Kolomiets, L. L.; Pilipenko, L. A.; Zhmud, I. M.; Panfilova, I. P. "Application of derivative spectrophotometry to the selective determination of nickel, cobalt, copper, and iron(III) with 4- (2-pyridylazo)resorcinol in binary mixtures" *J. Anal. Chem.* **1999**, *54*, 28-30.
- (6) Ni, Y. N. "Trace-metal determinations by spectrophotometry with a double chromogenic system and a chemometric approach" *Anal. Chim. Acta* **1993**, *284*, 199-205.
- (7) Ridder, C.; Norgaard, L. "Simultaneous determination of cobalt and nickel by flow- injection analysis and partial least-squares regression with outlier detection" *Chemometrics Intell. Lab. Syst.* **1992**, *14*, 297-303.
- (8) Mori, I.; Kawakatsu, T.; Fujita, Y.; Matsuo, T. "Selective spectrophotometric determination of gallium(III) with 2-(5-bromo-2-pyridylazo)-5-diethylaminophenol in the presence of sodium dodecylsulfate and Brij 35" *Anal. Lett.* **1999**, *32*, 613-622.
- (9) Taljaard, R. E.; van Staden, J. F. "Simultaneous determination of cobalt(II) and Ni(II) in water and soil samples with sequential injection analysis" *Anal. Chim. Acta* **1998**, *366*, 177-186.

- (10) Khalaf, K. D.; MoralesRubio, A.; DelaGuardia, M.; Garcia, J. M.; Jimenez, F.; Arias, J. J. "Simultaneous kinetic determination of carbamate pesticides after derivatization with p-aminophenol by using partial least squares" *Microchem J.* **1996**, *53*, 461-471.
- (11) Chakrapani, G.; Murty, D. S. R.; Mohanta, P. L.; Rangaswamy, R. "Sorption of PAR-metal complexes on activated carbon as a rapid preconcentration method for the determination of Cu, Co, Cd, Cr, Ni, Pb and V in ground water" *Journal of Geochemical Exploration* **1998**, *63*, 145-152.
- (12) Karve, M. A.; Khopkar, S. M. "Liquid-liquid-extraction of gallium with high-molecular-weight amines from ascorbate solutions" *Chem. Anal.* **1993**, *38*, 469-476.
- (13) Ming, X. Y.; Wu, Y. H.; Schwedt, G. "HPLC analysis of V, Co, Fe, and Ni By 4-(2-Pyridylazo)- Resorcinol, PAR, and H<sub>2</sub>O<sub>2</sub> and studies on complex properties influencing retention" *Fresenius J. Anal. Chem.* **1992**, *342*, 556-559.
- (14) Arruda, M. A. Z.; Zagatto, E. A. G.; Maniasso, N. "Kinetic determination of cobalt and nickel byflow-injection spectrophotometry" *Anal. Chim. Acta* **1993**, *283*, 476-480.
- (15) Blanco, M.; Coello, J.; Iturriaga, H.; Maspoch, S.; Riba, J.; Rovira, E. "Kinetic spectrophotometric determination of Ga(III)-Al(III) mixtures by stopped-flow injection-analysis using principal component regression" *Talanta* **1993**, *40*, 261-267.
- (16) Moore, J. W.; Pearson, R. G. *Kinetics and Mechanisms* ; Wiley: New York, 1991.
- (17) Mieling, G. E.; Pardue, H. L. "Kinetic method that is insensitive to variables affecting rate constants" *Anal. Chem.* **1978**, *50*, 1611-1618.

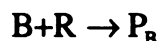
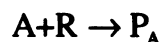
## CHAPTER 5

### KINETIC-SPECTROPHOTOMETRIC DETERMINATIONS IN SYSTEMS WITH NONLINEAR KINETICS

*When you can measure what you are speaking about,  
and express it in numbers, you know something about  
it. But when you cannot- your knowledge is of a  
meagre and unsatisfactory kind.*

--Lord Kelvin

Most kinetic determinations are carried out under conditions such that the kinetics of the reaction are pseudo first order in the analyte. In cases where multiple analytes are determined, conditions are usually arranged such that the analytes each react according to pseudo first order kinetics:



$$\frac{dA}{dt} = -k_A AR = -k'_A A$$

$$k'_A = k_A R$$

$$\frac{dB}{dt} = -k_B BR = -k'_B B$$

$$k'_B = k_B R$$

$$A_t = A_0 e^{-k'_A t}$$

$$B_t = B_0 e^{-k'_B t}$$

Under these conditions, the concentration of the analytes (and of their products) at any time  $t$  is linearly related to the initial concentration of the analytes. The

condition that must be met is that the concentration of the reagent be sufficiently large that it effectively remains constant over the course of the reaction.

Several factors can cause kinetic non-linearity. Most obviously, a low reagent concentration invalidates the assumptions necessary for pseudo first order kinetics. In this case, the concentration of the analyte at any given time is no longer linear with the initial concentration. For the case of a single analyte reacting with the reagent:

$$\begin{aligned}
 A+R &\rightarrow P_A \\
 \frac{dA}{dt} &= -k_A AR \\
 A_t &= \frac{A_0 R_0 \exp^{A_0 k_A t - R_0 k_A t}}{R_0}
 \end{aligned}$$

Here the concentration of the analyte at time  $t$  is a complex nonlinear function of the initial concentration of the analyte and reagent. When two or more analytes are present, a discreet solution for the concentration of an analyte at any time can not be written; rather, the set of differential equations

$$\begin{aligned}
 \frac{dA}{dt} &= -k_A \cdot A \cdot R \\
 \frac{dB}{dt} &= -k_B \cdot B \cdot R \\
 \frac{dR}{dt} &= -(k_A \cdot A \cdot R) - (k_B \cdot B \cdot R)
 \end{aligned}$$

must be solved numerically.

Some other conditions also result in nonlinear kinetics. Perhaps the most common of these is the existence of synergistic effects. Here the rate of reaction of

one analyte is a function of the concentration of the other, even if the reagent is present in large excess.

$$\frac{dA}{dt} = -k_A \cdot A \cdot R + f(B)$$

In all of these cases, most traditional methods for performing kinetic determinations fail.

Some work has been done in the area of performing kinetic determinations under conditions where nonlinear kinetics prevail. Modified nonlinear regression algorithms have been used<sup>1,2</sup> to determine analytes using second and third order reaction schemes. Several workers have used artificial neural networks to process kinetic data collected from reactions with nonlinear kinetics. Blanco and coworkers<sup>3</sup> used an artificial neural network to perform a determination of three analytes. Two react with the reagent according to pseudo first order kinetics; the third follows a complex multistep process that is nonlinear. The ANN produced predictions of acceptable accuracy for all three analytes and outperformed both PLS and PCR. In another study<sup>4</sup>, Blanco's group used simulated data to perform a detailed study of the use of PLS for nonlinear kinetic data. Here the nonlinearity was added through the addition of a synergistic term (see above equation). In all but the most nonlinear cases studied, the predictions returned by PLS were acceptably accurate.

Blanco and coworkers<sup>5</sup> have also explored the use of ANNs in situations where the nonlinearity is introduced by having the analytes present in sufficiently

high concentrations that the reaction is pseudo first order in reagent. Benzylamine and Butylamine were determined through their reaction with salicylaldehyde. The ANN outperformed PLS and predicted the concentration of the analytes with only 4% error.

Ventura et al.<sup>6</sup> used an ANN whose inputs were PCA factors to perform kinetic determinations in the presence of synergistic effects and the inherent nonlinearity of the continuous addition of reagent technique. The results of the experiments were quite impressive and the concentrations of the analytes were predicted with good accuracy (errors of prediction of about 5%).

In this chapter a standardized way of reporting the degree of kinetic non-linearity present in a system is developed. The results of simulations and experiments performed under conditions of kinetic non-linearity are presented.

## **5.1. EXPERIMENTAL**

### **5.1.1. Simulations**

Simulation studies were performed in a manner similar to that described in chapter 3. The degree of nonlinearity was controlled by varying the concentration of the reagent, and was measured as an angle from linearity.

The angle from linearity ( $\theta_L$ ) was calculated by plotting the concentration of the analyte at a fixed time vs. the initial concentration of the analyte for several samples with different concentrations of the two analytes. The angle  $\theta_L$  is related to the correlation between the initial and time-dependent concentrations.



$$\theta_{L_A} = \arccos \left( \frac{\sigma_{A_0 A_t}}{\sigma_{A_0} \cdot \sigma_{A_t}} \right)$$

where  $A_0$  and  $A_t$  are the concentrations of analyte A for several samples at times 0 and t, respectively,  $\sigma_{A_0}$  and  $\sigma_{A_t}$  are their standard deviations, and  $\sigma_{A_0 A_t}$  is the covariance of  $A_0$  and  $A_t$ . An angle from linearity of  $0^\circ$  indicates complete linearity, while an angle of  $90^\circ$  signifies complete nonlinearity. Practically, when the system is linear, the plot is linear; when there is kinetic nonlinearity the concentration of one analyte affects the concentration of the other at the fixed time. The following figure shows this plot for a situation where linear kinetics prevail.

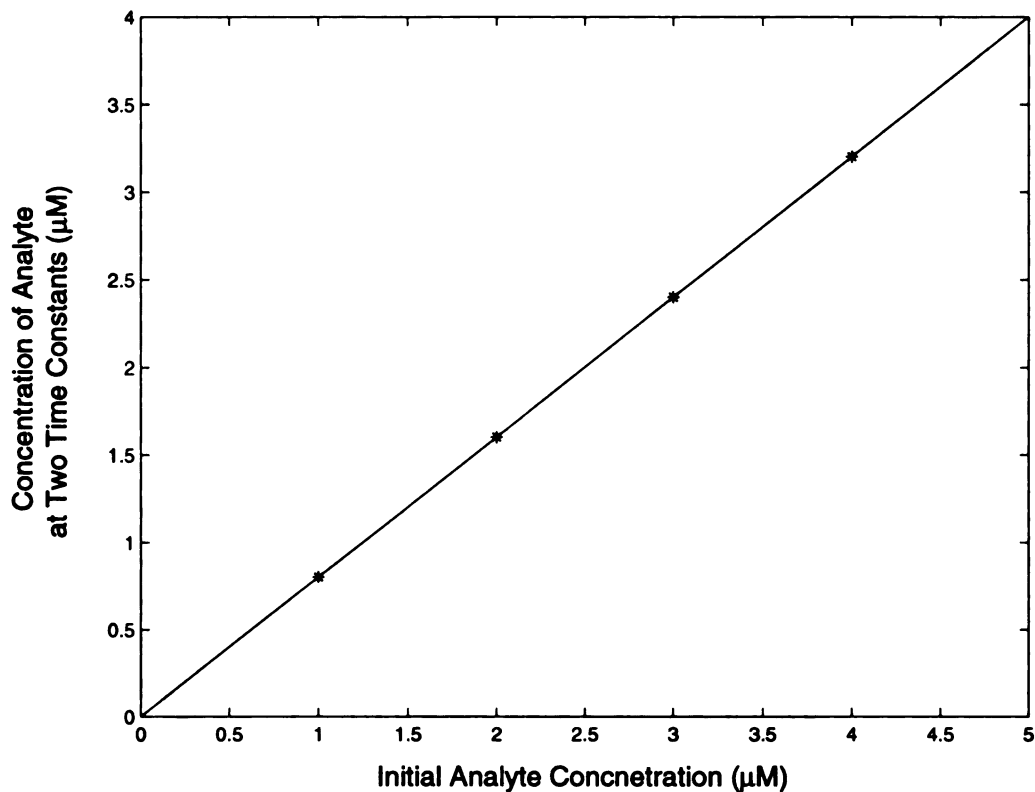


**Figure 5-1: Example of a linear (pseudo-first-order) kinetic system. This data was generated with a rate constant ratio of 1.7 and a kinetic angle of 10.2. The reagent was in 281 fold excess. The angle from linearity was 0.017.**

Kinetic nonlinearity causes samples with the same initial concentration of an analyte to have different concentrations of the analyte after a fixed time. Figure 5-2 shows this effect. The effect of the concentration of the second analyte on the kinetics of the first (because the second analyte uses up some reagent, thereby changing the reaction rate for the analyte in question) can be clearly seen.

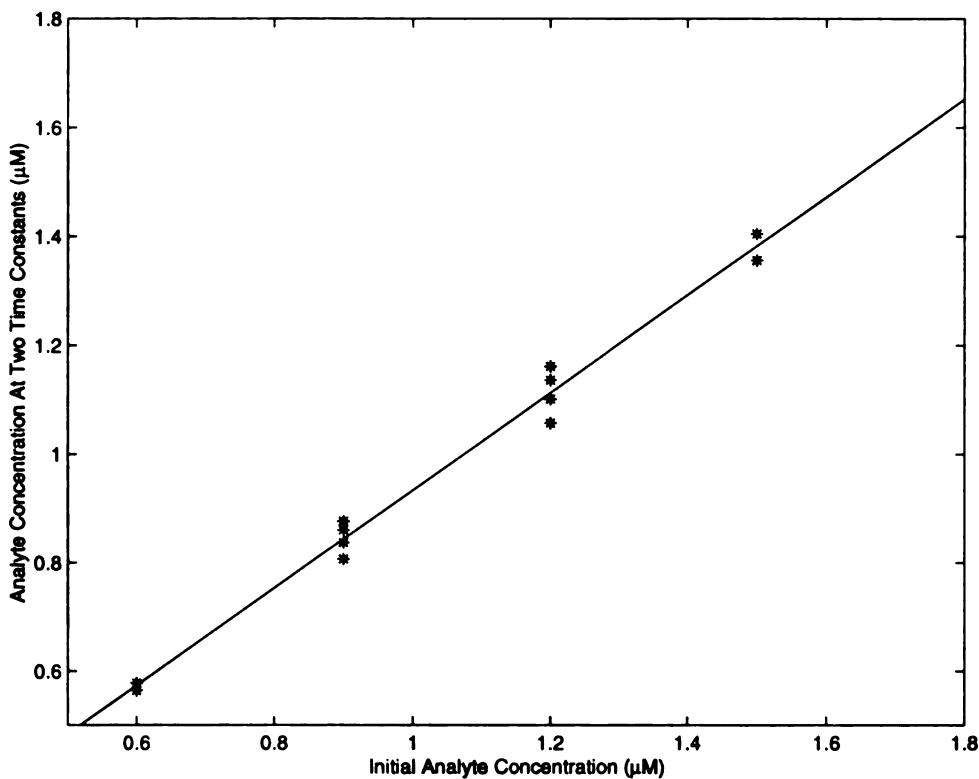


**Figure 5-2: Example of a nonlinear kinetic system. This data was generated with a rate constant ratio of 1.7 and a kinetic angle of 10.2. The reagent was in 1.4 fold excess. The angle from linearity was 6.449.**

### 5.1.2. Solution Preparation

Solutions of Ni(II) and Ga(III) were made in a pH 8.5 borate buffer as described in chapter 4. Solutions of PAR at concentrations of 1 mM and 40 μM were also made in the same buffer. The solutions prepared were positioned in the concentration space of the analytes as shown in Figure 5-3

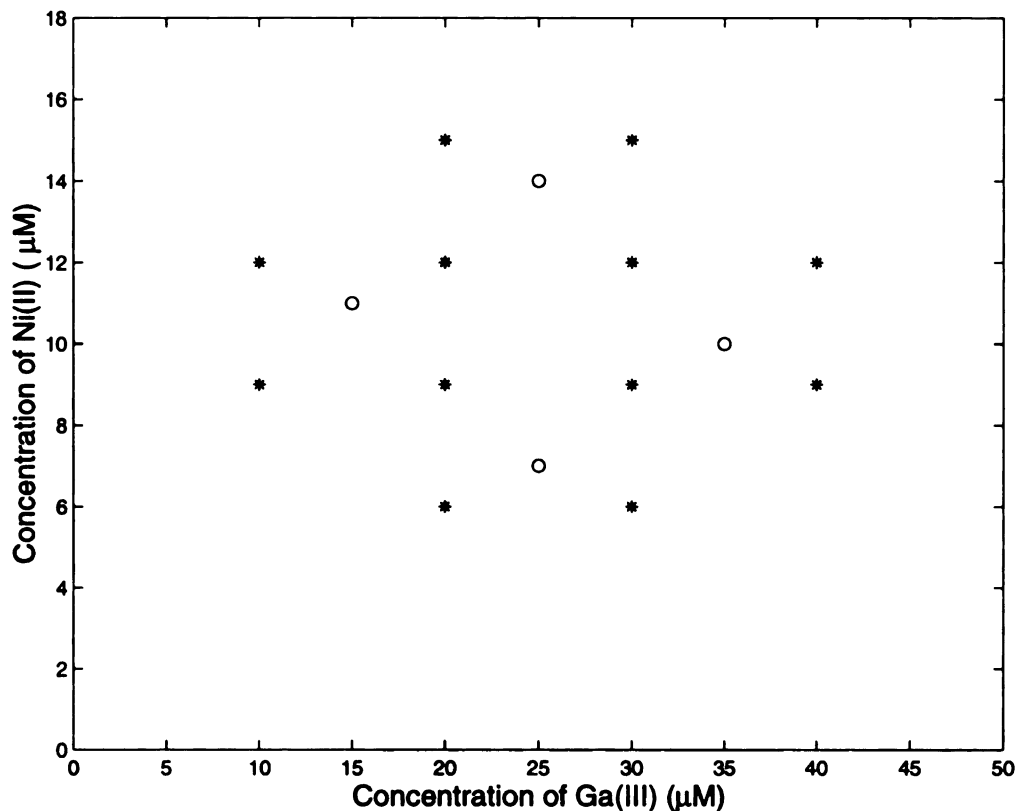


**Figure 5-3: Concentrations of calibration (stars) and unknown (open circles) samples used for the kinetic-spectrophotometric determinations of Ga(III) and Ni(II) under linear and nonlinear kinetic conditions.**

### 5.1.3. Kinetic-spectrophotometric Data Collection

Data were collected using the stopped-flow apparatus and diode array detector as described in chapter 4. One hundred spectra were acquired; the rate at which spectra were acquired was dependent on the concentration of the PAR. For the 1 mM PAR, 100 spectra were acquired over a period of 50 seconds; when the 40 µM PAR solution was used 100 spectra were acquired over a period of 200 seconds. For this study, a wavelength range of 500-550 nm was empirically

chosen. Absorbances were measured at 64 equally-spaced wavelengths in this range.

#### **5.1.4. Data processing**

Time-dependent spectra were collected in triplicate and averaged, i.e., each metal ion solution was reacted with PAR three times. The resulting three sets of kinetic-spectrophotometric data were averaged. Data were mean-centered before being input to the appropriate algorithms. Multivariate calibration algorithms provided in the PLS\_TOOLBOX (Eigenvector Technologies, Manson, WA.) and run in MATLAB were used to perform determinations.

## **5.2. SIMULATION STUDIES INVOLVING SYSTEMS WITH NONLINEAR KINETICS**

Detailed simulation studies that explored the effect of nonlinear kinetics on the accuracy of predictions generated by an array of chemometric techniques were conducted. Two limiting cases were considered. In the first, the synthetic spectra described in chapter 3 were used to generate data; in these spectra the reagent does not absorb. The second case was one where the reagent does absorb. These used the Ga(III)-PAR / Ni(II)-PAR spectra which were also used in the studies described in chapter 3.

### **5.2.1. Systems where the reagent does not absorb**

In the case where the reagent does not absorb, the only effect of kinetic nonlinearity is the type of effect seen in figure 5-2. The slower analyte is slightly more affected by the nonlinearity, as the faster analyte consumes some of the

reagent before the slower analyte has reacted to any appreciable extent. This effect is exaggerated at high kinetic angles where the difference between the reaction rates of the analytes is larger and the faster analyte consumes more of the reagent before the slower analyte begins to react.

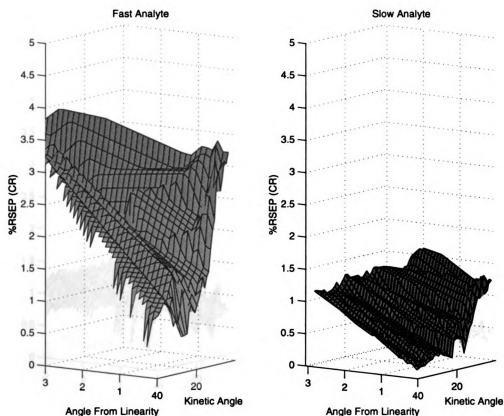


**Figure 5-4: Relative standard error of a CR prediction as a function of the kinetic angle and angle from linearity.**

Figure 5-4 shows the effect of kinetic angle and angle from linearity on the accuracy of a CR prediction. Error of prediction increases as the angle from linearity increases and kinetic angle decreases. The concentration of the slower analyte is predicted more accurately; this is expected, as when the determination is

limited by kinetic information the slower analyte is favored by the reaction scheme (see chapter 3). The spectral angle is low (8.6), and so the effects of the kinetic angle can easily be seen. The angle from linearity has a much larger effect at high kinetic angle than low ones (for the reasons already discussed).

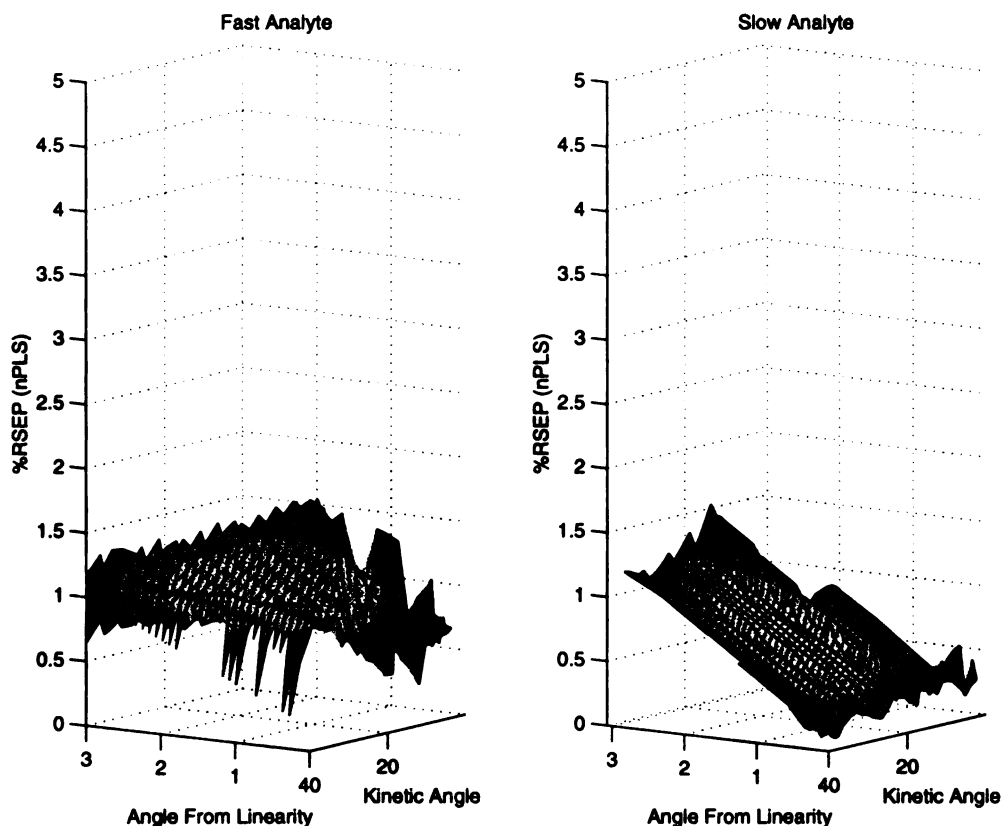


**Figure 5-5: Relative standard error of an nPLS prediction as a function of the kinetic angle and angle from linearity**

Figure 5-5 shows the response of multiway PLS to the same conditions depicted in figure 5-4. Here, it can be seen that the slower analyte is more affected by kinetic non-linearity, especially at high kinetic angles. It can also be seen through comparison with Figure 5-5 that multiway PLS produces more accurate

predictions than do the multivariate calibration techniques (of which CR is the best).

At a constant (low) kinetic angle the interaction of spectral angle with kinetic nonlinearity can be demonstrated.

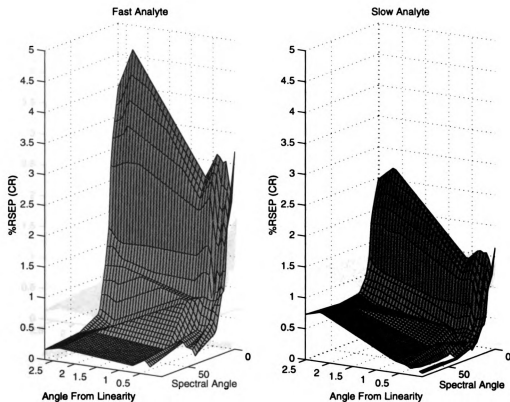


**Figure 5-6: Relative standard error of a CR prediction as a function of the spectral angle and angle from linearity. The kinetic angle for this data was  $\sim 10^\circ$ .**

In figure 5-6, it can be clearly seen that at high spectral angles kinetic nonlinearity has little affect on the accuracy with which multivariate calibration techniques can predict the concentration of the faster analyte. The prediction of the slower analyte is more strongly impacted by the angle from linearity. At low



spectral angles, the kinetic information becomes important, and the slower analyte is predicted with greater accuracy. The increase in error of prediction with increasing angle from linearity can be seen for both analytes.

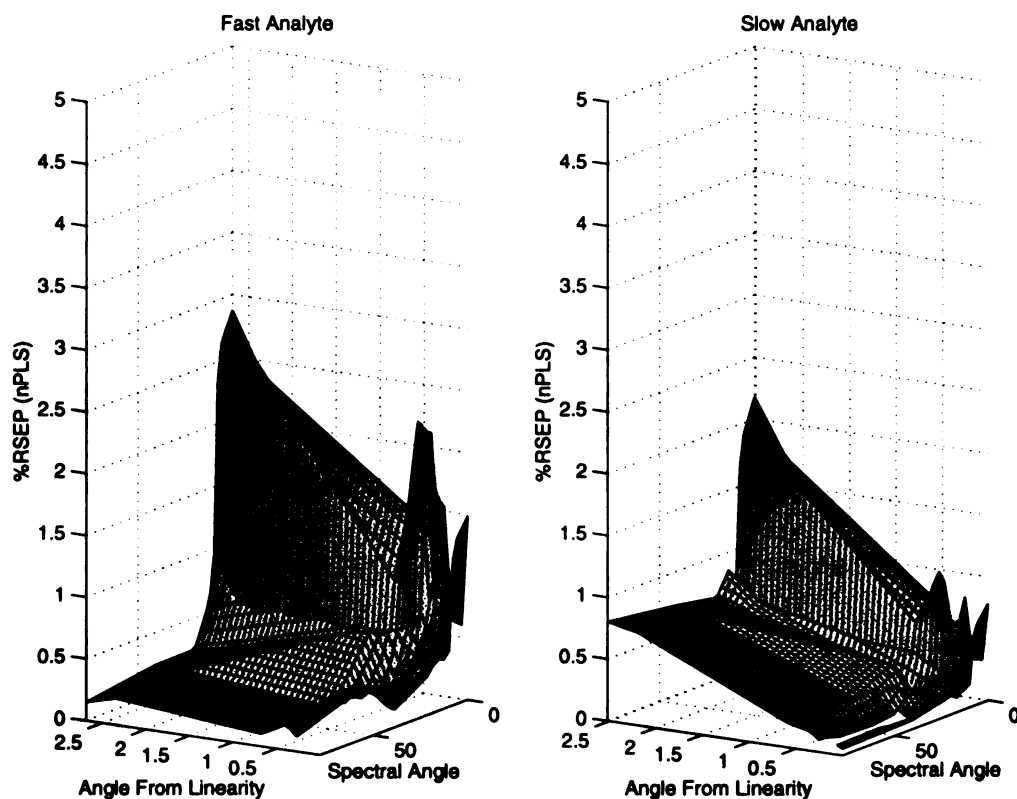


**Figure 5-7: Relative standard error of an nPLS prediction as a function of the spectral angle and angle from linearity. The kinetic angle for this data was  $\sim 10^\circ$ .**

Figure 5-7 depicts the response of multiway PLS to various spectral angles and angles from linearity. The same general trends described above are visible in these plots, but it is apparent that the errors of prediction are lower. Again, multiway PLS proves superior to traditional multivariate calibration techniques.

### **5.2.2. Systems where the reagent does absorb**

When the reagent absorbs in the spectral region of interest the effect of kinetic nonlinearity is complicated. In addition to a nonlinear relationship between initial and fixed-time analyte concentrations, the non-constant reagent concentration contributes a time-dependent rather than a constant spectral background. This effect becomes more pronounced as the reaction proceeds and the reagent is consumed. This results in less accurate determinations of the slower analyte, especially at high rate constant ratios where the faster reactant has used more of the reagent before the slower analyte has reacted to any appreciable degree. Figure 5-8 shows the results of a CR prediction for a system with the gallium-nickel spectra described in chapter 3. The determination of the faster analyte is not greatly affected by decreasing kinetic angle or reagent excess. The determination of the slower analyte, however, suffers loss of accuracy as the reagent excess decreases, especially at high rate constant ratios (kinetic angles).

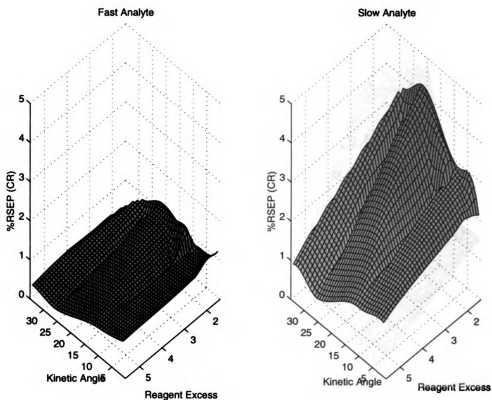


**Figure 5-8: Relative standard error of a CR prediction as a function of the kinetic angle and reagent excess. The gallium/nickel/PAR spectra (with the PAR absorbing) were used to generate the data. The spectral angle for this data was  $\sim 11^\circ$ .**

Figure 5-9 shows the results of applying nPLS to the same data used for Figure 5-8. In general, nPLS seems more adversely affected by increasing non-linearity than does CR.

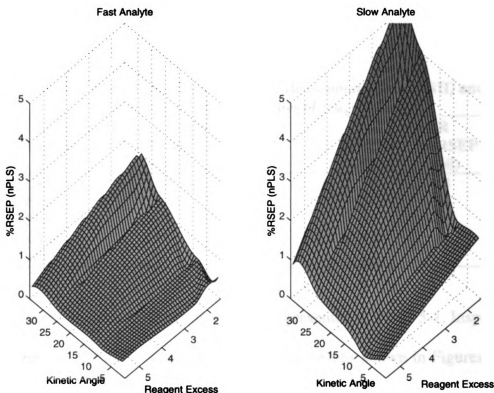


**Figure 5-9: Relative standard error of an nPLS prediction as a function of the kinetic angle and reagent excess. The gallium/nickel/PAR spectra (with the PAR absorbing) were used to generate the data. The spectral angle for this data was  $\sim 11^\circ$ .**

### **5.3. DETERMINATION OF GALLIUM (III) AND NICKEL (II) IN A SYSTEM WITH NONLINEAR KINETICS**

A determination of Ga(III) and Ni(II) was carried out as described in sections 5.1.2 through 5.1.4. The degree of nonlinearity was determined by varying the concentration of PAR. Two PAR concentrations were used. At the higher concentration (1.0 mM) there is an average reagent excess of 28.1 fold. Here the excess of reagent is calculated by dividing the PAR concentration by the

average sum of the analyte concentrations. At the lower PAR concentration (40  $\mu\text{M}$ ) the PAR is present in 1.2 fold excess.

**Table 5-1: Kinetic-spectrophotometric determination of Ga(III) and Ni(II) with two different values of reagent excess**

Method	1.0 mM PAR		40 $\mu\text{M}$ PAR	
	% RSEP (Ga)	% RSEP (Ni)	% RSEP (Ga)	% RSEP (Ni)
CR	19	4	28	4
PCR	19	6	34	4
PLS	19	4	43	6
MLR	26	14	56	4
nPLS	21	5	49	4

The results of these determinations are presented in Table 5-1. Inspection of the data reveals that, as is expected based on the results shown in Figures 5-8 and 5-9, the determination of Ni(II) is not affected by the change in PAR concentration. The determination of Ga(III) is more strongly affected by the kinetic nonlinearity present in the data due to the lower PAR concentration.

Figures 5-10 and 5-11 show the results of predictions using CR. As in chapter 4, the solid center line in these plots represents a perfect prediction (a slope of unity). The two dashed lines represent 10% error limits.

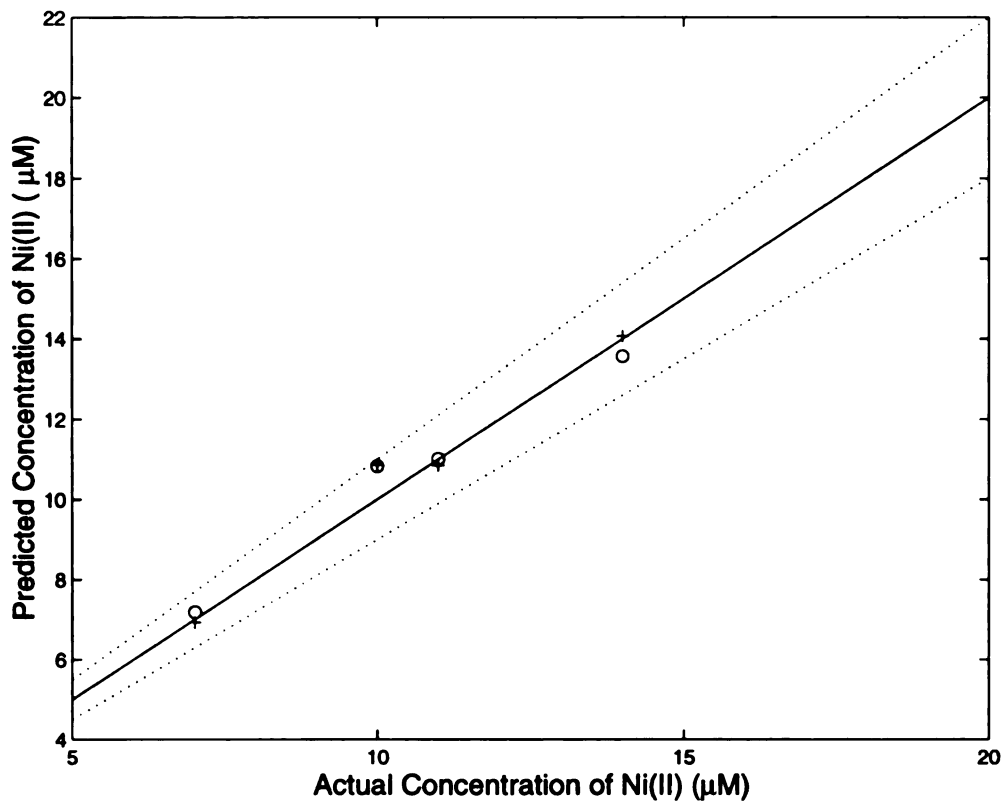


**Figure 5-10: CR determination of Ni(II) by reaction with 1mM PAR (circles) and 40 μM PAR (plus signs). At the PAR concentration of 1mM the average excess is 28 fold; at 40 μM it is 1.2 fold.**

Figure 5-10 depicts the prediction of nickel. The plot clearly shows that the prediction is largely unaffected by the kinetic nonlinearity.

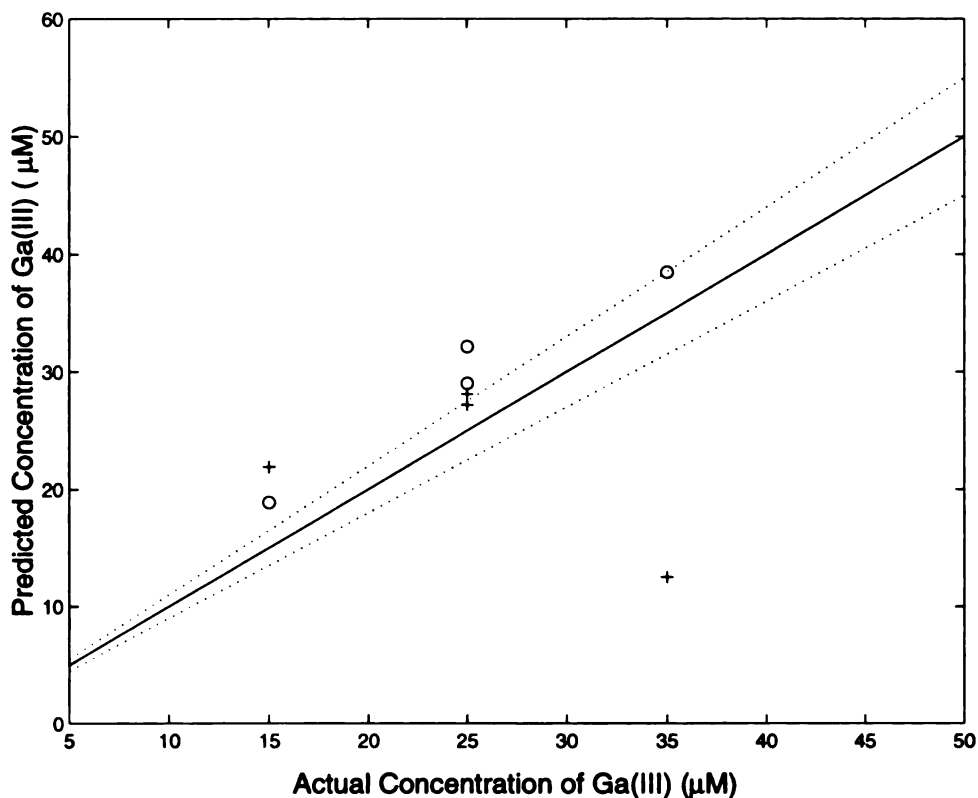


**Figure 5-11: CR determination of Ga(III) by reaction with 1mM PAR (circles) and 40 µM PAR (plus signs). At the PAR concentration of 1mM the average excess is 28 fold; at 40 µM it is 1.2 fold.**

In Figure 5-11 the results of the prediction of Ga(III) can be seen. The overall error is large (28%, see table 5-1), but three of the four unknown samples are predicted well. The fourth, with the highest concentration of Ga(III), is predicted quite poorly. The PAR is not in excess for this sample, and so the prediction fails. This result is of extreme interest, as it shows that reagent excesses of just a single fold are sufficient for accurate determinations and that only when the reagent is the limiting reactant does the kinetic-spectrophotometric determination fail. This is important, as it reveals that large excesses of extremely

high absorptivity reagents in order to ensure pseudo-first order conditions are not necessary. This, then, is perhaps one of the most compelling and powerful arguments for the use of multivariate calibration techniques for kinetic and kinetic-spectrophotometric determinations.

#### **5.4. REFERENCES**

- (1) Schechter, I.; Schroder, H. "Error-compensated kinetic determinations in systems of mixed 1st-order and 2nd-order reactions, without prior knowledge of reaction constants" *Anal. Chem.* **1992**, *64*, 325-329.
- (2) Schechter, I. "Simultaneous determination of mixtures by kinetic-analysis of general-order reactions" *Anal. Chem.* **1992**, *64*, 729-737.
- (3) Blanco, M.; Coello, J.; Iturriaga, H.; Maspoch, S.; Redon, M. "Artificial neural networks for multicomponent kinetic determinations" *Anal. Chem.* **1995**, *67*, 4477-4483.
- (4) Blanco, M.; Coello, J.; Iturriaga, H.; Maspoch, S.; Redon, M. "Partial least-squares regression for multicomponent kinetic determinations in linear and nonlinear-systems" *Anal. Chim. Acta* **1995**, *303*, 309-320.
- (5) Blanco, M.; Coello, J.; Iturriaga, H.; Maspoch, S.; Redon, M.; Villegas, N. "Artificial neural networks and partial least squares regression for pseudo-first-order with respect to the reagent multicomponent kinetic-spectrophotometric determinations" *Analyst* **1996**, *121*, 395-400.
- (6) Ventura, S.; Silva, M.; Perez-Bendito, D.; Hervas, C. "Computational neural networks in conjunction with principal component analysis for resolving highly nonlinear kinetics" *J. Chem. Inf. Comput. Sci.* **1997**, *37*, 287-291.



## CHAPTER 6

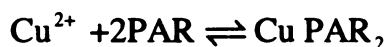
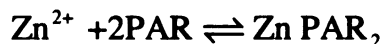
### DETERMINATION OF Zn(II) AND Cu(II) IN A DRINKING WATER SAMPLE

*Do, or do not. There is no try.*

--George Lucas: The Empire Strikes Back (Yoda)

The determination of zinc (II) and copper (II) in a standard drinking water sample was carried out using their reaction with PAR. Good accuracy was achieved in spite of the presence of interfering species.

Both Zn(II) and Cu(II) react with PAR according to a 1:2 stoichiometry<sup>1</sup>:



The determination of zinc and copper in environmental and clinical samples is of some importance<sup>2</sup>. While both metals are essential in small concentrations, they are toxic at higher concentrations<sup>2</sup>. The EPA has set limits of 1.3 ppm for copper in drinking water<sup>3</sup> and 5 ppm for zinc in drinking water<sup>3</sup>.

The use of PAR as a spectrophotometric reagent for the determination of copper and zinc has been reported in the literature<sup>4-13</sup>. Other workers have described the determination of zinc or copper using a chromatographic separation and either a pre-concentration step involving PAR or

a post-column reaction with PAR<sup>14-23</sup>. There have been a few reports of kinetic determinations of copper or zinc using PAR as a reagent<sup>20,24,25</sup>.

## 6.1. EXPERIMENTAL

The sample in which the Zn(II) and Cu(II) were determined was purchased from NSI Solutions, Inc. (Research Triangle Park, NC). It contained a mixture of 11 metal cations in a standard drinking water matrix. These metals were certified to be present in the following concentrations:

**Table 6-1**  
**Certified concentrations (ppb) of metal cations in a drinking water sample**

<b>Metal</b>	<b>Certified Concentration (ppb)</b>	<b>Certified Concentration <math>\mu</math>M</b>
Arsenic	113	1.5
Beryllium	5.17	0.6
Cadmium	15.4	0.1
Chromium	103	2.0
Copper	834	13.1
Lead	69.4	0.3
Manganese	222	4.0
Mercury	10.3	0.05
Nickel	246	4.2
Selenium	23.2	0.3
Zinc	1130	17.3

Of these metals, all but arsenic, beryllium and selenium will react with PAR<sup>1</sup>.

### 6.1.1. Solution Preparation.

All solutions were prepared with distilled water and reagent grade chemicals. A buffer of pH 8.5 was prepared from sodium borate and adjusted with nitric acid. All working solutions were prepared in this buffer, though some concentrated stock solutions were made in water and then diluted with buffer.

Twelve calibration mixtures in the micromolar concentration range were prepared from 1 mM stock solutions of the metal nitrates. The Cu(II) concentration was varied between 11 and 17  $\mu\text{M}$ ; the Zn(II) concentration ranged from 15 to 21  $\mu\text{M}$ . These were mixed and reacted in the stopped-flow system with a solution of 100  $\mu\text{M}$  PAR in pH 8.5 buffer. A plot of the calibration set in concentration space is given in figure 6-1.

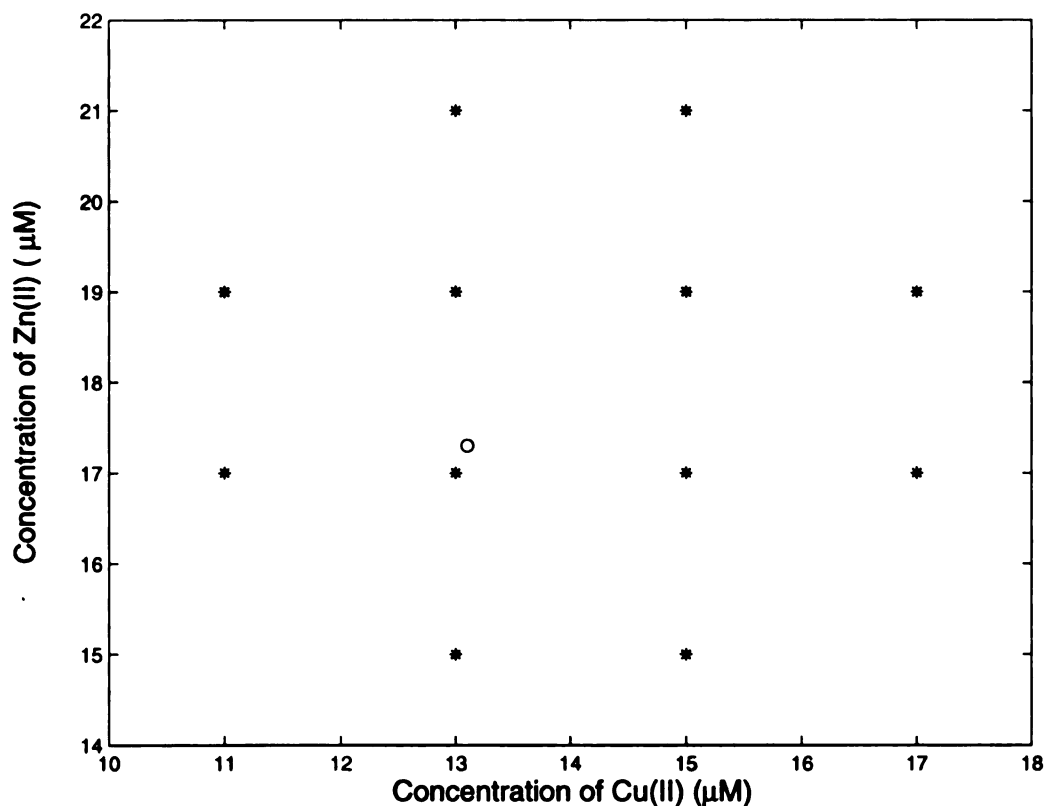


**Figure 6-1: Calibration set (stars) used in the determination of Zn(II) and Cu(II). The unknown sample is depicted by an open circle.**

### **6.1.2. Kinetic-spectrophotometric Data Collection**

Data were collected using a home-built stopped-flow apparatus interfaced to a thermoelectrically cooled Tracor Northern (Model TN-6123) 512 element intensified diode array (Tracor Northern, Philadelphia, PA) configured to acquire spectra in the 400-800 nm range as described in chapter 2.

In the wavelength range of interest (500-550 nm), absorbance was measured at 64 equally-spaced wavelengths. Kinetic information was obtained by acquiring 22 spectra at a rate of 10.5 spectra per second for a total acquisition time of 2.0 seconds. The spectra and kinetics of the analytes and their reaction products are described in detail later in this chapter.

### **6.1.3. Data processing**

Time dependent spectra were collected in quadruplicate and averaged, i.e., each metal ion solution was reacted with PAR four times. The resulting four sets of kinetic-spectrophotometric data were averaged. Data were mean-centered (as described in chapter 3) before being input to the appropriate algorithms. Multivariate calibration algorithms provided in the PLS\_TOOLBOX (Eigenvector Technologies, Manson, WA) and run in MATLAB were used to perform determinations.

## **6.2. DETERMINATION OF ZINC (II) AND COPPER (II)**

Zn(II) and Cu(II) were determined in both a standard drinking water sample and in a series of synthetic unknown samples. Ni(II) and Mn(II) were the major interfering species in the drinking water unknown and so these were added to the

calibration set solutions, and to several of the synthetic unknowns. The calibration samples were all 4.0  $\mu\text{M}$  in Mn(II) and 4.2  $\mu\text{M}$  in Ni(II). The concentrations of the analytes and the levels of the interferents present in each unknown sample are given in Table 6-2.

**Table 6-2**  
**Concentrations of analytes and interferents in the unknown samples in  $\mu\text{M}$  units**

	Drinking Water	Synthetic Unknown #1	Synthetic Unknown #2	Synthetic Unknown #3
<b>Cu</b>	13.1	13.1	13.1	13.1
<b>Zn</b>	17.3	17.3	17.3	17.3
<b>Mn</b>	4.0	4.0	13.1	4.0
<b>Ni</b>	4.2	--	--	4.2
<b>Cd</b>	0.1	--	--	--
<b>Cr</b>	2.0	--	--	--
<b>Pb</b>	0.3	--	--	--
<b>Hg</b>	0.05	--	--	--

The results of the determination of Cu(II) and Zn(II) in each of these samples are summarized in Table 6-3.

**Table 6-3**  
**Results of the determination of Cu(II) and Zn(II) in a series of unknown samples**

	Drinking Water		Synthetic Unknown #1		Synthetic Unknown #2		Synthetic Unknown #3	
Method	% RSEP (Cu)	% RSEP (Zn)	% RSEP (Cu)	% RSEP (Zn)	% RSEP (Cu)	% RSEP (Zn)	% RSEP (Cu)	% RSEP (Zn)
<b>PLS</b>	6	6	11	3	14	2	7	3
<b>PCR</b>	6	6	11	3	13	2	6	3
<b>MLR</b>	1	4	9	1	9	3	9	3
<b>CR</b>	5	1	11	3	14	2	11	1
<b>Parafac</b>	5	3	21	2	27	2	19	5
<b>nPLS</b>	6	6	11	3	14	2	7	3

The EPA has designated acceptance limits for the determination of Cu(II) and Zn(II) in the drinking water sample. The acceptable range for the determination of copper is  $\pm 9.8\%$  error. Acceptable determinations of zinc have

errors not larger than  $\pm 7.98\%$ . All of the chemometric techniques used produced predicted analyte concentrations of acceptable accuracy. Copper was determined with an error of approximately 5%; zinc with an error of 3-6%. Both are well within the EPA guidelines.

The presence of the interferents had little effect on the determination. In the second synthetic unknown, the manganese concentration is more than three times its level in the calibration set. The accuracy with which the analytes were predicted is only slightly worse (e.g., 14% vs. 11% error for the CR determination of copper) than it is for the first synthetic unknown. In the third synthetic unknown, which has the interfering species present in the same concentrations as the calibration set, the analytes are determined with better accuracy (an average decrease of 1-3% relative error compared to the first synthetic unknown). The calibration step compensates for the analytical signal due to the interfering species, and so the third unknown is least affected by the interferents. The other two synthetic unknowns are missing Ni(II) (see Table 6-2) , and so are not well described by the calibration set, which does contain nickel.

In all cases, zinc is determined more accurately than is copper; the error with which Zn(II) is determined is generally half to one third that of Cu(II) (see Table 6-3). This can be explained by examining the spectral and kinetic contributions to the net analyte signal for each analyte. As a first step, the spectra of the analytes (or specifically, of their reaction products with PAR) can be compared.

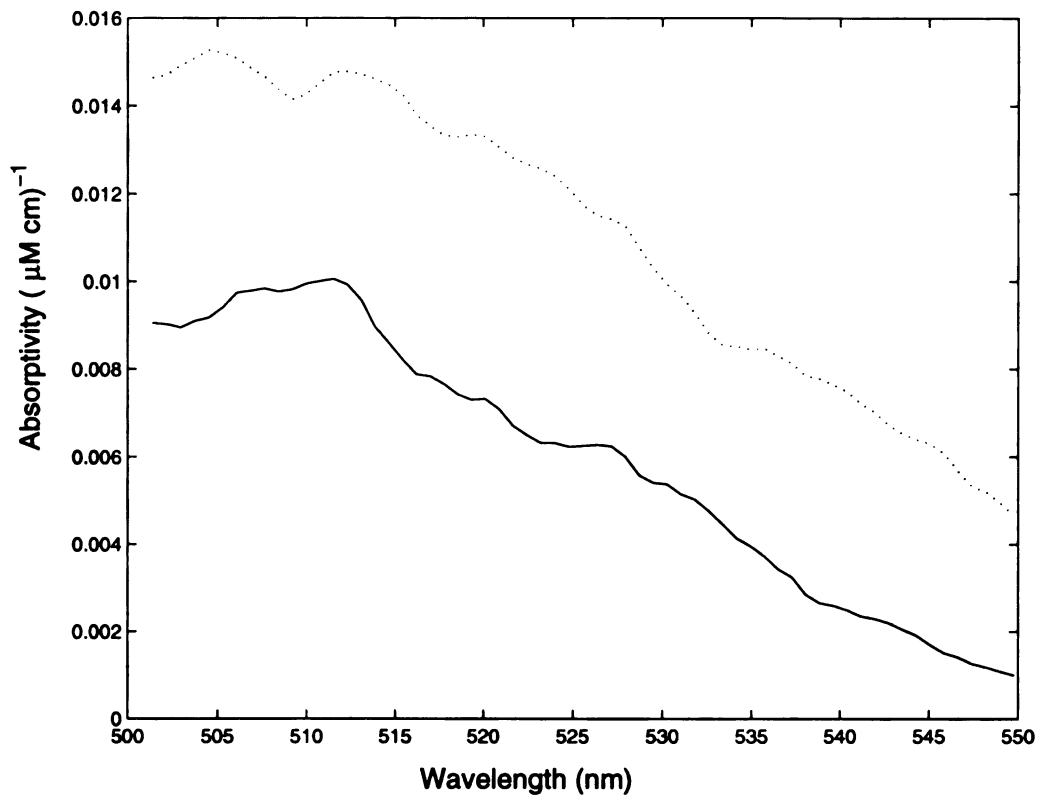


**Figure 6-2: Spectra of the PAR complexes of Zn(II) and Cu(II). The zinc complex is shown as a solid line, the copper complex as a dotted line.**

The spectral angle can be computed to be 17.1, a sufficiently high value to suggest that a reasonable determination might be attempted. The spectral net analyte signals reveal that zinc is likely to be more accurately predicted than copper; zinc's spectral net analyte signal is 5.8 times larger than copper's. This is true because although the copper complex has a higher molar absorptivity, zinc is present in a high concentration.

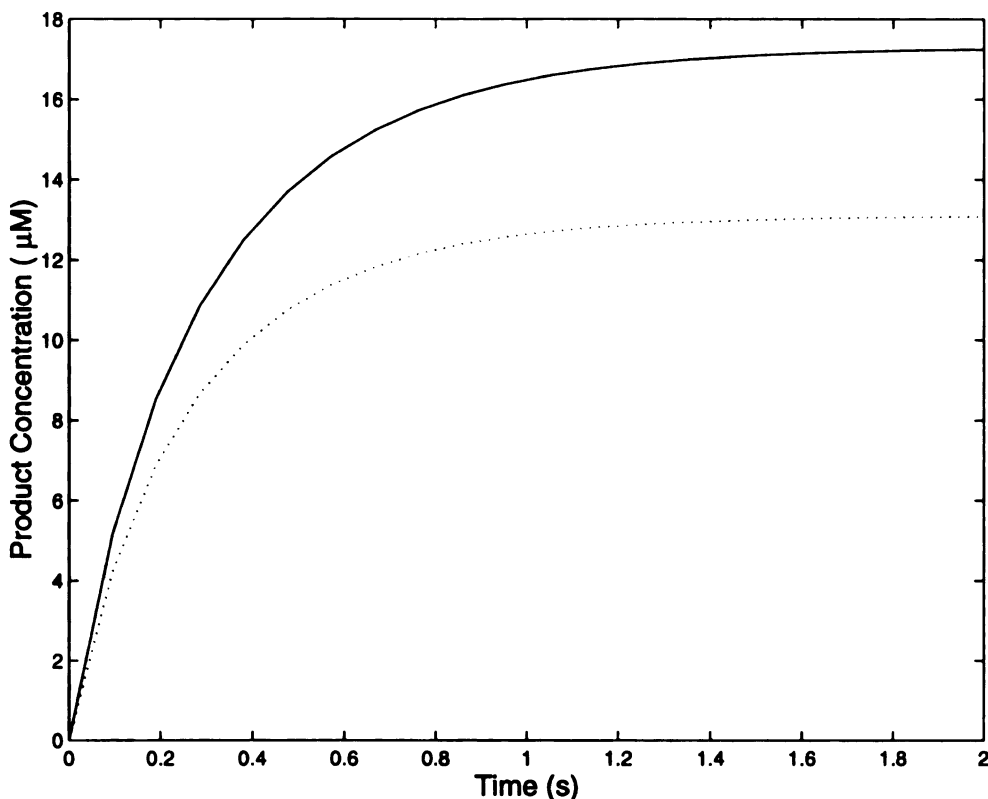


**Figure 6-3: Kinetic profiles of the formation of the PAR complexes of Zn(II) and Cu(II). The zinc complex is shown as a solid line, the copper complex as a dotted line.**

The kinetics of the reactions under the conditions in which the drinking water sample were determined are shown in Figure 6-3. The rate constants for the two reactions are very close; the ratio of the rate constants is 1.1, and the kinetic angle is 2.4. The kinetic data provides slightly more information about the slower reaction of zinc with PAR; zinc's kinetic net analyte signal is 1.3 times larger than copper's. Since zinc has both a larger kinetic and spectral net analyte signal, it is not surprising that it is determined with greater accuracy (usually between half and a third the error of the copper determinations—see Table 6-3).



### 6.3. REFERENCES

- (1) Shibata, S., "2-Pyridylazo compounds in analytical chemistry", in *Chelates in Analytical Chemistry*; Flaschka, H. A., Barnard, A. J., Jr, Eds.; Marcel Dekker: New York, 1972; Vol. 4.
- (2) Lobinski, R.; Marczenko, Z. *Spectrochemical Trace Analysis for Metals and Metalloids* Wilson and Wilson's Comprehensive Analytical Chemistry, ; Elsevier: New York, 1996.
- (3) Environmental Protection Agency Office of Ground Water and Drinking Water, "Technical Drinking Water and Health Contaminant Fact Sheets" [Online] Available <http://www.epa.gov/OGWDW/dwh/t-ioc/zinc.html>, 1999
- (4) Bobrowska Grzesik, E.; Grossman, A. M. "Derivative spectrophotometry in the determination of metal ions with 4-(pyridyl-2-azo) resorcinol (PAR)" *Fresenius J. Anal. Chem.* **1996**, *354*, 498-502.
- (5) Engstrom, E.; Jonebring, I.; Karlberg, B. "Assessment of a screening method for metals in seawater based on the non-selective reagent 4-(2-pyridylazo)resorcinol (PAR)" *Anal. Chim. Acta* **1998**, *371*, 227-234.
- (6) Fernandez deCordova, M. L.; Molina Diaz, A.; Pascual Reguera, M. I.; Capitan Vallvey, L. F. "Determination of Trace Amounts of Copper With 4-(2- Pyridylazo)Resorcinol By Solid-Phase Spectrophotometry" *Fresenius J. Anal. Chem.* **1994**, *349*, 722-727.
- (7) Gomez, E.; Estela, J. M.; Cerda, V.; Blanco, M. "Simultaneous spectrophotometric determination of metal-ions with 4-(Pyridyl-2-Azo)Resorcinol (PAR)" *Fresenius J. Anal. Chem.* **1992**, *342*, 318-321.
- (8) Kolomiets, L. L.; Pilipenko, L. A.; Zhmud, I. M.; Panfilova, I. P. "Application of derivative spectrophotometry to the selective determination of nickel, cobalt, copper, and iron(III) with 4- (2-pyridylazo)resorcinol in binary mixtures" *J. Anal. Chem.* **1999**, *54*, 28-30.
- (9) Manouri, O. C.; Papadimas, N. D.; Salta, S. E.; Ragos, G. C.; Demertzis, M. A.; Issopoulos, P. B. "Three approaches to the analysis of zinc(II) in pharmaceutical formulations by means of different spectrometric methods" *Farmaco* **1998**, *53*, 563-569.

- (10) Molina, M. F.; Nechar, M.; Bosque-Sendra, M. "Determination of zinc in environmental samples by solid phase spectrophotometry: Optimization and validation study" *Analytical Sciences* **1998**, *14*, 791-797.
- (11) Ni, Y. N. "Trace-metal determinations by spectrophotometry with a double chromogenic system and a chemometric approach" *Anal. Chim. Acta* **1993**, *284*, 199-205.
- (12) Pollak, M.; Kuban, V. "Comparison of spectrophotometric methods of determination of Zinc(II) in biological-material and study of its complex-formation reactions with 4-(2-Pyridylazo)Resorcinol" *Collection of Czechoslovak Chemical Communications* **1979**, *44*, 725-741.
- (13) Ren, S. X.; Gao, L. "Simultaneous spectrophotometric determination of copper(II), lead(II) and cadmium(II)" *Journal of Automatic Chemistry* **1995**, *17*, 115-118.
- (14) Al-Shawi, A. W.; Dahl, R. "The determination of cadmium and six other heavy metals in nitrate phosphate fertilizer solution by ion chromatography" *Anal. Chim. Acta* **1999**, *391*, 35-42.
- (15) Cardellicchio, N.; Dell'Atti, A.; Giandomenico, S.; Di Leo, A.; Cavalli, S. "Determination of transition metals in mineral waters by ion chromatography and spectrophotometric detection" *Annali Di Chimica* **1998**, *88*, 819-827.
- (16) Cardellicchio, N.; Cavalli, S.; Ragone, P.; Riviello, J. M. "New strategies for determination of transition metals by complexation ion-exchange chromatography and post column reaction" *J. Chromatogr. A* **1999**, *847*, 251-259.
- (17) Chakrapani, G.; Murty, D. S. R.; Mohanta, P. L.; Rangaswamy, R. "Sorption of PAR-metal complexes on activated carbon as a rapid preconcentration method for the determination of Cu, Co, Cd, Cr, Ni, Pb and V in ground water" *Journal of Geochemical Exploration* **1998**, *63*, 145-152.
- (18) de Jesus, D. S.; Casella, R. J.; Ferreira, S. L. C.; Costa, A. C. S.; de Carvalho, M. S.; Santelli, R. E. "Polyurethane foam as a sorbent for continuous flow analysis: Preconcentration and spectrophotometric determination of zinc in biological materials" *Anal. Chim. Acta* **1998**, *366*, 263-269.

- (19) Hardy, S.; Jones, P.; Riviello, J. M.; Avdalovic, N. "Construction and investigation of a post-capillary reactor for trace metal analysis by capillary electrophoresis" *J. Chromatogr. A* **1999**, *834*, 309-320.
- (20) Lucy, C. A.; Dinh, H. N. "Kinetics and equilibria of the Zn-EDTA-PAR postcolumn reaction detection system for the determination of alkaline-earth metals" *Anal. Chem.* **1994**, *66*, 793-797.
- (21) Nagaosa, Y.; Tanizaki, M. "Simultaneous determination of zinc(II) and iron(III) in human serum by liquid chromatography using post-column derivatization with 4-(2-pyridylazo)-resorcinol" *Journal of Liquid Chromatography & Related Technologies* **1997**, *20*, 2357-2366.
- (22) Shotyk, W.; Immenhauser Potthast, I. "Determination of Cd, Co, Cu, Fe, Mn, Ni and Zn in coral skeletons by chelation ion chromatography" *J. Chromatogr. A* **1995**, *706*, 167-173.
- (23) Vasconcelos, M. T.; Gomes, C. A. R. "Limitations of ion chromatography with postcolumn reaction for determination of heavy-metals in waters containing strong chelating-agents" *J. Chromatogr. A* **1995**, *696*, 227-234.
- (24) Cladera, A.; Gomez, E.; Estela, J. M.; Cerda, V.; Cerda, J. L. "Computer method for the simultaneous kinetic determination of compounds in mixtures based on the use of diode-array spectrophotometry" *Anal. Chim. Acta* **1993**, *272*, 339-344.
- (25) Taljaard, R. E.; van Staden, J. F. "Simultaneous determination of cobalt(II) and Ni(II) in water and soil samples with sequential injection analysis" *Anal. Chim. Acta* **1998**, *366*, 177-186.

## CHAPTER 7

### CONCLUSIONS AND FUTURE PERSPECTIVES

*Data without generalization is just gossip.*  
--Robert Pirsig

The preceding chapters have described the application of chemometric data processing techniques to kinetic-spectrophotometric data under a variety of circumstances. In this chapter, the work as a whole is summarized, and thoughts on future work are presented.

#### 7.1. CONCLUSIONS AND SUMMARY

Chapter one presents a fairly detailed overview of the fields of chemometrics and kinetics as applied to analytical chemistry and highlights the application of chemometric techniques to kinetic data. Multivariate calibration algorithms are described in detail; some attention is given to artificial neural networks, multiway algorithms, and other techniques as well.

A new data acquisition system was designed and built. This redesign of the existing system involved the fabrication of a new optical path for the stopped-flow apparatus as well as the creation of a new computerized interface for the diode array detection system. The new system was characterized; the results of this characterization and the details of the new designs are found in chapter two. The

redesign of the system made possible the collection of the kinetic-spectrophotometric data analyzed in the remaining chapters.

In chapter three the results of a series of simulated experiments are described. In these simulation studies the effect of an array of experimental variables on the accuracy of a kinetic-spectrophotometric determination of a two component mixture are explored. Methods for quantifying the amount of kinetic and spectral information present in kinetic-spectrophotometric data were discussed. The kinetic and spectral angles were introduced and shown to be good measures of the quantity of information available in each dimension. Kinetic and spectral net analyte signals were also developed and were shown to be good predictors of the relative accuracy with which analytes can be determined. Simply put, the kinetic and spectral angles allow prediction of the general feasibility of a determination and the dimension (kinetic or spectral) that will be relied upon most heavily. From these data and the net analyte signals it is possible to infer which analyte will be determined most accurately. As an example, the case of gallium and nickel discussed in chapter four can be cited. The kinetic and spectral angles make it clear that spectral information is more heavily relied upon than kinetic in this case. Thus, although gallium has a higher kinetic net analyte signal, nickel's greater spectral net analyte signal indicates that it will be determined more accurately. This indeed is the result of both the simulated and experimental determinations.

The kinetic angle was shown to have several contributing factors. The ratio of the analyte rate constants is the largest contributor, but the fraction of the slower reaction for which data is acquired and the number of spectra acquired also impact the kinetic angle.

Chapter four describes the determination of Ga(III) and Ni(II). In the studies discussed, the effect of the kinetic angle was explored experimentally; the determination was carried out at two different values of solution pH where the ratios of the reaction rate constants are different. The expected results were obtained; the determination was more accurate at the pH (8.5) where the kinetic angle was largest. A comparison was drawn between the various chemometric algorithms and it was found that continuum regression generally out-performed the other multivariate calibration techniques, but that partial least squares regression and principal component regression were nearly as good. PARAFAC was found to be useful only in limited circumstances, and multiway PLS showed an ability to compete with and often surpass the best of the multivariate calibration techniques when dealing with multiway data.

In chapter five the effect of kinetic non-linearity was examined. Causes of kinetic non-linearity were discussed and recent work in the area of kinetic determinations in nonlinear systems was highlighted. The degree of kinetic non-linearity was measured as an angle from linearity. This angle was shown to be a good predictor of the accuracy with which a determination could be performed. The degree of non-linearity was varied in a series of simulations. In general, it was

found that the techniques used were fairly tolerant of nonlinear kinetics, but that at very large angles from linearity the determinations became inaccurate. Experimental studies in which the degree of linearity was varied were also described. In these studies Ga(III) and Ni(II) were determined under two sets of experimental conditions with varying degrees of non-linearity. The results obtained paralleled the simulations and were quite encouraging. Again, the various chemometric algorithms were compared, and similar results to those found in chapter three were obtained. Continuum regression and nPLS proved best suited to handling the nonlinear kinetic data.

Chapter six presents the determination of Cu(II) and Zn(II) in a real sample with clinical and environmental relevance. The accuracy of the determination was within the EPA's acceptance limits for both analytes. The kinetic and spectral angles and net analyte signals were used to explain the relative accuracy with which the analytes were determined.

## **7.2. REFLECTIONS ON FUTURE DIRECTIONS**

All of the work described in this document has focused on the determination of two analytes. The extension to three or more analytes is certainly logical, but also is highly challenging and will present many difficulties. Not least of these will be the need to develop new methods for quantifying the amount of kinetic and spectral information available. Ratios of rate constants and angles between profiles lose meaning when more than two analytes are present. Net analyte signals are better, but are still not capable of the necessary resolution. The

net analyte signals reveal the degree to which a profile (kinetic or spectral) is overlapped by other profiles, but do not reveal which specific profiles overlap the profile of interest; e.g., an analyte might be highly spectrally and kinetically overlapped, but by different species. In this situation, the net analyte signals will both be small, but the determination can still be accurately performed since the analyte is not overlapped in both dimensions by the same species. Other problems that will be encountered include the determination of an unoverlapped analyte in the presence of two other highly overlapped analytes, and the economics of scale associated with three-analyte calibration sets.

The trend in chemometrics is toward the wider use of multiway algorithms. As they become more popular, their use with multiway data will supercede the use of first order algorithms on unfolded multiway data. This has had and will continue to have an impact on the way in which data are collected and used. The use of multiway algorithms for kinetic-spectrophotometric data has been briefly explored in this work, and it is expected that it will continue to be an active area of study.

In 1993 Crouch<sup>1</sup> identified seven trends in kinetic methods of analysis. Several of these are relevant to the work discussed in this document. These trends are:

1. Increasing use of “intelligent automation”
2. Growing utilization of multidimensional instrumentation
3. Continuing development of sophisticated data processing techniques



4. Additional progress in error-compensation techniques
5. Innovations in multicomponent kinetic procedures
6. Expanding applications of kinetic determinations
7. Enlarging the kinetic approach to include miscellaneous time-dependent responses

The work in this thesis is testament to the continuation of trends 2, 3, 4, and 5. As the field of chemometrics continues to advance and to become more widely accessible and accepted, trend three will hold as new (at least to kinetics researchers) chemometric techniques are applied to kinetic data.

It is the contention of this author that wider accessibility of and familiarity with chemometric techniques and the proliferation of multidimensional instrumentation will eventually result in an increase in the number of analytical measurements employing kinetic or other time-dependent data. This is in accordance with the sixth and seventh trends listed above. As Crouch<sup>1,2</sup> and Mottola<sup>3</sup> have pointed out, most analytical methods involve some sort of kinetic or transient response. Often, great pains are taken to ensure that these time-dependent responses are avoided or that they are compensated for in the data processing. Modern multiway chemometric data processing options are able to correctly handle higher order data and can separate and make use of several data dimensions. This implies that time-dependent data can be used in almost all analytical measurements, resulting in increases in selectivity and (in many cases) sensitivity<sup>1,3-5</sup>. Some of the areas in which the transient data is already being

applied include luminescence lifetime spectroscopy, fluorescence lifetime imaging microscopy, sequential injection analysis and transient electroanalytical chemistry.

In all, the future of analytical chemistry appears bright. Greater computing power allows the acquisition of more data in more dimensions and grants the ability to use these data to perform more and better determinations. The field of kinetic methods will no doubt benefit from this trend, and the field of chemometrics will continue to grow. This thesis is but one example, a simple harbinger of this new direction and focus.

### **7.3. REFERENCES**

- (1) Crouch, S. R. "Trends in kinetic methods of analysis" *Anal. Chim. Acta* **1993**, 283, 453-470.
- (2) Crouch, S. R. "Kinetic methods of analysis - how do they rate" *J. Chin. Chem. Soc.* **1994**, 41, 221-229.
- (3) Mottola, H. A. *Some Kinetic Aspects of Analytical Chemistry* ; Wiley: New York, 1988.
- (4) Perez-Bendito, D.; Silva, M. *Kinetic Methods in Analytical Chemistry* ; Ellis Horwood: Chichester, 1988.
- (5) Perez-Bendito, D.; Silva, M. "Recent advances in kinetometrics" *Trac-Trends Anal. Chem.* **1996**, 15, 232-240.

## APPENDIX

## APPENDIX

### MATLAB CODE FOR GENERATING SIMULATED KINETIC-SPECTROPHOTOMETRIC DATA

*You think you know when you learn, are more sure  
when you can write, even more when you can teach,  
but certain when you can program.*

--Alan J. Perlis

*Anyone who considers arithmetical methods of  
producing random digits is, of course, in a state of sin.*

--John von Neumann

Code designed to generate simulated kinetic-spectrophotometric data was written in MATLAB's native programming language. The main program is *mulgen\_a.m*. This program calls several others.

*Mulgen\_a* begins by collecting the necessary information for the generation of simulated data. The user provides a matrix of absorptivities for each reactant, reagent, and product, a matrix of the initial concentrations of each reactant, the fraction of the slower reaction to observe, the initial reagent concentration, the desired levels of instrumental noise and rate constant fluctuation, and the number of spectra to generate.

The program then uses the variable *perrxn* (the input fraction of the slower reaction to observe), and calculates the time at which to cease "data acquisition."

It does this by making the initial, worst-case assumption that the faster reaction will have reached equilibrium by the time the slower reaction has had time to begin. Using this assumption, the time at which the slower reaction will have reached the desired fractional completion is calculated. Five hundred points are then generated for the parallel reaction of the two reactants with the reagent between zero and this calculated time. The time at which the concentration of the slower product reaches the threshold determined by the fraction of the reaction to be observed is noted, and 500 more points are generated between time zero and this new time. Again, the time at which the product concentration reaches the threshold level is found, and this time is used as the stopping time for the data generation in all future calculations.

The program proceeds to calculate the concentration of all species at all times in all samples. The absorptivities are then used to calculate the absorbance of each species, and these absorbances are summed to generate the final data matrix.

Calculations of the concentration of the reactants, reagent, and products at any time during the reaction are performed by the program *kinetic.m*. This program sets up and calls the MATLAB routines for numerically solving systems of ordinary differential equations. These routines require a model of the system that includes the differential equations to be solved. This model is supplied by the function *vary\_k.m*.

The code of *mulgen\_a.m*, *kinetic.m*, and *vary\_k.m* are found below.

## MULGEN\_A

```
function [signal,signal3,Dim_signal,tfinal] =...
    mulgen_a(absorbs,concentrations,perrxn,concr0,...
        noisek,noisei,pts)
% [signal,signal3,Dim_signal,tfinal] = ...
%     mulgen_a(absorbs,concentrations,perrxn,concr0,..
%         noisek,noisei,pts);
%
% generates absorbance data for a specified # of wavelengths
% over a specified time period. It uses the kinetic.m routine,
% and so can handle any kinetic system that can be modeled
% by ode45.
%
% Molar absorbtivities should be organized in columns:
%
%     eps1  eps2  ...  epsreagent  epsp1  epsp2  ...
%
% Concentrations should be also be arranged in columns.
%
%     comp1samp1 comp2samp1
%     comp1samp2 comp2samp2
%
%         .         .
%         .         .
%         .         .
%
% This version handles 2 components, any # of wavelengths, and
% any # of samples.
% It allows the user to input the amount of variation in the
% rate constants, the level of instrumental noise, and the
% percent completion of the slower reaction.
%
% It requires that k1 and k2 be declared as global variables
%
% The output "signal" is in the form:
%
%     s1w1t1  s1w2t1  s1w3t1 ...  s1w1t2  s1w2t2 ...
%     s2w1t1  s2w2t1  s2w3t1 ...  s2w1t2  s2w2t2 ...
%     s3w1t1  s3w2t1  s3w3t1 ...  s3w1t2  s3w2t2 ...
%
%         .         .         .         .         .
%         .         .         .         .         .
%         .         .         .         .         .
%
% The output "Dim_signal" is in the form:
%
%     [samples waves pts]
%
%
% The output "signal3" has each row as a time, each column as a
% wavelength, and each sample as a page.
%
```

```

%
%
%
% Created 9/20/95 by Tom Cullen
% Last Updated 6:04 PM 8/16/99 by Tom Cullen
%

%*****
% Get info from user
%*****
[samples,comp]= size(concentrations);
[waves,xcomp] = size(absorbs);

global k1
global k2

%*****
% Determine stopping time
%*****

[lowk,which_one_low]=min([k1,k2]);
[highk,which_one_high]=max([k1,k2]);
if k1==k2
    lowk=k2;
    highk=k1
    which_one_low=2;
    which_one_high=1;
end

medianconcs=median(concentrations);
medianconcl=medianconcs(which_one_high);
medianconcl2=medianconcs(which_one_low);
medianconcr=concr0-medianconcl-medianconcl2;

concratio=medianconcl./medianconcl2;
medianconcs=[medianconcl medianconcl2];
reagtextexcess=concr0 ./ (medianconcl+medianconcl2);

newtf=(-log(1-(perrxn)))/ ...
    (lowk*(concr0-medianconcs(which_one_high)));
[profile1,profile2,profiler] = ...
    kinetic(medianconcs,concr0,0,newtf,'vary_k',500);
if which_one_high==1
    slow_profile=profile2;
else
    slow_profile=profile1
end
times=linspace(0,newtf,500);
for i=1:500

```

```

        if slow_profile(i) < (1-perrxn)*medianconcs(which_one_low)
            newtf=times(i);
            break;
        end;
    end;
end;

[profile1,profile2,profiler] = ...
    kinetic(medianconcs,concr0,0,newtf,'vary_k',500);
if which_one_high==1
    slow_profile=profile2;
else
    slow_profile=profile1
end
times=linspace(0,newtf,500);
for i=1:500
    if slow_profile(i) < (1-perrxn)*medianconcs(which_one_low)
        newtf=times(i);
        break;
    end;
end;
tfinal=newtf;

%*****
% Expand scalar data into matrices... prepare other matrices
%*****

c01 = ones(samples,pts);
c02 = ones(samples,pts);
for i=1:pts
    c01(:,i) = concentrations(:,1);
    c02(:,i) = concentrations(:,2);
end;

k1_array = k1*ones(samples,pts);
k2_array = k2*ones(samples,pts);
k1_noisy_array = noise(k1_array,noisek);
k2_noisy_array = noise(k2_array,noisek);
k1_noise = abs(k1_array - k1_noisy_array);
k2_noise = abs(k2_array - k2_noisy_array);
noisesign = sign(rand(samples,pts));
time = linspace(0,tfinal,pts);
times = ones(samples,pts);
for i=1:samples
    times(i,:)=time;
end;

for s=1:samples
    for c = 1:comp
        eval(['con' int2str(c) '_' int2str(s) ' =...
            ones(waves,pts);'])
        eval(['comp' int2str(c) '_' int2str(s) ' =...

```



```

        ones(waves,pts);'])
    eval(['abs' int2str(c) '_' int2str(s) ' =...
        ones(waves,pts);'])
    eval(['absps' int2str(c) '_' int2str(s) ' =...
        ones(waves,pts);'])
end;
end;
absr = ones(waves,pts);

datapoints = waves*pts;
signal = ones(datapoints,samples);

%*****
% Calculate concentrations as a function of time
%*****

[profile1,profile2,profiler] =...
    kinetic(concentrations,concr0,0,tfinal,'vary_k',pts);
k1t_noise = exp(-k1_noise .* times .* profiler) .* noisesign;
k2t_noise = exp(-k2_noise .* times .* profiler) .* noisesign;
profile1 = profile1 .* k1t_noise;
profile2 = profile2 .* k2t_noise;
profiler = profiler .* k1t_noise .* k2t_noise;
profilep1 = c01 - profile1;
profilep2 = c02 - profile2;

for s=1:samples
    for c = 1:comp
        for i = 1:waves
            eval(['con' int2str(c) '_' int2str(s) '([i,:)=...
                profile' int2str(c) ' (s,:);'])
            eval(['comp' int2str(c) '_' int2str(s) '([i,:)=...
                profilep' int2str(c) ' (s,:);']);
            eval(['conr_' int2str(s) '([i,:)=...
                profiler(s,:);']);
        end;
    end;
end;

%*****
% Convert absorptivities into a useful form
%*****

for c = 1:comp
    eval(['eps' int2str(c) ' = absorbs(:, ' int2str(c) ');'])
    eval(['epsp' int2str(c) ' =...
        absorbs(:, ' int2str(c+comp+1) ');'])
end;
eval(['epsr = absorbs(:, ' int2str(comp+1) ');'])

```

```

for c= 1:comp
    eval(['extinct' int2str(c) ' = ones(waves,pts);'])
    eval(['extinctp' int2str(c) ' = ones(waves,pts);'])
end;
extinctr = ones(waves,pts);

for c= 1:comp
    for i = 1:pts
        eval(['extinct' int2str(c) ' (:,[i]) =...
            eps' int2str(c) ' (:,1);'])
        eval(['extinctp' int2str(c) ' (:,[i]) =...
            epsp' int2str(c) ' (:,1);'])
    end;
end;
for i = 1:pts
    extinctr(:,[i]) = epsr(:,1);
end;

%*****
% Calculate absorbances
%*****

for s= 1:samples
    for c= 1:comp
        eval(['abs' int2str(c) '_' int2str(s) ' = extinct'...
            int2str(c) ' .* con' int2str(c) '_' int2str(s) ';'])
        eval(['absps' int2str(c) '_' int2str(s) ' =extinctp'...
            int2str(c) ' .* conp' int2str(c) '_' int2str(s) ';'])
        eval(['absr_' int2str(s) ' = conr_' int2str(s) '...
            .* extinctr;'])
    end;
end;

for s= 1:samples
    eval(['sig_' int2str(s) ' = absr_' int2str(s) ';'])
    for c= 1:comp
        eval(['sig_' int2str(s) ' =...
            sig_' int2str(s) ' + abs' int2str(c) '_' int2str(s) '...
            + absps' int2str(c) '_' int2str(s) ' ;'])
    end;
end;

%*****
% Reshape data and add instrumental noise
%*****

for s= 1:samples
    eval(['signal_' int2str(s) ' =...
        reshape(sig_' int2str(s) ',datapoints,1);'])
    eval(['signal(:,s) = signal_' int2str(s) ';'])
end;

```

```
signal = noise(signal,noisei);
signal = signal';

Dim_signal=[samples waves pts];

signal3=reshape(signal,samples,waves,pts);
signal3=permute(signal3,[3 2 1]);

%*****
% All done!!!!
%*****
```

## KINETIC

```
function [profile1,profile2,profiler] =...
    kinetic(concs,r0,t0,tfinal,model,pts)
% [profile1,profile2,profiler] =...
% kinetic(concs,r0,t0,tf,model,pts);
% is a general-purpose m-file that uses the ode45
% function to generate kinetic profiles. It must be given
% initial concentrations, beginning and ending times,
% and the filename of the ode45 function that describes the
% system. This m-file uses a cubic spline to interpolate
% as it generates a user-supplied number of data points
% per profile.
%

global k1
global k2

[mcon,ncon] = size(concs);
profile1=zeros(mcon,pts);
profile2=zeros(mcon,pts);
profiler=zeros(mcon,pts);
for zz= 1:mcon
    c0= [concs(zz,:),r0];
    [t,c]=ode45(model,[t0 tfinal],c0);
    ti=linspace(t0,tfinal,pts);
    ci=interp1(t,c,ti,'spline');
    ci=ci';
    profile1(zz,:)=ci(1,:);
    profile2(zz,:)=ci(2,:);
    profiler(zz,:)=ci(3,:);
end;
```

## VARY\_K

```
function cdot=varyk(t,c);
% function cp=varyk(t,c);
% m-file that returns state derivatives when given state and
% time value for a second order kinetic process given by:
% A+R=PA
% B+R=PB
% Created 8/7/96 by Tom Cullen

global k1
global k2

% Define c1=A, c2=B, and c3=R
% c1' = -k1 .* c1 .* c3
% c2' = -k2 .* c2 .* c3
% c3' = (-k1 .* c1 .* c3) + (-k2 .* c2 .* c3)

cdot=[(-k1)*c(1)*c(3);(-k2)*c(2)*c(3);((-k1)*c(1)*c(3))+...
      (-k2*c(2)*c(3))];
```



MICHIGAN STATE UNIV. LIBRARIES



31293020582064